A STUDY OF THE DIVERSE T DWARF POPULATION REVEALED BY WISE

Gregory N. Mace[a,b], J. Davy Kirkpatrick[b], Michael C. Cushing[c], Christopher R. Gelino[b], Roger L. Griffith[b], Michael F. Skrutskie[d], Kenneth A. Marsh[e], Edward L. Wright[a], Peter R. Eisenhardt[f], Ian S. McLean[a], Maggie A. Thompson[g], Katholeen Mix[b], Vanessa Bailey[h], Charles A. Beichman[b], Joshua S. Bloom[i], Adam J. Burgasser[j,k], Jonathan J. Fortney[l], Philip M. Hinz[h], Russell P. Knox[h], Patrick J. Lowrance[b], Mark S. Marley[m], Caroline V. Morley[l], Timothy J. Rodigas[h], Didier Saumon[n], Scott S. Sheppard[o], and Nathan D. Stock[h]

[a]Department of Physics and Astronomy, UCLA, 430 Portola Plaza, Box 951547, Los Angeles, CA 90095-1547, USA; gmace@astro.ucla.edu

[b]Infrared Processing and Analysis Center, MS 100-22, California Institute of Technology, Pasadena, CA 91125, USA

[c]Department of Physics and Astronomy, MS 111, University of Toledo, 2801 W. Bancroft St., Toledo, OH 43606-3328, USA

[d]Department of Astronomy, University of Virginia, Charlottesville, VA 22904, USA

[e]School of Physics and Astronomy, Cardiff University, Cardiff CF24 3AA, UK

[f]NASA Jet Propulsion Laboratory, 4800 Oak Grove Drive, Pasadena, CA 91109, USA

[g]Department of Astrophysical Sciences, Princeton University, Peyton Hall, 4 Ivy Lane, Princeton, NJ 08544-1001, USA

[h]Steward Observatory, The University of Arizona, 933 N. Cherry Ave., Tucson, AZ 85721, USA

[i]Department of Astronomy, University of California, Berkeley, CA 94720, USA

[j]Department of Physics, University of California, San Diego, CA 92093, USA

[k]Department of Physics, Massachusetts Institute of Technology, 77 Massachusetts Ave, Cambridge, MA 02139, USA

[l]Department of Astronomy and Astrophysics, University of California, Santa Cruz, CA 95064, USA

[m]NASA Ames Research Center, Moffett Field, CA 94035, USA

[n]Los Alamos National Laboratory, Los Alamos, NM 87545, USA

[o]Department of Terrestrial Magnetism, Carnegie Institution of Washington, 5241 Broad Branch Rd. NW, Washington, DC 20015, USA

ABSTRACT

We report the discovery of 87 new T dwarfs uncovered with the Wide-field Infrared Survey Explorer (WISE) and three brown dwarfs with extremely red near-infrared colors that exhibit characteristics of both L and T dwarfs. Two of the new T dwarfs are likely binaries with L7±1 primaries and mid-type T secondaries. In addition, our follow-up program has confirmed 10 previously identified T dwarfs and four photometrically-selected L and T dwarf candidates in the literature. This sample, along with the previous WISE discoveries, triples the number of known brown dwarfs with spectral types later than T5. Using the WISE All-Sky Source Catalog we present updated color-color and color-type diagrams for all the WISE-discovered T and Y dwarfs. Near-infrared spectra of the new discoveries are presented, along with spectral classifications. To accommodate later T dwarfs we have modified the integrated flux method of determining spectral indices to instead use the median flux. Furthermore, a newly defined J-narrow index differentiates the early-type Y dwarfs from late-type T dwarfs based on the J-band continuum slope. The K/J indices for this expanded sample show that 32% of late-type T dwarfs have suppressed K-band flux and are blue relative to the spectral standards, while only 11% are redder than the standards. Comparison of the Y/J and K/J index to models suggests diverse atmospheric conditions and supports the possible re-emergence of clouds after the L/T transition. We also discuss peculiar brown dwarfs and candidates that were found not to be substellar, including two young stellar objects and two active galactic nuclei. The substantial increase in the number of known late-type T dwarfs provides a population that will be used to test models of cold atmospheres and star formation. The coolest WISE-discovered brown dwarfs are the closest of their type and will remain the only sample of their kind for many years to come.

Subject headings: infrared: stars — stars: low-mass, brown dwarfs — binaries: general — Galaxies: active

1. Introduction

Brown dwarfs were initially theorized nearly 50 years ago as the lowest mass products of star formation (Kumar 1963; Hayashi & Nakano 1963). Without the energy provided by hydrogen burning, brown dwarfs cool as they age and transition to later spectral types (e.g.

Burgasser 2004, Figure 2). As a result, older field brown dwarfs can have higher masses than young brown dwarfs, even though they have the same effective temperature and spectral type (Baraffe et al. 2003; Burrows et al. 1997). Brown dwarfs are classified by their spectral morphology, which is primarily related to effective temperature, but is also modulated by metallicity, clouds, gravity, and binarity. The cooling process results in a dearth of field L dwarfs and a surplus of T dwarfs relative to the initial mass function (Burgasser 2004). Since Gl 229B was discovered in 1995 (Nakajima et al. 1995), the T dwarf sample has increased in spurts thanks primarily to the Two Micron All Sky Survey (2MASS; Skrutskie et al. 2006), the Sloan Digital Sky Survey (SDSS; York et al. 2000), the United Kingdom Infrared Telescope Infrared Deep Sky Survey (UKIDSS; Lawrence et al. 2007), and the Canada France Hawaii Telescope Legacy Survey (CFHTLS; Delorme et al. 2008). T dwarfs are classified by increased methane, water and molecular hydrogen collision-induced absorption (CIA) in the near-infrared (Burgasser et al. 2002, 2006; Geballe et al. 2002), and have inferred temperatures between ∼500 and ∼1300K (Cushing et al. 2008, 2011; Stephens et al. 2009).

The cool brown dwarfs discovered by the Wide-field Infrared Survey Explorer (WISE; Wright et al. 2010) will provide the most robust tests of cool atmospheric models. Recent analysis of the T9 spectral standard UGPS J072227.51−054031.2 (Lucas et al. 2010; Bochanski et al. 2011; Leggett et al. 2012), and the Y dwarfs presented by Cushing et al. (2011), highlights the shortcomings of current models to match the low-flux near-infrared spectra of the coolest known objects. One promising avenue is the recent work of Morley et al. (2012) to include sulfide clouds in modeling the coolest brown dwarf atmospheres.

Tight constraints on the field mass function can be imposed by a complete census of the low-mass component of the solar neighborhood, of which the local T-dwarf component is a vital part. Our knowledge of the functional form of the mass function has a compounding influence on models of galaxy, star and planet formation processes. Also, knowledge of the low-mass component of the solar neighborhood can be used to determine the minimum mass for star formation (Burgasser 2004; Allen et al. 2005). To approach a complete volume-limited census, we have chosen brown dwarf candidates from the WISE All-Sky Source Catalog by imposing methane sensitive color constraints. Employing various near-infrared spectrographs, which provide diverse resolution and wavelength coverage, we have produced accurate classifications for these candidates through comparison to spectroscopic standards. Astrometric monitoring of the coolest objects provides trigonometric parallax measurements, as discussed by Marsh et al. (2013) and Beichman et al. (2013). Kirkpatrick et al. (2012) use this information to determine absolute magnitude relationships and constrain the mass function.

In this paper we present the spectra of 100 T dwarfs, including 90 newly reported

sources, which comprise approximately one-third of the present sample. Combined with the 89 T dwarfs reported by Kirkpatrick et al. (2011), WISE has more than tripled the number of brown dwarfs with spectral types later than T5. In §2 we discuss our photometric selection criteria and present WISE All-Sky photometry for all the objects in Kirkpatrick et al. (2011) and the new brown dwarfs presented here. In §3 we present our follow-up photometry and spectroscopy for the new T dwarfs and a few objects in the literature. Spectral classification, indices, and further analysis are presented in §4, along with comments on noteworthy objects. In §5 we present a dedicated discussion on the re-emergence of clouds in late-type T dwarfs. Interlopers, that mimic brown dwarfs in WISE color space, are discussed in §6. Our results are summarized in §7. In the Appendix we discuss our motivation for redefining spectral indices as the median flux over a wavelength range rather than the integrated flux.

2.   Candidate Selection

The WISE All-Sky Data Release (Cutri et al. 2012) is the culmination of a two-pass all-sky survey at 3.4, 4.6, 12, and 22 μm, hereafter referred to as bands $W1$, $W2$, $W3$, and $W4$, respectively (Wright et al. 2010). Designed as a variant of the methane imaging technique (Tinney et al. 2005), the $W1 - W2$ color compares the flux from the deep 3.3 μm CH_4 absorption band to the bright 4.6 μm flux in T and Y dwarfs (Mainzer et al. 2011). Cooler T and Y dwarf atmospheres possess redder $W1 - W2$ colors than M and L dwarfs. In $W3$ and $W4$, past the blackbody peak for the coolest T dwarf, the flux decreases and is further reduced by NH_3 absorption (Saumon et al. 2003; Burrows et al. 2003). Objects with $W2 - W3 \geq 4.0$ can be disregarded as brown dwarf candidates, and only two of thirteen candidates with $W2 - W3 > 3.0$ are T dwarfs (see §6).

Initial candidate selection, as described by Kirkpatrick et al. (2011), was made using the WISE Preliminary Data Release[1]. Our search required $W1 - W2$ colors (or limits) greater than 1.5 mag, which corresponds roughly to types $\geq$T5, and $W2 - W3 < 3.0$ mag, which reduces the number of very red extragalactic contaminants and sources embedded in star formation regions. To identify brown dwarfs earlier than T5 we searched for objects with $W1 - W2 > 0.4$ mag and no association with a 2MASS source (implying that the $J - W2$ color is either very red or the object has moved). Extragalactic contaminants were culled from the bright source candidates using the following criteria: $W1 - W2 > 0.96(W2 - W3) - 0.96$ (as shown in Figure 3 of Kirkpatrick et al. (2011)). Spectroscopic follow-up of our initial candidates confirmed ∼100 new brown dwarfs. Kirkpatrick et al.

---

[1]See http://wise2.ipac.caltech.edu/docs/release/prelim/expsup/ .

(2011) provide photometry from the WISE Preliminary Data Release for these new objects and the objects in Mainzer et al. (2011) and Burgasser et al. (2011).

Making use of the WISE All-Sky Data Release[2], specifically the database of extractions from the atlas images that is a union of the WISE All-Sky Source Catalog and the WISE All-Sky Reject Table, we modified our selection criteria to identify the reddest candidates. The details of our query method can be found in Kirkpatrick et al. (2012). Briefly, we required $W1 - W2 > 2.0$ mag, $W2 - W3 < 3.5$ mag, signal-to-noise ratio (SNR) > 3 per frame at $W2$, that the source is not blended with another source in visual inspection, that the source is point-like, and that the absolute Galactic latitude be greater than three degrees if its Galactic longitude falls within twenty degrees of the Galactic Center. To aid in follow-up, finder charts of a $2'$x$2'$ field around each candidate were constructed using DSS2 BRI (epoch $\sim$1980s), SDSS $ugriz$ (where available; epoch $\sim$2000), 2MASS JHK_s (epoch $\sim$2000), and WISE four-band data (epoch $\sim$2010). Prioritization was accomplished by visually inspecting each of these finder charts[3]. T dwarf candidates that were detected at visual wavelengths, and showed no clear proper motion, were excluded from further follow-up.

Comparison of the WISE photometry in the Preliminary Data Release and the All-Sky Data Release reveals measurements biases of $\sim$0.3, 0.05, and 0.4 magnitudes in $W1$, $W2$ and $W3$, respectively. This is a known difference in the catalogs and is further discussed in Section 6.3 of the WISE Explanatory Supplement[4]. The Pass-2 source extraction, which produced the All-Sky Source Catalog, implemented a number of improvements listed in section 4.1 of the Explanatory Supplement. Because the WISE All-Sky Data Release is the premier data product from the WISE mission, we present this new photometry in Table 1 for the brown dwarfs in Kirkpatrick et al. (2011) and in Table 2 present photometry for our newly confirmed brown dwarfs.

Figures 1 & 2 present the updated $W1 - W2$ and $W2 - W3$ colors as a function of spectral type for objects in Tables 1 & 2 and for Y dwarfs from Kirkpatrick et al. (2012). Similar plots were included in Kirkpatrick et al. (2011) for M, L, T, and Y dwarfs, but here we focus on the T dwarf sequence. The gradual onset of methane absorption at 3.3 μm (Noll et al. 2000) complicates the functional form of the $W1 - W2$ color around the L-T transition. Although the dispersion in the $W1 - W2$ color for the late-type T dwarfs is large ($\sim$1.5 mag), early-type T dwarfs display a considerably smaller dispersion until T4 or T5.

---

[2]See http://wise2.ipac.caltech.edu/docs/release/allsky/.

[3]In lieu of creating $\sim$90 additional figures for the finder charts of the new objects, we point the readers to the excellent DSS+SDSS+2MASS+WISE Finder Chart Service at IRSA (http://irsa.ipac.caltech.edu/).

[4]See http://wise2.ipac.caltech.edu/docs/release/allsky/expsup/.

Most objects later than T9 only have $W2$ and $W3$ detections, resulting in $W1 - W2$ lower limits. The gap between the limits and the verified detections of the late-type sources implies that the $W1$ limit is an overestimate and the resultant $W1 - W2$ color limits are artificially high. Upper limits in $W2 - W3$ are a result of non-detections in $W3$, which is the case for many of our new T dwarfs. The dispersion in the $W1 - W2$ and $W2 - W3$ colors is likely caused by clouds and/or non-equilibrium chemistry in T dwarf atmospheres (Saumon et al. 2003), and are largest for spectral types later than T4.

3. Follow-up Photometry and Spectroscopy

T dwarf candidates selected by WISE colors alone are reliable when they fall within the core of the T dwarf $W1 - W2$ versus $W2 - W3$ color-color diagram in Figure 3. However, near the periphery of this region the number of non-stellar interlopers increases. Additional photometry of WISE candidates allows us to identify sources that have near-infrared colors characteristic of brown dwarfs, and provides near-IR magnitudes that guide facility selection for spectroscopic observation.

3.1. Follow-up Photometric Observations

Most of our photometric observations are described in Cushing et al. (2011) and Kirkpatrick et al. (2011, 2012). We have separated the 2MASS and Mauna Kea Observatories Near-Infrared (MKO; Simons & Tokunaga 2002; Tokunaga et al. 2002) systems since care should be taken when making comparisons between the two filter systems whose different bandpasses produce slightly different magnitudes. Some of our photometry is provided by the 2MASS All-Sky Point Source Catalog and the Reject Table[5]. Other follow-up ground-based photometry on the 2MASS system is from the 2MASS camera on the 1.5 m Kuiper Telescope at Steward Observatory and the Peters Automated Infrared Imaging Telescope (PAIRITEL; Bloom et al. 2006) on the 1.3 m telescope at Fred Lawrence Whipple Observatory. Photometry on the MKO system is from the Wide-field Infrared Camera (WIRC; Wilson et al. 2003) at the 5 m Hale Telescope at Palomar Observatory, the Persson's Auxilliary Nasmyth Infrared Camera (PANIC; Martini et al. 2004) on the 6.5 m Magellan telescope at Las Campanas Observatory, and the NOAO Extremely Wide Field Infrared Imager (NEWFIRM; Autry et al. 2003) on the 4 m Victor M. Blanco Telescope at Cerro Tololo Inter-American Observatory (CTIO). Ten of our candidates are available in UKIDSS (the UKIRT Infrared Deep

---

[5]See http://www.ipac.caltech.edu/2mass/releases/allsky/doc/explsup.html for details.

Sky Survey) Data Release 8 (Hewett et al. 2006; Lawrence et al. 2007; Casali et al. 2007; Hambly et al. 2008; Hodgkin et al. 2009). Photometric filters installed in the Ohio State Infrared Imager/Spectrometer (OSIRIS; Depoy et al. 1993) use Barr filters which produce T dwarf photometry most similar to the MKO system (Kirkpatrick et al. 2012, Section 2.2.5), so they are listed with the MKO measurements. All images were acquired between 2010 August and 2012 August, and source extractions from our observations use source apertures that are 1.5×FWHM of the source point-spread function.

Figures 5, 7, and 8 of Kirkpatrick et al. (2011) specify the $J-H$, $J-W2$, and $H-W2$ colors of M, L, T, and Y dwarfs. Objects lacking photometry in Table 3 of that paper, but having follow-up photometry now, are presented in Table 3 of this paper. Photometry of new T dwarf candidates is listed in Table 4. For the figures in this paper we use magnitudes on the 2MASS system. MKO magnitudes are depicted in Kirkpatrick et al. (2011, 2012).

The $J-H$ color-type diagram for WISE-discovered T and Y dwarfs is shown in Figure 4. The reversal in the $J-H$ color shown in Figure 7 of Kirkpatrick et al. (2012) can also be seen in Figure 4 around T7±1. However, the turnaround in the $J-H$ color is driven by only a few objects later than T8 and there are large uncertainties in our colors, making a clear identification of the reversal location difficult.

The $J-W2$ and $H-W2$ colors, shown in Figures 5 & 6, of early-type T dwarfs are slightly bluer (or flat) for successive types before they become redder for late-type T dwarfs. These colors are complicated as H_2 CIA, non-equilibrium CO and CO_2 absorption, and the shift of the Planck peak to longer wavelengths influence the emergent flux (Linsky 1969; Borysow et al. 1997; Frommhold et al. 2010; Saumon et al. 2012; Abel et al. 2012).

The Infrared Array Camera (IRAC; Fazio et al. 2004) onboard the *Spitzer Space Telescope* (Werner et al. 2004) was used during the warm *Spitzer* mission to obtain deeper photometry in its 3.6 and 4.5 μm channels (hereafter, $ch1$ and $ch2$, respectively) allowing the WISE $W1$ and $W2$ filters to be robustly measured. These observations were made as part of Cycle 7 and Cycle 8 programs 70062 and 80109 (Kirkpatrick, PI). *Spitzer*/IRAC photometry is listed in Tables 3 & 4 along with our ground-based photometry. The $ch1-ch2$ color, as a function of spectral type, is shown in Figure 7. The trend is similar to the WISE $W1-W2$ colors (Figure 1), but differences in the WISE and *Spitzer*/IRAC passbands (Mainzer et al. 2011) result in a shallower slope in the $ch1-ch2$ color, as a function of spectral type, than the $W1-W2$ color. Figure 8 directly compares the $ch1-ch2$ and $W1-W2$ colors for T dwarfs. Figure 1 of Griffith et al. (2012) shows the $ch1-ch2$ and $W1-W2$ colors of many WISE candidate and confirmed brown dwarfs, clearly identifying the dip in $ch1-ch2$ at the L/T transition and the dispersion in colors at later spectral types that are also seen in Figure 8.

3.2. Follow-up Spectroscopic Observations

Summaries of the spectroscopic follow-up observations of the 90 new brown dwarfs and fourteen known objects from the literature are given in Tables 5 & 6, respectively. Our observation and data reduction procedures are discussed in detail in Kirkpatrick et al. (2011, 2012). The analysis by Kirkpatrick et al. (2012) of the low-mass end of the field brown dwarf mass function used objects observed prior to 2012 May 1 (UT) and spectral types for WISE J152305.10+312537.6, WISE J180901.07+383805.4, WISE J201404.13+042408.5, and WISE J201920.76−114807.5 have been adjusted by half spectral types in this paper. An improved spectrum of the T9 dwarf WISE J033515.01+431045.1 has increased the precision of the spectral type provided by Kirkpatrick et al. (2012).

No changes were made in our procedures for spectra acquired with SpeX (Rayner et al. 2003) at NASA's Infrared Telescope Facility (IRTF), the Triple Spectrograph (TSpec; Herter et al. 2008) at Palomar Observatory, or the Wide Field Camera 3 (WFC3; Kimble et al. 2008) on-board the *Hubble Space Telescope* (HST). Non-peculiar T dwarf spectra from SpeX and TSpec are sorted by spectral type (see §4.1 for classification procedure) and shown in Figures 9 and 10, respectively. Figure 11 shows the WFC3 confirmed T9.5 dwarf WISE J154214.00+223005.2.

We spectroscopically confirmed seven of our candidates employing the Gemini Near-InfaRed Spectrograph (GNIRS; Elias et al. 2006) at the Gemini-North Telescope on Mauna Kea, HI. We used the cross-dispersed mode with the 32 lines/mm grating and a 1″-wide slit which provided an R of 540 over the 0.8 to 2.5 μm wavelength range. A series of 300 sec exposures were obtained at two positions along the 7″-long slit. An A0 V standard star was obtained either before or after each science target for telluric correction and flux calibration purposes. The data were reduced with a modified version of the Spextool data reduction package (Cushing et al. 2004). The raw frames were first cleaned of fixed patterns using the `cleanir.py` routine provided by Gemini Observatory. A normalized flat-field image was then generated using the nightly calibration frames. Pairs of images taken at two different positions along the slit were then pair-subtracted and flat-fielded. The spectra were then extracted after subtracting off residual background and wavelength calibrated using the night sky OH emission lines. The raw spectra were corrected for telluric absorption using the spectra of the associated A0 V standard star and the technique described in Vacca et al. (2003). Finally the spectra from the individual orders were merged to produce a continuous 0.8 to 2.4 μm spectrum. The GNIRS spectra of our new T dwarfs are shown in Figure 10 and are colored blue to differentiate them from the other instruments.

Since the publication of Kirkpatrick et al. (2011), the reduction procedure has changed for spectra from the Folded-port Infrared Echellette (FIRE; Simcoe et al. 2008, Simcoe et al.

2010) instrument at the 6.5m Walter Baade Telescope on Cerro Manqui at the Las Campanas Observatory, Chile. FIRE reductions in this paper make use of the FIREHOSE package for low-dispersion data following the procedure in the online "cookbook."[6] The FIREHOSE package uses NeAr arc lines for the calibrator, and OH sky emission lines for target, wavelength solutions. For our faintest objects, pair subtraction of the 2-D spectra prior to insertion into the pipeline greatly improved the accuracy of the bspline sky-line fitting procedure. Although the automated continuum fitting worked well for most of our targets, the faint sources required manual selection of the continuum position when sky-lines were poorly subtracted. Spectra were extracted using the optimal spectral extraction process, where an iterative, local background model is fit to improve estimates of the sky flux for subtraction. The combined spectrum was then corrected for telluric absorption and flux calibrated using the observations of an A0 V star and the technique described in Vacca et al. (2003) and the XTELLCOR program from SpeXtool (see Cushing et al. 2004). FIRE spectra are presented in Figure 10 and are colored red to differentiate them from the other instruments.

Observations with the Near-Infrared Spectrometer (NIRSPEC, McLean et al. 1998, 2000) at the 10 m W. M. Keck Observatory on Mauna Kea, Hawai'i, were made with slit widths of $0\rlap{.}''38$, $0\rlap{.}''57$, or $0\rlap{.}''76$ to reduce slit-loss for specific seeing conditions. These slit widths result in spectral resolutions at 1.27μm of R$\sim$ 2250, 1500, and 1100, respectively. After being confirmed in our J-band (N3) observations, two of our new T dwarfs were observed with the H-band (N5) filter with a $0\rlap{.}''76$ slit (R$\sim$1400 at 1.58μm). Observations from multiple epochs used the same instrument configurations and were combined into a single spectrum. Data reduction made use of the publicly available REDSPEC package, with modifications to remove residuals from the sky-subtracted pairs prior to 1-D spectral extraction. Normalized Keck/NIRSPEC J-band spectra are shown in Figure 12, and objects with both J- and H-band observations are shown in Figure 13. The H-band spectra were scaled relative to the J-band data using the ratio of peak fluxes produced by REDSPEC (McLean et al. 2003).

4. T Dwarf Spectral Analysis

After collecting near-IR spectra for each candidate we determined spectral types through comparison to the spectral standards (Burgasser et al. 2006 and Cushing et al. 2011). Some of the objects are noteworthy for their peculiarity. Fourteen of our candidates have been published by others since we first identified or confirmed them, and we discuss each one individually. For all the T dwarfs presented here and in Kirkpatrick et al. (2011), as well

---

[6]See http://www.mit.edu/people/rsimcoe/FIRE/ob_data.htm for details.

as the Y dwarfs from Cushing et al. (2011) and Kirkpatrick et al. (2012), we derive spectral indices using the median flux method.

4.1. Spectral Classification

We derived the spectral types for each of our near-IR spectra by visual comparison to the T0-to-T8 spectral standards of Burgasser et al. (2006) and the T9 and Y0 standards defined by Cushing et al. (2011). Classifications are based on the complete near infrared flux when it is available. Normalization at $\sim$1.27 μm makes the J-band morphology the easiest to compare to the standards and emphasizes peculiarities in the Y, H, and K bands. Half spectral types are assigned where the spectrum falls consistently between two adjacent spectral standards. In cases where the spectrum deviates from the standards in a way that is inconsistent with the spectral sequence (e.g. the J band is narrower than a T7 and wider than a T8, but the H- and K-band fluxes are consistent with a T6) we have identified these objects as peculiar. We identify spectral types of low SNR spectra with ':' to indicate that they are more uncertain than the standard $\pm$0.5 type uncertainty. The extremely red brown dwarfs defy classification and are discussed in detail in §4.2. Our binary candidates are given spectral types and marked as 'sb' to denote that they are peculiar and best matched with combined spectral templates. Assigned spectral types for all the objects in Table 2 are listed in column 2 of Tables 5 and 6.

4.2. Are the Extremely Red Brown Dwarfs L or T Type?

The T dwarf spectral standards from Burgasser et al. (2006) were chosen for their progressively stronger H_2O and CH_4 absorption features throughout the near infrared. It is the CH_4 features in T dwarfs like the prototype Gl 229B (Geballe et al. 1996) that makes these objects stand apart from L dwarfs. Kirkpatrick et al. (2010) outlined the procedure for defining a near infrared L dwarf sequence that varies smoothly between spectral types and is tied closely with the optical spectral types. For this L dwarf sequence, spectra are normalized at the J-band flux peak ($\sim$1.27μm) and the type is determined from only the 0.9-1.4μm spectral shape. From this initial classification, the spectral morphology from 1.4-2.5μm identifies the source as either "red" or "blue" relative to the spectral standard. Based on these systems, we have identified three objects (WISE J064205.58+410155.5, WISE J075430.95+790957.8, and WISE J173859.27+614242.1) that defy classification.

As the number of red L dwarfs with near-IR spectra has increased, classification and

physical interpretation of the spectra has become more complicated. Many of the known red L dwarfs are early-type and have accompanying optical spectra to facilitate classification and analysis (Looper et al. 2008; Kirkpatrick et al. 2006, 2010). At later spectral types, L dwarf $J - K$ colors redden by nearly 1.5 magnitudes relative to L0's (as cloud opacity increasingly dominates at shorter wavelengths) and the red L dwarfs mark the upper boundary of these colors (Gizis et al. 2012, Figure 4). Recently, as a result of 2MASS proper motion surveys and the WISE mission, the sample of red, late-type L dwarfs has been expanded (Kirkpatrick et al. 2011; Gizis et al. 2012). Since the reddest L dwarfs are a few magnitudes fainter at visible wavelengths, high-quality optical spectra of these objects are rare.

Infrared spectra of red L dwarfs are primarily influenced by temperature, metallicity and gravity differences, but also by possible binarity and cloud morphology. Looper et al. (2008) discuss the influence of low surface gravity and high metallicity on reddening near-IR colors, and the unlikely reddening from binarity and interstellar extinction. Allers et al. (2010, Figure 3) show how dust and low surface gravity alters near-IR spectra for adjacent spectral types. Other extremely red objects, like 2MASS J035523.37+113343.7 (Faherty et al. 2013), 2MASS 1207b (Patience et al. 2010; Barman et al. 2011) and the HR 8799 planets (Bowler et al. 2010; Barman et al. 2011; Marley et al. 2012) have low surface gravity, appear to be dusty, resemble the L dwarf standards, and lack the methane features of T dwarfs. Gizis et al. (2012) present an extremely red L dwarf (WISEP J004701.06+680352.1) that they can best classify as an L7.5pec based on rough comparison to the spectral standards and other red L dwarfs in the literature, but they also discuss the difficulty in determining spectral types and estimating surface gravities for such red sources, which may not be very young. The extremely red objects shown in this paper don't show the 'peakiness' associated with youth, but instead display a broader plateau in the H band, and are most similar to WISEP J0047+6803 and 2MASSW J2244316+204343 (Dahn et al. 2002; McLean et al. 2003; Looper et al. 2008).

WISE J0754+7909 is the least red of the three new objects. Figure 14 shows the Palomar/TSpec spectrum of this object along with the L9 and T2 spectral standards. Comparison to the L9 standard produces the best match to the integrated flux, but poorly matches the H_2O and CH_4 absorption depths. Classification based solely on the J-band peak, as was done by Kirkpatrick et al. (2010), pushes the classification of this object into the T sequence. However, given the noise of this spectrum it is difficult to fully identify CH_4 features, ruling out its classification as a T dwarf using the scheme of Burgasser et al. (2006). Near-IR colors for this object are consistent with the T2 classification and WISE colors are similar to sources at the L/T transition. However, this object is blended in the *Spitzer* images with a source that is not visible in our near-IR imaging, so WISE and *Spitzer* colors should be used cautiously.

Burgasser et al. (2010) used the SpeX Prism Library to identify possible binary systems based on the composite of L and T dwarf spectra. Using the same analysis, we find that WISE J0754+7909 is poorly matched by composite spectra and is likely not a binary. The spectrum of SDSS J1516+3053 is also included in Figure 14 since it matches the spectrum of WISE J0754+7909 well at shorter wavelengths. SDSS J151643.01+305344.4 has been classified as a T0.5±1 (Chiu et al. 2006) and T1.5±2 (Burgasser et al. 2010), and is a weak binary candidate based on their analysis. The large uncertainties in the SDSS J1516+3053 classifications are due to the difficulty in classifying this source using the methods in the literature.

The Palomar/TSpec spectrum of WISE J0642+4101 is shown in Figure 15 with the L9 and T2 spectral standards. Just like WISE J0754+7909, classification of this object based on the J band only requires that we classify this object as a T dwarf. However, there is a clear absence of CH_4 in this spectrum. Compared to SDSS J1516+3053, WISE J0642+4101 is significantly redder. The red L7.5±2 dwarf 2MASS J2244+2043 is one of the reddest late-type L dwarfs and is very similar to WISEP J0047+6803 (L7.5pec; Gizis et al. 2012). Figure 15 shows that WISE J0642+4101 is nearly as red as 2MASS J2244+2043 in the H band, but has a significantly lower K-band flux.

The reddest object that we have identified, WISE J1738+6142, is shown in Figure 16. We observed this object with Palomar/TSpec on 2011 July 13 (UT) and with IRTF/SpeX on 2012 July 23 (UT). Although the Palomar/TSpec spectrum is noisy, comparison of these two spectra reveals that the near-infrared flux of WISE J1738+6142 is extremely variable.[7] Photometry of this object from PAIRITEL produces $J-K_s$=2.55±0.16, which is equivalent with the extremely red L dwarf WISE J0047+6803. The WISE $W1-W2$=0.72±0.04 color for this source is slightly redder than the similar red L dwarfs WISEP J0047+6803 ($W1-W2$=0.65±0.03) and 2MASS J2244+2043 ($W1-W2$=0.67±0.03). Comparison of the WISE J1738+6142 IRTF/SpeX spectrum to 2MASS J2244+2043 reveals excess flux on the blue side of the H and K bands, possibly hinting at the presence of a T dwarf secondary. Since the red L dwarf phenomenon isn't entirely understood, having a coeval T dwarf companion with similar metallicity or low gravity indicators will help reveal the cause of the cloudiness in the L dwarfs, should any of these extremely red objects prove to be an L+T binary.

Although gravity, metallicity, and temperature changes are the primary variables in modeling these red objects, the variability seen in WISE J1738+6142 hints at considerably rapid changes in atmospheric conditions. If we assume that the source of reddening is common to all these objects, then surface gravity and metallicity are not likely the mechanisms

---

[7]The airmass of each A0 standard was less than 0.05 away from the mean value for WISE J1738+6142.

at work. The proper motions of these three objects, determined by comparing 2MASS and WISE coordinates [WISE J0642+4101 (0.37 ± 0.03 ″/yr), WISE J0754+7909 (0.43 ± 0.04 ″/yr), and WISE J1738+6142 (0.28 ± 0.04 ″/yr)] is consistent with the red L dwarfs from Kirkpatrick et al. (2010) that are likely part of an older field population. That is inconsistent with either high metallicity or low gravity. Although analysis of the underlying physical mechanisms will require detailed analysis and modeling of higher resolution optical and near-IR spectroscopy, identifying companions to these red objects and disentangling their spectral features are good initial tests. We believe that further analysis (i.e. optical spectroscopy, high-resolution imaging, and time domain observations) are warranted before final classifications are made for these extremely red objects at the L/T transition.

4.3.   Comments on Interesting T Dwarf Discoveries

In the following subsection we discuss the peculiar objects individually, along with noteworthy objects that warrant separate discussion.

4.3.1.   WISE J0336−0143 - T8:

This object is a clear outlier in Figure 7 ($ch1 - ch2 = 2.64 \pm 0.06$) and is undetected in the WISE $W1$ filter ($W1 - W2 > 3.42$). These colors are more consistent with a Y dwarf than a T8, but the Keck/NIRSPEC J-band spectrum is broad. WISE J0336−0143 may be a T+Y binary, with the Y dwarf contributing more flux at the WISE passbands than in the near-IR bands. Follow-up photometry and broader near-IR spectroscopy of this source are warranted.

4.3.2.   WISE J0413−4750 - T9

The A nod position of the pair subtracted 2-D spectra for this source was contaminated by a galaxy. The spectrum of the galaxy was extracted from the B-position images and fit with a line. This linear fit was then subtracted from the final extracted spectrum of WISE J0413−4750, which is shown in Figure 10.

4.3.3. WISE J0629+2418 - T2 sb

The IRTF/SpeX spectrum for this object is presented in Figure 17 along with the T2 standard, which is the best overall match to the CH_4 and H_2O absorption troughs. Relative to the T2 standard, the H band is wider and displays greater CH_4 absorption redward of the flux peak and the K-band flux is high. Using the statistical method described by Burgasser et al. (2010) we identify WISE J0629+2418 as a strong binary candidate with a L7±1 primary and T5.5±0.5 secondary (ΔJ_{MKO}=0.47±0.28, ΔH_{MKO}=1.67±0.30). The best composite match to WISE J0629+2418 is also shown in Figure 17.

4.3.4. WISE J1523+3125 - T6.5 pec

Figure 18 shows the Gemini/GNIRS spectrum for this object. Comparison to the T6 standard produces the best match to the H-band flux, while the J band is better matched by the T7 standard. The Y- and K-band fluxes are inconsistent with the standards. These features are similar to the metal-poor T dwarfs 2MASSI J0937347+293142 (T6pec; Burgasser et al. 2002) and BD +01° 2920B (T8pec; Pinfield et al. 2012). However, we also observed BD +01° 2920B (§4.4.5) and find that, other than a suppressed K band, it matches the T8 standard well and we do not classify it as peculiar.

4.3.5. WISE J1542+2230 - T9.5

The HST/WFC3 spectrum for this object is shown in Figure 11, compared to the T9 and Y0 spectral standards from Cushing et al. (2011). WISE J1542+2230 has a measured F140W(Vega) magnitude of 20.3. Located 2″0 west is a neighbor that has a measured F140W(Vega) magnitude of 22.8. The slitless grism image of this field revealed that the neighbor has a flux peak coincident with the H-band flux peak in cool brown dwarfs, however we detect no flux in the J-band opacity window at 1.27 μm. Additional high resolution images of WISE J1542+2230 were obtained using the Keck II LGS-AO system (Wizinowich et al. 2006; van Dam et al. 2006) with NIRC2 on 2012 April 14 (UT). Very good seeing ($\approx$0″3) and clear skies allowed us to use the relatively faint (R=18.5) USNO-B star 1124-0287738 (Monet et al. 2003) as the tip-tilt reference star. Observations were obtained in the MKO H filter with the wide camera (nominal plate scale 40mas/pixel) on NIRC2. Twenty-one frames with durations of 120sec each were collected using a 3-point dither pattern that was repeated seven times with position offsets 1.5–5″. The images were dark subtracted, flat-fielded, shifted to a common grid, and median averaged to make a

single mosaic image with a total exposure time of 42 minutes in the central region. From this imaging we measured the proper motion of WISE J1542+2230 to be $\mu_\alpha = -0.82 \pm 0.07$ arcsec/yr and $\mu_\delta = -0.41 \pm 0.06$ arcsec/yr, while the neighbor remained stationary, thus ruling out binarity.

4.3.6.   WISE J1730+4207 - T0 sb

This object's spectrum is very similar to WISE 0629+2418 (§4.3.3), with the integrated flux most similar to the T0 standard (see Figure 17). This source is matched well by a composite of L7.5±1 and T3±1 spectra. With ΔJ_{MKO}=-0.31±0.27 and ΔH_{MKO}=0.38±0.36, this system is likely a flux-reversal binary. The best composite match to WISE J1730+4207 is also shown in Figure 17, and is well within the uncertainties of the average fit L7.5+T3.

4.3.7.   WISE J2014+0424 - T6.5 pec

Much like WISE J1523+3125 (§4.3.4), comparison to the T6 standard produces the best match to the H-band flux, while the J band is better matched by the T7 standard. The Y- and K-band fluxes are inconsistent with the standards. Figure 18 shows the Gemini/GNIRS spectrum for this object.

4.4.   Comments on Known and Candidate Brown Dwarfs in the Literature

Some of our candidates were identified and/or confirmed but subsequently published by others as independent discoveries. Table 6 lists these objects along with their discovery papers and previous spectral classifications. Spectra for these objects are shown in Figure 19 unless noted otherwise.

4.4.1.   WISE J0920+4538 - L9 sb?

Aberasturi et al. (2011) performed a cross correlation of the 2MASS Point Source, SDSS Data Release 7, and WISE Preliminary Release Catalogs to identify six brown dwarf candidates based on photometric colors and proper motion. Based on a temperature derived from spectral energy distribution fitting, they estimated the spectral type of this object as L4 or L5. However, comparison to spectral standards reveals that this object is best classi-

fied as an L9 and a weak binary candidate. Figure 17 shows the Palomar/TSpec spectrum for this source and the best fitting composite spectrum with a L7.5±1.5 primary and a T1.5±1.5 secondary (ΔJ_{MKO}=-0.17±0.33 and ΔH_{MKO}=0.22±0.33). The composite fit to WISE J0920+4538 is highly uncertain, but fitting to a single object spectrum is also a poor fit and binarity may be the source of the discrepant photometric colors and spectral features of this source.

4.4.2. ULAS J095047.28+011734.3 - T8

Photometry, and a T8 spectral type, for this object was reported by Leggett et al. (2012). Our Magellan/FIRE spectrum for this source is consistent with the T8 standard, but displays a slightly higher flux in the Y and H band, and is slightly suppressed in the K band. However, these deviations are within our noise estimates and so we do not classify this object as peculiar.

4.4.3. WISE J1246−3139 - T1

This source was first identified in the literature by Andrei et al. (2011) as one of the targets in their parallax program. Based on preliminary photometry they estimated the spectral type as T1.0. The Palomar/TSpec spectrum for this source is shown in Figure 19 and we classify this object as a T1.

4.4.4. LHS 2803B - T5.5

This wide separation, common proper motion companion to the M4.5±0.5 dwarf LHS 2803 was reported by Deacon et al. (2012) and classified as a T5.5. We produce the same T5.5 classification from our IRTF/SpeX spectrum.

4.4.5. BD +01° 2920B - T8

Pinfield et al. (2012) identify BD +01° 2920B as a T8pec dwarf companion to BD +01° 2920 (HIP 70319), a metal-poor ([Fe/H] = −0.38 ± 0.06) G1 dwarf at a distance of 17.2 pc. We observed BD +01° 2920B and find that, other than a suppressed K band, the object matches the T8 standard. Since our analysis (§4.5.5) shows that suppressed K-band flux is

fairly common in late-type T dwarfs we do not classify it as peculiar.

4.4.6.   WISE J1449+1147 - T5 pec

In a search for high proper motion T dwarf candidates between the UKIDSS DR6 and SDSS DR7 databases, Scholz (2010) identified this source as a candidate T7±2 (ULAS J144901.90+114711.3). This object was observed with two instruments, Gemini/GNIRS and Palomar/TSpec. Figure 18 shows the near-IR spectra from each instrument along with the T5 spectral standard. The J- and H-band flux match the T5 standard, but the Y band displays a flux excess and the K band is more heavily suppressed than the standard. These are the same low-metallicity features seen in the other peculiar objects.

4.4.7.   Repeats from Deacon et al. (2011)

Deacon et al. (2011) identified four new T dwarfs by their proper motions between the PanSTARRS 1 commissioning data and 2MASS. We independently identified three of these objects in the WISE catalog and they were observed prior to publication by Deacon et al. (2011); PSO J226.2599−28.8959 (WISE J1505-2853), PSO J246.4222+15.4698 (WISE J1625+1528), and PSO J247.3273+03.5932 (WISE J1629+0335). Our derived spectral types are consistent with their visually derived types, but with higher uncertainties. The fourth object observed by Deacon et al. (2011), PSO J201.0320+19.1072, is not included in the partial sky coverage of the WISE Preliminary Release Source Catalog and was not observed by us after it was published by Deacon et al. (2011).

4.4.8.   VHS J154352.78−043909.6 - T5:

Our IRTF/SpeX spectrum for this source is fairly low signal-to-noise. Lodieu et al. (2012) photometrically selected this object from the first data release of the VISTA Hemisphere Survey and the WISE Preliminary Data Release. They derive a spectral type of T4.5 based on a Magellan/FIRE spectrum of the source, which is constant with the uncertain T5: classification that we produce.

4.4.9. Repeats from Kirkpatrick et al. (2011)

Two objects from Kirkpatrick et al. (2011), WISE J1717+6129 and WISE J2344+1034, were observed again with Gemini/GNIRS to provide more wavelength coverage than the original Keck/NIRSPEC observations. The classifications from Kirkpatrick et al. (2011) remain unchanged at T8 and T9, respectively.

4.4.10. WISE J1809+3838 - T7.5

Luhman et al. (2012) used the WISE All-Sky Source Catalog along with the 2MASS Point Source Catalog to search for proper motion companions. From their IRTF/SpeX spectrum they produce a type of T7±1, while we classify the object as T7.5±0.5.

4.4.11. WISE J2342+0856 - T6.5

This object was also identified by Scholz (2010) as a candidate T7±2 (ULAS J234228.96+085620.1). We classify this object as a T6.5 based on the IRTF/SpeX spectrum for this object.

4.5. Median Derived Spectral Indices

Burgasser et al. (2006) defined a number of primary spectral indices that compare the ratio of the integrated J- and H-band flux peaks to the blueward H_2O and redward CH_4 absorption features; H_2O-J, CH_4-J, H_2O-H, and CH_4-H. K-band indices were also defined, but K-band fluxes reduced by H_2 CIA results in low SNR K-band spectra and highly uncertain K-band indices. The Y/J and K/J color ratios, defined by Burgasser et al. (2004, 2006), serve as proxies for the broadband $Y - J$ and $J - K$ colors. Two additional indices that correlate well with the T dwarf spectral sequence are W_J (Warren et al. 2007) and NH_3-H (Delorme et al. 2008), which approximate the slope of the J- and H-band flux peaks, respectively.

In addition to these indices, we have derived an H/J color ratio as a proxy for the $J - H$ color,

$$\mathrm{H/J} = \frac{\widetilde{F}_{1.560-1.600\mu m}}{\widetilde{F}_{1.250-1.290\mu m}}, \tag{1}$$

and the J-narrow index which is designed to differentiate Y dwarfs from T dwarfs based

on their narrow J-band flux peaks,

$$\text{J-narrow} = \frac{\widetilde{F}_{1.245-1.260\mu m}}{\widetilde{F}_{1.260-1.275\mu m}}, \qquad (2)$$

where $\widetilde{F}$ is the *median* flux between the subscripted wavelengths in microns. Figure 20 depicts the wavelengths over which these indices are derived for a series of Palomar/TSpec spectra from this paper.

Although indices in the literature are defined as the integrated flux over the desired wavelength range, this method is unreliable when trying to compute indices for low-SNR spectra. Even with moderate SNR spectra, the flux in the numerator of most indices is minuscule for late-type T dwarfs and easily modulated by noisy pixels and poor telluric correction. For this reason, we have computed all of our indices *over the classical wavelengths* but use the *median* flux instead of the integrated flux. This method reduces the scatter in index values as a function of spectral type, especially at later types. Further discussion about using median fluxes to compute indices is deferred to the Appendix, where we also include the integrated flux indices for all our WISE discoveries.

We computed the index values using a Monte Carlo model of each spectrum. This was accomplished by randomly drawing from a normal distribution with means given by the flux densities at each wavelength and standard deviations given by the uncertainty in the flux densities. For 1000 realizations of each spectrum, the index is given as the mean and standard deviation of the distribution of index values. Table 7 lists the index values for the T and Y dwarf spectra in Kirkpatrick et al. (2011, 2012) and Cushing et al. (2011), the new WISE T dwarf discoveries in this paper, and for objects from Table 6.

Spectral indices for the WISE-discovered T and Y dwarfs are shown in Figures 21 to 25 along with the T0-to-Y0 spectral standards. Because our sample is mostly T dwarfs later than T5, indices for the T dwarfs in the SpeX Prism Library (Burgasser et al., in prep.) are also included in our figures. The average index value and standard deviation, for the ∼320 unique T and Y dwarfs shown in the figures, are listed in Table 8 for each half spectral type from T0 to Y0. In the subsections below we discuss each index in detail.

4.5.1. Primary Indices from Burgasser et al. (2006)

The primary classification indices for T dwarfs were designed by Burgasser et al. (2002) and Geballe et al. (2002), and then revised by Burgasser et al. (2006). We modify these as

follows to incorporate median fluxes:

$$\mathrm{H_2O-J} = \frac{\widetilde{F}_{1.140-1.165\mu m}}{\widetilde{F}_{1.260-1.285\mu m}} \tag{3}$$

$$\mathrm{CH_4-J} = \frac{\widetilde{F}_{1.315-1.340\mu m}}{\widetilde{F}_{1.260-1.285\mu m}} \tag{4}$$

$$\mathrm{H_2O-H} = \frac{\widetilde{F}_{1.480-1.520\mu m}}{\widetilde{F}_{1.560-1.600\mu m}} \tag{5}$$

$$\mathrm{CH_4-H} = \frac{\widetilde{F}_{1.635-1.675\mu m}}{\widetilde{F}_{1.560-1.600\mu m}}. \tag{6}$$

These indices each show a general trend of having a maximum value at the earliest T spectral type and a steady decrease at later spectral types. However, by the end of the T sequence theses indices have saturated and are less useful for classification. For Y dwarfs, these indices have highly uncertain and spurious values since the numerator in each case has essentially no flux and is dominated by background noise.

4.5.2. W_J and NH_3-H Indices for Late-type T Dwarfs

The W_J index was defined by Warren et al. (2007) to characterize the J band width. The original integrated flux definition required that the denominator be multiplied by a factor of two in order to compensate for the larger width numerator. When modified to use the median flux, the index becomes,

$$\mathrm{W}_J = \frac{\widetilde{F}_{1.180-1.230\mu m}}{\widetilde{F}_{1.260-1.285\mu m}}, \tag{7}$$

and it is no longer necessary to keep this factor in the denominator. We have chosen to remove it in our analysis. This produces index values between 0.0 and 0.9, which is consistent with the integrated flux results in the literature. The flux from 1.180-1.230 μm gradually and consistently decreases with spectral type, producing unique index values all the way to the T/Y boundary, as seen by Cushing et al. (2011).

Delorme et al. (2008) defined the $\mathrm{NH_3-H}$ index to probe the blue wing of the H band in later T dwarfs. We modify this index to incorporate median fluxes,

$$\mathrm{NH_3-H} = \frac{\widetilde{F}_{1.530-1.560\mu m}}{\widetilde{F}_{1.570-1.600\mu m}}. \tag{8}$$

This index is not useful at identifying T dwarfs earlier than T7, but has a large dynamic range for for the latest T dwarfs and the Y0s. Cushing et al. (2011) identified the break in the NH_3-H index at Y0, suggesting that near infrared NH_3 absorption begins at the T/Y boundary. This break is still clearly identified in our median flux index.

4.5.3. Y/J Ratio

The Y/J index was defined by Burgasser et al. (2006) as a possible tracer of variations in metallicity. We modify this index to incorporate median fluxes,

$$Y/J = \frac{\widetilde{F}_{1.005-1.045\mu m}}{\widetilde{F}_{1.250-1.290\mu m}}. \tag{9}$$

The Y-band spectra that we have acquired are from the low-resolution, multi-band spectrographs IRTF/SpeX, Palomar/TripleSpec, Magellan/FIRE, and Gemini/GNIRS. From lower resolution spectra we derive indices with larger uncertainties. This index shows significant scatter compared to the H/J and K/J ratios and the spectral standards produce a trend with redder Y/J flux ratios relative to the rest of the population. The dispersion in this index is smallest for T4's and later objects show the largest scatter.

4.5.4. H/J Ratio

Burgasser et al. (2002) defined a broader version of the H/J index that encompasses most of the T dwarf flux contributing to the broadband $J - H$ color, and noted a possible reversal at later types. It is not one of the indices revised in Burgasser et al. (2006) and so we have constructed the H/J index, presented in Equation 1, employing the wavelengths used by Burgasser et al. (2006) to define other indices. This index shows a tight trend with an average dispersion of 0.1 and shows a similar reversal as the 2MASS $J-H$ colors in Figure 4. As discussed in §3.1, the turnaround of the $J - H$ color is evident before the T/Y boundary, and appears to occur around T6±1 for the H/J index. However, Y dwarfs show a significant scatter in H/J. The Y0s break the trend of the T dwarfs, and the H/J index drops, possibly due to the onset of NH_3 absorption. WISE J182831.08+265037.8 has been typed as $\geq$ Y2 (Kirkpatrick et al. 2012) based on the near-equal heights of the J- and H-band flux peaks and has an index value equivalent to the earliest T dwarfs. This dichotomy of H/J flux ratios hints at drastically different atmospheric conditions for Y0s and later type Y dwarfs.

4.5.5. K/J Ratio

The wavelengths used for the K/J ratio were initially defined by Burgasser et al. (2002) to compare the K-band flux peak to the J-band flux peak, and modified here to incorporate median fluxes,

$$\mathrm{K/J} = \frac{\widetilde{F}_{2.060-2.100\mu m}}{\widetilde{F}_{1.250-1.290\mu m}}. \tag{10}$$

Models have long predicted dominant H_2 CIA of the K-band flux in cool brown dwarf atmospheres, (Saumon et al. 1994, 2012; Marley et al. 1996; Allard et al. 1996) which has been observationally verified and is evident in Figure 22. The large dispersion in the late-type T K/J index was pointed out by Burgasser et al. (2006) and we find that the dispersion is smallest at T4 and flares at both earlier and later types. Although the early-type T dwarf standards fall near the mean of each spectral bin, the late-type T spectral standards are on the redder side of the mean. Figure 23 shows the K/J indices for T dwarfs, sorted by instrument. We find that the average K/J index for the T5-T9 spectral standards is 0.147 ± 0.013 and only $\sim11\%$ (18 out of 170; 8 WISE discoveries and 10 from the SpeX Prism Library) are redder than the 3σ upper limit. However, 47 of the 126 WISE-discovered and 7 of the 44 SpeX Prism Library late-type T dwarfs are below the 3σ lower limit (shown in Figure 23). In total 54 out of 170, *approximately one third*, of the T5 or later dwarfs are blue relative to the standards.

The largest dispersion (~1.5 mags) in the K/J ratio is in the T7-T8 spectral bins, in which the number of known T dwarfs has been quintupled by WISE. The T dwarf sample prior to WISE peaked at T5 (Kirkpatrick et al. 2011, Figure 28), and WISE discoveries shift this peak to T6, with the number of T8's nearly as bountiful. Figure 23 shows that, although the spectral standards all have similar K/J ratios, the value of the index for late-type T dwarfs gradually decreases at later types. The small number of late-type T dwarfs in the SpeX Prism Library, and the steady decrease in the K/J index with spectral type, results in a smaller fraction of blue T dwarfs from the SpeX Prism Library ($\sim16\%$) relative to the WISE discoveries ($\sim37\%$).

Although $\sim32\%$ of the late-type T dwarfs are blue (K band suppressed) and $\sim11\%$ are red, the current spectral standards still provide the best overall match to the bulk of observed spectra. The spectral standards match the mean H/J indices very well. It is possible that the standards, which were chosen to be bright in order to be easily observed, are also younger. If younger than the mean of the sample, the standards would generally be more luminous for their effective temperature (larger), have a lower surface gravity (reduced collision induced absorption), and be metal-rich. All of these factors would result in the redder colors seen in the K/J index and bluer Y/J index values. Objects with blue or red

K/J index values, relative to the J band normalized standards, are most commonly called peculiar in the literature. Because this is fairly common in our sample, the objects we classify as peculiar deviate from the standards in more than one band.

4.5.6. J-narrow Index

The J-narrow index is defined in Equation 2 and also presented in Kirkpatrick et al. (2012). This index was derived empirically from the spectra presented in this paper in order to produce a useful index for classifying Y dwarfs using a spectral index. As discussed above, many of the indices derived for T dwarfs have saturated before the T/Y boundary and are no longer useful for Y dwarfs. The KI doublet at 1.243 and 1.254 μm is a feature present in M though T dwarfs down to mid-type T. The numerator in this index encloses the red member of the J-band neutral potassium doublet and the denominator captures the J-band flux peak. Variations in the KI feature are what produce the dispersion and undulation seen in Figure 24 for the T dwarf sequence. Most of our spectra are lower resolution IRTF/SpeX and Palomar/TSpec spectra and the KI 1.254μm line is barely resolved. In these data, there is no significant difference in the J-narrow index when using the median or the integrated flux. In higher resolution spectra the integrated flux produces slightly lower index values than the median method while increasing the dispersion in each spectral bin by including more spectral variation. To minimize this variability we use the median flux to derive this index. McLean et al. (2003, Figure 15) shows how the KI lines broaden towards later spectral types, before also decreasing in strength around T6 (McLean et al. 2007). It is this broadening that causes the J-narrow index to decrease from T0-T6, and the disappearance of the line in late-type T dwarfs that causes the slight increase in the index before falling for the Y dwarfs as a result of the narrowing J-band flux peak.

As discussed in Kirkpatrick et al. (2012), because our by-eye classification of Y dwarfs requires that the J-band peak be narrower than the Y0 standard, WISE J173835.52+273258.9, all the other Y0s have smaller J-narrow indices. Also, this index is only useful for distinguishing very early-type Y dwarfs from late-type T dwarfs since it does not appear to work well for WISE J1828+2650, which is either much later in type or spectroscopically peculiar. Future use of the J-narrow index for higher-resolution spectra may provide a means of sorting each spectral bin by surface gravity by employing the KI feature (McLean et al. 2003), a pursuit that may be aided by computing the index using the integrated flux.

5. Clouds and Metallicity at the T/Y Boundary

Burrows et al. (2006) developed a set of brown dwarf models that combined cloudy and cloudless models to reproduce the observed $J - K$ colors of L and T dwarfs, respectively. Similar synthetic colors were derived by Saumon & Marley (2008) that matched the overall brown dwarf sequence. Both models failed to match the late-type T dwarf dispersion, which they could modulate through variations in metallicity and binarity (see Figure 15 in Saumon & Marley 2008). Burgasser et al. (2011) utilized the Saumon & Marley (2008) models to determine the best fit parameters for their five WISE-discovered T dwarfs and found that cloudy, low surface gravity models provided the best match to observed spectra.

The addition of sulfide clouds to the brown dwarf models by Morley et al. (2012) reproduces the dispersion of the late-type T dwarf photometry. The flux reversal we see in the $J - H$ color (and the H/J index) around T7 corresponds to the turn-off of the late-type T dwarfs from the cloudless models of Morley et al. (2012). Based on this turn-off, the spectral sequence beyond T7 (Teff ≤800K) is possibly dominated by cloudy atmospheres that have redder H/J and K/J indices. This includes the T dwarf spectral standards and the Y dwarfs later than Y0. The bluest H/J and K/J indices continue the trend of the early-type T dwarfs and are still consistent with cloudless atmospheres. The Y0s in this case stand-out in the H/J index as breaking the trend, and may be less cloudy than the later Y dwarfs. Thus, the spectral sequence of the late-type T dwarfs and the early-type Y dwarfs may no longer be correlated directly to temperature, but also to the atmospheric conditions.

The top panel of Figure 25 shows the objects that we have computed indices for, sorted by spectral type. Early-type T dwarfs are uniquely identified by their K/J index, while late-type T dwarfs have a larger Y/J dispersion. The T5-T9 spectral standards all have similar index values, and the T8 dwarfs show the largest spread in index values.

The middle panel in Figure 25 depicts the index values for the Morley et al. (2012) sulfide cloud models with solar metallicity, and various gravity and condensate sedimentation efficiencies (f_{sed}), between 400K and 1300K. These models do not include silicate clouds, and so they do not replicate the early-type T dwarfs. The cloudless models predict a range of Y/J index values for the coolest objects when gravity is varied, but relatively little difference for most T dwarfs. Both the Y and J bands are impacted by the alkali opacity and small variations to the broadening produces large changes in the Y/J index, so our interpretation here is limited. For f_{sed}=5, the models predict a slight increase in both the Y/J and K/J indices before they both decrease, and this matches our measured index values. However, for f_{sed}=4 only the log g=4.5 model remains consistent with our measurements. Smaller f_{sed} values have Y/J ≤ 0.5 and large K/J values that are inconsistent with our measurements.

In the bottom panel of Figure 25 we show the index values for the cloudy (Case E) and cloudless models presented in Burrows et al. (2006), for log g=5.0, T_{eff}s from 800K to 1700K, and various metallicities. The highest temperature is marked with a square and the lowest temperature is marked with a circle in the figure. Here we see that the K/J index produced for the cloudless models, for a specific temperature, do not match the early-type T dwarfs. This figure shows that the cloudy models trace the early-type T dwarfs well and identifies a similar cloudy late-type T population as the Morley et al. (2012) models. Although both the cloudy and cloudless -0.5 dex tracks enclose the increasing Y/J index values, the cloudless sub-solar metallicity model best matches our measurements.

Overall, the T dwarf spectral standards occupy a minimum in the Y/J index for the bulk of the late-type T dwarfs. Objects with Y/J indices below the spectral standards are best matched to cloudy models and possibly oversolar metallicities. Objects with a Y/J index greater than the standards are best matched to cloudless models and sub-solar metallicities. The K/J index can be modulated by temperature, metallically, and surface gravity (Leggett et al. 2007). However, objects with the lowest K/J values, also have the highest Y/J indices, which is consistent with many K band suppressed late-type T dwarfs that are best matched to low-metallicity models.

6. Interlopers in WISE Color Space

Some of the brown dwarf candidates survived the photometric selection process but were spectroscopically identified as contaminants in our sample. In cases where the acquired spectrum did not match a brown dwarf, we saved images at the telescope to later verify pointing. In the few cases where pointing was questioned, the candidate was added back to the candidate list and the observations were attempted again. If pointing was confirmed, and the observed flux was not that of a brown dwarf, we logged the object as an interloper.

WISE All-Sky photometry for the interlopers is listed in Table 9. Figure 3 shows where these sources encroach on the WISE $W1 - W2$ versus $W2 - W3$ color space of T and Y dwarfs. Although many are located on the periphery, some look like legitimate brown dwarf candidates because they fall squarely in the brown dwarf color-color space. Interlopers that were observed with *Spitzer* are logged in Table 10 and shown in Figure 8. Only a few of the interlopers are distinguishable from brown dwarfs in this figure.

Spectroscopic observations are listed in Table 11 along with descriptions of the spectra. In most cases we observe faint near-IR continuum and no discernible spectral features. However, some objects are unique and we discuss those sources in the following subsections.

6.1. Young Stellar Objects

Two of the interlopers, WISE J0421+3721 and WISE J0546+2639, were selected from candidates in our L-dwarf color selection process ($W1 - W2 > 0.4$ mag and no association with a 2MASS source). Both objects are missing from the 2MASS All-Sky PSC, but are listed in the 2MASS Survey Point Source Reject Table. WISE J0421+3721 has 2MASS magnitudes J=17.0±0.2, H=15.0±0.1, and K_s=14.1±0.1 mag. WISE J0546+2639 is flagged as an artifact contaminated source with J=15.88±0.07, H=14.50±0.06, K_s=13.26±0.03 mag. These two sources have very similar near-IR colors, and consistent $W1 - W2$ colors. The IRTF/SpeX spectra of these sources are shown in Figure 26 with prominent spectral features marked.

We identify these sources as YSOs based on comparisons to the survey of 110 young stellar objects (YSOs) by Connelley & Greene (2010). We find that a few of their YSO spectra have similar morphologies to our newly identified YSOs in that they that lack emission features, peak around 1.8μm, and show weak H and CO absorption features. The best spectral match Elias 2-25 (16:26:34.167 −24:23:28.26 J2000) is a T Tauri star with similar near-IR colors to the new YSOs ($J - H$=1.598, $H - K_s$=0.943, and $J - K_s$=2.542). The other T Tauri objects from Connelley & Greene (2010) with similar colors and spectral morphologies are V806 Tau, FS Tau A, and LZK 12.

Employing the α spectral index, defined as the slope of $\log(\lambda F_\lambda)$ versus $\log(\lambda)$ (Lada 1987), over the WISE passbands we find α=-1.63 and -1.42 for WISE J0421+3721 and WISE J0546+2639, respectively. Inclusion of the K_s and $W3$ magnitudes for WISE J0421+3721 produces α=-1.45. These values are consistent with evolved T Tauri stars, between Class II and Class III, in the proximity of Taurus-Auriga.

6.2. Active Galactic Nuclei

Although many of the interlopers show faint continuum flux, two of them show spectral features indicative of AGN. WISE J1530−2617 and WISE J1754+3233 have *Spitzer* and WISE colors consistent with reddened extragalactic sources (Wright et al. 2010; Eisenhardt et al. 2012; Stern et al. 2012).

Figure 27 shows the Keck/NIRSPEC J-band spectrum of WISE J1530−2617. We identify Hα, [NII]λ6583, and broad [SII]$\lambda\lambda$6716, 6731 at 1.3136, 1.3158 and 1.3313, 1.3334 μm, respectively. This produces a redshift z=1.00 and line flux ratio N[II]/Hα = 1.314, which is typical for an AGN (Veilleux & Osterbrock 1987). Also, $W1 - W2$=3.89±0.50 for this source, which is even redder than the $W1W2$-dropouts shown in Figure 1 of Eisenhardt et al.

(2012).

The HST/WFC3 spectrum of WISE J1754+3233 is shown in Figure 28. We determine that z=1.92 for Hβ and [O III]$\lambda\lambda$4959, 5007 at 1.4192, 1.4471 and 1.4611μm, respectively. Although [O III]λ5007/H$\beta = 1.129$ is not unique to AGN, its WISE colors identify it as an AGN (Wright et al. 2010). This object is one that was initially identified as a candidate in the Preliminary Data Release, but its updated All-Sky Data Release photometry moved it outside our selection criteria (see Figure 3).

7. Conclusions

We present the spectra of $\sim$100 T dwarfs uncovered with the Wide-field Infrared Survey Explorer (WISE). Spectral types were derived by visual comparison to spectral standards, and modified median-flux spectral indices were computed for WISE brown dwarf discoveries. We also define the J-narrow index to help better identify future early-type Y dwarf discoveries. Along with the 89 T dwarfs reported by Kirkpatrick et al. (2011), our follow-up triples the number of known brown dwarfs with spectral types later than T5.

Using the classification schemes in the literature, we identify three extremely red brown dwarfs that can not easily be classified as L or T type. These objects display Y- and J-band spectral morphologies most similar to T dwarfs, have red $J - K$ colors, and lack distinct CH$_4$ absorption features. Although gravity, metallicity, and temperature variations can all contribute to the reddening in these objects, variability seen in WISE J1738+6242 hints at rapid (on the order of a year) atmospheric changes. Perhaps the discrepant features we see in these extremely red objects are due to an unresolved redL + T binary. If the T dwarf component of this system constrains other physical parameters, such as the age or metallicity of the system, this would shed light on the underlying cause of the red L dwarf phenomenon. Alternatively, these objects may bridge the L dwarf sequence to the HR 8799 planets and provide a greater understanding of both with further investigation.

Along with the spectral indices, we derive the Y/J, H/J and K/J peak flux ratios for $\sim$320 T and Y dwarfs. The H/J ratio traces the $J - H$ color and shows a reversal around T7. The Y0s stand-out in the H/J index as breaking the trend, and may be less cloudy than the later Y dwarfs. Thus, the spectral sequence of the late-type T dwarfs and the early-type Y dwarfs may no longer be correlated directly to temperature, but also to other atmospheric conditions like cloud fraction, metallicity, grain size, and surface gravity. The K/J index shows a large dispersion of $\sim$1.5 mag, which can be matched by the sulfide cloud models presented by Morley et al. (2012) and not by previous cloudless models used for

late-type T dwarfs. We find that although most late-type T dwarfs match the J- and H-band morphology of the spectral standards, one-third show significantly suppressed K-band flux relative to the standards (smaller K/J values), which implies higher surface gravities, cloudless atmospheres, and/or low metallicities. Comparison to atmospheric models reveals that the small Y/J peak flux ratios of late-type T dwarfs are best matched to cloudy models and/or oversolar metallicities. Objects with a Y/J index greater than the standards are best matched to cloudless models and/or sub-solar metallicities. However, we can not disentangle the physical parameters modulating T dwarf colors until model grids are extended to include various cloud species at lower temperatures and non-solar metallicities.

8. Acknowledgments

Appendix A: Integrated Flux Indices for WISE Discovered Brown Dwarfs

Spectral indices from the literature are defined as integrated flux ratios such that,

$$\text{integrated flux index} = \int F_{\lambda_1 - \lambda_2} \, d\lambda \, / \, \int F_{\lambda_3 - \lambda_4} \, d\lambda,$$

where the numerator, integrated between $\lambda_1 - \lambda_2$, covers a specified absorption region and the denominator, integrated between $\lambda_3 - \lambda_4$, includes the corresponding peak flux. This results in index values generally less than unity and greater than zero. In this paper we redefine the spectral indices using the median flux ratios which when defined as,

$$\text{median flux index} = \widetilde{F}_{\lambda_1 - \lambda_2} \, / \, \widetilde{F}_{\lambda_3 - \lambda_4},$$

for the same wavelengths produce consistent index values with the integrated flux method, but decreased dispersion per spectral type bin.

For each of the WISE discovered brown dwarfs listed in Table 7 we first derived the integrated flux ratios from Burgasser et al. (2006), Warren et al. (2007), and Delorme et al. (2008). These are listed in Table A1. Indices were derived as described in §4.5, using a Monte Carlo method with 1000 realizations of the spectrum. Figure A1 shows the median flux and integrated flux indices plotted as a function of spectral type, like Figure 21, but color coded by spectrograph. The Y/J, H/J, and K/J flux ratios computed using the median flux and integrated flux methods are shown in Figure A2, also color coded by spectrograph.

The integrated flux indices show a clear instrumental bias, where the indices from IRTF/SpeX spectra sit distinctly above the others. This offset is the result of differences in spectral resolution between instruments, and between near-infrared bands for the same instrument. To properly compare integrated flux spectral indices between instruments we would first need to interpolate the spectra onto similar wavelength scales. Even for the same instrument, changes in the resolution as a function of wavelength would need to be removed by interpolation. Using the median flux, rather than the integrated flux, sidesteps this issue and reduces the likelihood of errors when comparing spectra from numerous instruments, like we have done here. Another, less significant, source of this offset is a negative noise bias of all non-IRTF/SpeX spectra reduced with Spextool. This is clearly seen in Figure 18, where the scatter in the per pixel flux is more often below the mean. This bias in the reduced spectrum results in smaller integrated fluxes and consequently, smaller index values. Employing the *median* flux instead of the integrated flux reduces data reduction and instrumental influences on the computed indices.

REFERENCES

Abel, M., Frommhold, L., Li, X., & Hunt, K. L. C. 2012, J. Chem. Phys., 136, 044319

Aberasturi, M., Solano, E., & Martín, E. L. 2011, A&A, 534, L7

Allard, F., Hauschildt, P. H., Baraffe, I., & Chabrier, G. 1996, ApJ, 465, L123

Allen, P. R., Koerner, D. W., Reid, I. N., & Trilling, D. E. 2005, ApJ, 625, 385

Allers, K. N., Liu, M. C., Dupuy, T. J., & Cushing, M. C. 2010, ApJ, 715, 561

Andrei, A. H., Smart, R. L., Penna, J. L., et al. 2011, AJ, 141, 54

Autry, R. G., Probst, R. G., Starr, B. M., et al. 2003, Proc. SPIE, 4841, 525

Baraffe, I., Chabrier, G., Allard, F., & Hauschildt, P. 2003, Brown Dwarfs, 211, 41

Barman, T. S., Macintosh, B., Konopacky, Q. M., & Marois, C. 2011, ApJ, 735, L39

Barman, T. S., Macintosh, B., Konopacky, Q. M., & Marois, C. 2011, ApJ, 733, 65

Beichman, C. A., Gelino, C. R., Kirkpatrick, J. D., et al. 2013, arXiv:1301.1669

Bloom, J. S., Starr, D. L., Blake, C. H., Skrutskie, M. F., & Falco, E. E. 2006, Astronomical Data Analysis Software and Systems XV, 351, 751

Bochanski, J. J., Burgasser, A. J., Simcoe, R. A., & West, A. A. 2011, AJ, 142, 169

Borysow, A., Jorgensen, U. G., & Zheng, C. 1997, A&A, 324, 185

Bowler, B. P., Liu, M. C., Dupuy, T. J., & Cushing, M. C. 2010, ApJ, 723, 850

Burgasser, A. J., Cushing, M. C., Kirkpatrick, J. D., et al. 2011, ApJ, 735, 116

Burgasser, A. J., Cruz, K. L., Cushing, M., et al. 2010, ApJ, 710, 1142

Burgasser, A. J., Geballe, T. R., Leggett, S. K., Kirkpatrick, J. D., & Golimowski, D. A. 2006, ApJ, 637, 1067

Burgasser, A. J., Burrows, A., & Kirkpatrick, J. D. 2006, ApJ, 639, 1095

Burgasser, A. J. 2004, ApJS, 155, 191

Burgasser, A. J., McElwain, M. W., Kirkpatrick, J. D., Cruz, K. L., Tinney, C. G., & Reid, I. N. 2004, AJ, 127, 2856

Burgasser, A. J., Kirkpatrick, J. D., Brown, M. E., et al. 2002, ApJ, 564, 421

Burrows, A., Sudarsky, D., & Hubeny, I. 2006, ApJ, 640, 1063

Burrows, A., Sudarsky, D., & Lunine, J. I. 2003, ApJ, 596, 587

Burrows, A., Marley, M., Hubbard, W. B., et al. 1997, ApJ, 491, 856

Casali, M., Adamson, A., Alves de Oliveira, C., et al. 2007, A&A, 467, 777

Chiu, K., Fan, X., Leggett, S. K., et al. 2006, AJ, 131, 2722

Connelley, M. S., & Greene, T. P. 2010, AJ, 140, 1214

Cushing, M. C., Kirkpatrick, J. D., Gelino, C. R., et al. 2011, ApJ, 743, 50

Cushing, M. C., Marley, M. S., Saumon, D., et al. 2008, ApJ, 678, 1372

Cushing, M. C., Vacca, W. D., & Rayner, J. T. 2004, PASP, 116, 362

Cutri, R. M., & et al. 2012, VizieR Online Data Catalog, 2311, 0

Dahn, C. C., Harris, H. C., Vrba, F. J., et al. 2002, AJ, 124, 1170

Deacon, N. R., Liu, M. C., Magnier, E. A., et al. 2012, ApJ, 757, 100

Deacon, N. R., Liu, M. C., Magnier, E. A., et al. 2011, AJ, 142, 77

Delorme, P., Willott, C. J., Forveille, T., et al. 2008, A&A, 484, 469

Delorme, P., Delfosse, X., Albert, L., et al. 2008, A&A, 482, 961

Depoy, D. L., Atwood, B., Byard, P. L., Frogel, J., & O'Brien, T. P. 1993, Proc. SPIE, 1946, 667

Eisenhardt, P. R. M., Wu, J., Tsai, C.-W., et al. 2012, ApJ, 755, 173

Elias, J. H., Joyce, R. R., Liang, M., et al. 2006, Proc. SPIE, 6269,

Faherty, J. K., Rice, E. L., Cruz, K. L., Mamajek, E. E., & Núñez, A. 2013, AJ, 145, 2

Fazio, G. G., Ashby, M. L. N., Barmby, P., et al. 2004, ApJS, 154, 39

Frommhold, L., Abel, M., Wang, F., et al. 2010, Molecular Physics, 108, 2265

Geballe, T. R., Knapp, G. R., Leggett, S. K., et al. 2002, ApJ, 564, 466

Geballe, T. R., Kulkarni, S. R., Woodward, C. E., & Sloan, G. C. 1996, ApJ, 467, L101

Gelino, C. R., Kirkpatrick, J. D., Cushing, M. C., et al. 2011, AJ, 142, 57

Gizis, J. E., Faherty, J. K., Liu, M. C., et al. 2012, AJ, 144, 94

Griffith, R. L., Kirkpatrick, J. D., Eisenhardt, P. R. M., et al. 2012, AJ, 144, 148

Hambly, N. C., Collins, R. S., Cross, N. J. G., et al. 2008, MNRAS, 384, 637

Hayashi, C., & Nakano, T. 1963, Progress of Theoretical Physics, 30, 460

Herter, T. L., Henderson, C. P., Wilson, J. C., et al. 2008, Proc. SPIE, 7014,

Hewett, P. C., Warren, S. J., Leggett, S. K., & Hodgkin, S. T. 2006, MNRAS, 367, 454

Hodgkin, S. T., Irwin, M. J., Hewett, P. C., & Warren, S. J. 2009, MNRAS, 394, 675

Kimble, R. A., MacKenty, J. W., O'Connell, R. W., & Townsend, J. A. 2008, Proc. SPIE, 7010,

Kirkpatrick, J. D., Gelino, C. R., Cushing, M. C., et al. 2012, ApJ, 753, 156

Kirkpatrick, J. D., Cushing, M. C., Gelino, C. R., et al. 2011, ApJS, 197, 19

Kirkpatrick, J. D., Looper, D. L., Burgasser, A. J., et al. 2010, ApJS, 190, 100

Kirkpatrick, J. D., Barman, T. S., Burgasser, A. J., et al. 2006, ApJ, 639, 1120

Kumar, S. S. 1963, ApJ, 137, 1121

Lada, C. J. 1987, Star Forming Regions, 115, 1

Lawrence, A., Warren, S. J., Almaini, O., et al. 2007, MNRAS, 379, 1599

Leggett, S. K., Saumon, D., Marley, M. S., et al. 2012, ApJ, 748, 74

Leggett, S. K., Marley, M. S., Freedman, R., et al. 2007, ApJ, 667, 537

Linsky, J. L. 1969, ApJ, 156, 989

Lodieu, N., Burningham, B., Day-Jones, A., et al. 2012, A&A, 548, A53

Looper, D. L., Kirkpatrick, J. D., Cutri, R. M., et al. 2008, ApJ, 686, 528

Lucas, P. W., Tinney, C. G., Burningham, B., et al. 2010, MNRAS, 408, L56

Luhman, K. L., Loutrel, N. P., McCurdy, N. S., et al. 2012, ApJ, 760, 152

Mainzer, A., Cushing, M. C., Skrutskie, M., et al. 2011, ApJ, 726, 30

Marley, M. S., Saumon, D., Cushing, M., et al. 2012, ApJ, 754, 135

Marley, M. S., Saumon, D., Guillot, T., et al. 1996, Science, 272, 1919

Marsh, K. A., Wright, E. L., Kirkpatrick, J. D., et al. 2013, ApJ, 762, 119

Martini, P., Persson, S. E., Murphy, D. C., et al. 2004, Proc. SPIE, 5492, 1653

McLean, I. S., Prato, L., McGovern, M. R., et al. 2007, ApJ, 658, 1217

McLean, I. S., McGovern, M. R., Burgasser, A. J., Kirkpatrick, J. D., Prato, L., & Kim, S. S. 2003, ApJ, 596, 561

McLean, I. S., Graham, J. R., Becklin, E. E., Figer, D. F., Larkin, J. E., Levenson, N. A., & Teplitz, H. I. 2000, Proc. SPIE, 4008, 1048

McLean, I. S., Becklin, E. E., Bendiksen, O., et al. 1998, Proc. SPIE, 3354, 566

Monet, D. G., Levine, S. E., Canzian, B., et al. 2003, AJ, 125, 984

Morley, C. V., Fortney, J. J., Marley, M. S., et al. 2012, ApJ, 756, 172

Nakajima, T., Oppenheimer, B. R., Kulkarni, S. R., et al. 1995, Nature, 378, 463

Noll, K. S., Geballe, T. R., Leggett, S. K., & Marley, M. S. 2000, ApJ, 541, L75

Patience, J., King, R. R., de Rosa, R. J., & Marois, C. 2010, A&A, 517, A76

Pinfield, D. J., Burningham, B., Lodieu, N., et al. 2012, MNRAS, 422, 1922

Rayner, J. T., Toomey, D. W., Onaka, P. M., et al. 2003, PASP, 115, 362

Saumon, D., Marley, M. S., Abel, M., Frommhold, L., & Freedman, R. S. 2012, ApJ, 750, 74

Saumon, D., & Marley, M. S. 2008, ApJ, 689, 1327

Saumon, D., Marley, M. S., & Lodders, K. 2003, arXiv:astro-ph/0310805

Saumon, D., Bergeron, P., Lunine, J. I., Hubbard, W. B., & Burrows, A. 1994, ApJ, 424, 333

Scholz, R.-D., Bihain, G., Schnurr, O., & Storm, J. 2011, A&A, 532, L5

Scholz, R.-D. 2010, A&A, 515, A92

Simcoe, R. A., Burgasser, A. J., Bochanski, J. J., et al. 2010, Proc. SPIE, 7735,

Simcoe, R. A., Burgasser, A. J., Bernstein, R. A., et al. 2008, Proc. SPIE, 7014,

Simons, D. A., & Tokunaga, A. 2002, PASP, 114, 169

Skrutskie, M. F., Cutri, R. M., Stiening, R., et al. 2006, AJ, 131, 1163

Stephens, D. C., Leggett, S. K., Cushing, M. C., et al. 2009, ApJ, 702, 154

Stern, D., Assef, R. J., Benford, D. J., et al. 2012, ApJ, 753, 30

Tinney, C. G., Burgasser, A. J., Kirkpatrick, J. D., & McElwain, M. W. 2005, AJ, 130, 2326

Tokunaga, A. T., Simons, D. A., & Vacca, W. D. 2002, PASP, 114, 180

Vacca, W. D., Cushing, M. C., & Rayner, J. T. 2003, PASP, 115, 389

van Dam, M. A., Bouchez, A. H., Le Mignant, D., et al. 2006, PASP, 118, 310

Veilleux, S., & Osterbrock, D. E. 1987, ApJS, 63, 295

Warren, S. J., Mortlock, D. J., Leggett, S. K., et al. 2007, MNRAS, 381, 1400

Werner, M. W., Roellig, T. L., Low, F. J., et al. 2004, ApJS, 154, 1

Wilson, J. C., Eikenberry, S. S., Henderson, C. P., et al. 2003, Proc. SPIE, 4841, 451

Wizinowich, P. L., Le Mignant, D., Bouchez, A. H., et al. 2006, PASP, 118, 297

Wright, E. L., Eisenhardt, P. R. M., Mainzer, A. K., et al. 2010, AJ, 140, 1868

York, D. G., Adelman, J., Anderson, J. E., Jr., et al. 2000, AJ, 120, 1579

Table 1. Updated WISE All-Sky Photometry for Discoveries from Kirkpatrick et al. (2011)

Object Name (1)	NIR Sp. Type (2)	$W1$ (mag) (3)	$W2$ (mag) (4)	$W3$ (mag) (5)	$W4$ (mag) (6)	$W1 - W2$ (mag) (7)	$W2 - W3$ (mag) (8)
WISE J000849.75−173922.9	T6	16.41 ± 0.09	14.56 ± 0.07	> 12.15	> 8.49	1.86 ± 0.12	< 2.40
WISE J003119.76−384036.1	L2 pec (blue)	12.40 ± 0.03	12.01 ± 0.02	11.56 ± 0.17	> 8.76	0.39 ± 0.04	0.45 ± 0.17
WISE J004928.48+044059.9	L9	13.45 ± 0.03	12.97 ± 0.03	12.01 ± 0.29	8.39 ± 0.27	0.48 ± 0.04	0.96 ± 0.29
WISE J010637.07+151852.8	M8 pec	13.08 ± 0.03	12.73 ± 0.03	12.49 ± 0.37	> 8.81	0.35 ± 0.04	0.24 ± 0.38
WISE J012333.23+414203.8	T7	17.04 ± 0.11	15.03 ± 0.07	12.99 ± 0.45	> 9.20	2.01 ± 0.14	2.03 ± 0.46
WISE J013836.58−032221.2	T3	14.43 ± 0.03	13.40 ± 0.03	12.35 ± 0.35	> 9.30	1.03 ± 0.05	1.05 ± 0.35
WISE J014807.25−720258.7	T9.5	> 18.94	14.69 ± 0.05	> 12.86	> 9.52	> 4.25	< 1.83
WISE J015010.89+382724.1	T0	13.65 ± 0.03	12.98 ± 0.03	11.74 ± 0.19	> 9.04	0.67 ± 0.04	1.24 ± 0.20
WISE J020625.27+264023.6	L9 pec (red)	13.40 ± 0.03	12.82 ± 0.03	11.33 ± 0.22	> 8.88	0.59 ± 0.04	1.49 ± 0.22
WISE J022105.97+384203.2	T6.5	16.87 ± 0.15	14.70 ± 0.08	> 12.69	> 9.24	2.18 ± 0.17	< 2.00
WISE J022322.36−293257.2	T7/7.5	17.16 ± 0.12	14.02 ± 0.04	12.64 ± 0.32	> 9.64	3.13 ± 0.13	1.39 ± 0.32
WISE J022623.98−021142.8	T7	17.60 ± 0.19	14.59 ± 0.06	> 12.86	> 9.18	3.01 ± 0.20	< 1.74
WISE J025409.51+022358.6	T8	15.76 ± 0.05	12.74 ± 0.03	11.49 ± 0.14	> 9.44	3.02 ± 0.06	1.25 ± 0.14
WISE J030533.51+395434.6	T6	17.38 ± 0.24	14.69 ± 0.07	> 12.64	> 9.12	2.69 ± 0.25	< 2.05
WISE J030724.59+290447.4	T6.5	17.22 ± 0.21	14.99 ± 0.11	> 12.39	> 8.74	2.23 ± 0.24	< 2.60
WISE J031325.94+780744.3	T8.5	15.88 ± 0.06	13.19 ± 0.03	11.32 ± 0.12	9.00 ± 0.37	2.69 ± 0.07	1.87 ± 0.12
WISE J032337.53−602554.5	T8.5	18.10 ± 0.32	14.50 ± 0.05	> 12.73	> 9.18	3.61 ± 0.33	< 1.76
WISE J033349.34−585618.1	T3	13.99 ± 0.03	13.25 ± 0.03	12.30 ± 0.21	> 9.20	0.75 ± 0.04	0.95 ± 0.22
WISE J041022.71+150248.4	Y0	> 18.33	14.18 ± 0.06	> 11.86	> 8.90	> 4.15	< 2.32
WISE J041054.48+141131.1	T6	17.02 ± 0.16	15.08 ± 0.10	> 12.10	> 9.01	1.95 ± 0.19	< 2.98
WISE J044853.28−193548.6	T5 pec	16.52 ± 0.09	14.30 ± 0.05	> 12.49	> 9.17	2.22 ± 0.10	< 1.81
WISE J045853.89+643452.5	T8.5	16.67 ± 0.11	13.03 ± 0.03	12.60 ± 0.41	> 9.28	3.64 ± 0.12	0.43 ± 0.41
WISE J050003.04−122343.2	T8	17.66 ± 0.24	13.94 ± 0.04	11.56 ± 0.15	8.99 ± 0.36	3.72 ± 0.25	2.38 ± 0.15
WISE J051317.27+060814.7	T6.5	15.82 ± 0.07	13.86 ± 0.05	> 12.40	> 9.10	1.97 ± 0.08	< 1.46
WISE J052536.35+673952.6	T6 pec	> 17.98	15.04 ± 0.09	> 12.81	> 9.20	> 2.94	< 2.23
WISE J052844.51−330823.9	T7 pec	17.73 ± 0.23	14.60 ± 0.06	12.27 ± 0.24	> 9.33	3.13 ± 0.24	2.33 ± 0.25
WISE J053957.00−103436.7	T5.5	17.28 ± 0.22	14.83 ± 0.08	> 12.64	> 8.95	2.46 ± 0.23	< 2.18
WISE J054231.26−162829.1	T6.5	16.39 ± 0.09	13.98 ± 0.05	> 12.35	> 8.78	2.41 ± 0.10	< 1.63
WISE J061135.13−041024.0	T0	13.57 ± 0.03	12.93 ± 0.03	> 12.06	> 9.08	0.63 ± 0.04	< 0.88
WISE J061208.69−492024.2	T3.5	15.41 ± 0.03	14.11 ± 0.03	12.81 ± 0.27	> 9.78	1.30 ± 0.05	1.30 ± 0.27
WISE J061213.85−303612.5	T6	16.35 ± 0.07	14.03 ± 0.04	12.96 ± 0.45	> 8.93	2.32 ± 0.08	1.07 ± 0.45
WISE J061407.49+391235.9	T6	16.47 ± 0.12	13.65 ± 0.04	12.02 ± 0.28	> 9.07	2.83 ± 0.12	1.63 ± 0.28
WISE J062309.94−045624.6	T8	17.33 ± 0.20	13.82 ± 0.04	> 12.63	> 9.07	3.52 ± 0.20	< 1.18
WISE J062542.21+564625.4	T6	16.33 ± 0.08	14.38 ± 0.06	12.44 ± 0.35	> 8.77	1.95 ± 0.10	1.94 ± 0.36
WISE J062720.07−111428.0	T6	15.00 ± 0.04	13.26 ± 0.03	11.53 ± 0.21	> 8.96	1.74 ± 0.05	1.73 ± 0.21
WISE J065609.59+420531.9	T3	14.31 ± 0.03	13.22 ± 0.03	12.04 ± 0.30	> 8.72	1.09 ± 0.05	1.18 ± 0.30
WISE J074457.25+562821.0	T8	17.08 ± 0.15	14.49 ± 0.06	12.48 ± 0.36	> 9.17	2.59 ± 0.16	2.01 ± 0.36
WISE J075003.78+272545.4	T8.5	> 18.11	14.46 ± 0.07	> 12.69	> 8.96	> 3.65	< 1.78
WISE J075108.80−763449.5	T9	17.54 ± 0.13	14.52 ± 0.04	11.44 ± 0.08	> 9.21	3.01 ± 0.14	3.08 ± 0.09
WISE J075946.98−490454.0	T8	> 17.92	13.86 ± 0.04	> 12.95	> 9.15	> 4.05	< 0.92
WISE J081958.05−033528.5	T4	14.38 ± 0.03	13.08 ± 0.04	11.83 ± 0.28	> 8.81	1.31 ± 0.05	1.25 ± 0.28
WISE J082131.64+144319.2	T5.5	16.49 ± 0.12	14.37 ± 0.07	> 12.58	> 8.96	2.12 ± 0.14	< 1.78
WISE J083641.10−185947.0	T8 pec	> 18.41	15.18 ± 0.10	> 12.47	> 9.18	> 3.23	< 2.71
WISE J085716.24+560407.6	T8	17.49 ± 0.21	14.11 ± 0.05	> 12.49	> 9.29	3.37 ± 0.22	< 1.63
WISE J090649.35+473538.5	T8	17.48 ± 0.23	14.65 ± 0.08	> 12.06	> 8.96	2.83 ± 0.24	< 2.59
WISE J092906.77+040957.9	T6.5	16.63 ± 0.12	14.23 ± 0.06	> 11.91	> 9.07	2.40 ± 0.13	< 2.32
WISE J095259.29+195508.1	T6	16.87 ± 0.16	14.34 ± 0.06	> 12.18	> 8.99	2.53 ± 0.17	< 2.16
WISE J101808.04−244557.9	T8	17.38 ± 0.21	14.17 ± 0.05	> 12.55	> 9.17	3.21 ± 0.22	< 1.62
WISE J101905.62+652954.2	T6	16.42 ± 0.07	14.03 ± 0.04	> 12.40	> 9.44	2.39 ± 0.08	< 1.63
WISE J104245.23−384238.3	T8.5	> 18.57	14.52 ± 0.06	> 12.95	> 9.26	> 4.06	< 1.57
WISE J112254.72+255022.2	T6	16.20 ± 0.08	13.97 ± 0.05	> 12.39	> 8.99	2.22 ± 0.10	< 1.58
WISE J115013.85+630241.5	T8	16.99 ± 0.11	13.40 ± 0.03	12.32 ± 0.24	> 9.23	3.59 ± 0.11	1.08 ± 0.25
WISE J121756.90+162640.8	T9	16.80 ± 0.13	13.09 ± 0.03	12.12 ± 0.31	> 8.90	3.71 ± 0.14	0.97 ± 0.31
WISE J131106.20+012254.3	T9:	18.27 ± 0.46	14.76 ± 0.09	> 12.32	> 9.25	3.50 ± 0.47	< 2.45
WISE J131141.92+362924.7	L5 pec (blue)	13.51 ± 0.03	13.11 ± 0.03	12.74 ± 0.44	> 8.88	0.40 ± 0.04	0.38 ± 0.44
WISE J132004.16+603426.3	T6.5	16.94 ± 0.11	14.41 ± 0.05	> 12.42	> 9.43	2.52 ± 0.12	< 2.00
WISE J132233.64−234016.8	T8	16.99 ± 0.14	13.93 ± 0.04	> 12.70	8.78 ± 0.35	3.06 ± 0.14	< 1.23
WISE J134806.99+660328.4	L9	14.43 ± 0.03	13.76 ± 0.03	12.65 ± 0.29	> 9.62	0.68 ± 0.04	1.11 ± 0.30
WISE J140518.39+553421.3	Y0 (pec?)	> 18.82	14.10 ± 0.04	12.43 ± 0.27	> 9.40	> 4.72	1.67 ± 0.28
WISE J143602.20−181421.9	T8 pec	17.21 ± 0.14	14.71 ± 0.06	> 12.28	> 9.23	2.50 ± 0.16	< 2.43
WISE J145715.03+581510.2	T7	16.83 ± 0.08	14.47 ± 0.04	13.34 ± 0.53	> 9.64	2.36 ± 0.09	1.13 ± 0.53
WISE J150649.97+702736.1	T6	13.39 ± 0.02	11.27 ± 0.02	10.15 ± 0.03	> 9.07	2.12 ± 0.03	1.12 ± 0.04
WISE J151906.63+700931.4	T8	17.17 ± 0.09	14.14 ± 0.03	13.44 ± 0.47	> 9.86	3.03 ± 0.10	0.70 ± 0.47
WISE J154151.65−225024.9	Y0.5	16.74 ± 0.17	14.25 ± 0.06	> 12.31	> 8.89	2.49 ± 0.18	< 1.93
WISE J161215.94−342028.5	T6.5	> 18.19	13.96 ± 0.05	> 12.47	> 9.12	> 4.23	< 1.49

Table 1—Continued

Object Name (1)	NIR Sp. Type (2)	$W1$ (mag) (3)	$W2$ (mag) (4)	$W3$ (mag) (5)	$W4$ (mag) (6)	$W1 - W2$ (mag) (7)	$W2 - W3$ (mag) (8)
WISE J161441.46+173935.5	T9	> 17.90	14.25 ± 0.05	> 12.45	> 9.21	> 3.65	< 1.80
WISE J161705.74+180714.1	T8	17.12 ± 0.15	14.16 ± 0.05	12.49 ± 0.36	> 9.38	2.96 ± 0.16	1.67 ± 0.36
WISE J162208.93−095934.4	T6	16.50 ± 0.14	14.17 ± 0.06	> 12.55	> 8.53	2.33 ± 0.15	< 1.62
WISE J162725.65+325524.6	T6	16.25 ± 0.07	13.60 ± 0.04	12.56 ± 0.35	> 9.25	2.65 ± 0.08	1.04 ± 0.35
WISE J164715.57+563208.3	L9 pec (red)	13.60 ± 0.02	13.09 ± 0.02	12.06 ± 0.09	> 9.62	0.52 ± 0.03	1.03 ± 0.10
WISE J165311.05+444422.8	T8	16.49 ± 0.07	13.81 ± 0.04	12.26 ± 0.23	> 9.49	2.68 ± 0.08	1.55 ± 0.24
WISE J171104.60+350036.8	T8	> 18.15	14.72 ± 0.06	> 12.76	> 9.45	> 3.43	< 1.96
WISE J171717.02+612859.3	T8	18.42 ± 0.20	15.09 ± 0.05	13.51 ± 0.38	> 10.07	3.33 ± 0.20	1.58 ± 0.39
WISE J172844.93+571642.7	T6	17.96 ± 0.18	15.01 ± 0.05	> 13.49	> 9.84	2.95 ± 0.19	< 1.51
WISE J173835.53+273259.0	Y0	> 18.41	14.55 ± 0.06	11.93 ± 0.19	> 8.98	> 3.86	2.62 ± 0.20
WISE J174124.25+255319.6	T9	15.38 ± 0.04	12.33 ± 0.03	10.83 ± 0.09	> 8.60	3.05 ± 0.06	1.50 ± 0.09
WISE J180435.37+311706.4	T9.5:	> 18.64	14.70 ± 0.06	> 12.55	> 9.42	> 3.94	< 2.15
WISE J181210.85+272144.3	T8.5:	17.80 ± 0.29	14.23 ± 0.05	> 12.26	> 9.31	3.58 ± 0.29	< 1.97
WISE J182831.08+265037.7	≥Y2	> 18.47	14.39 ± 0.06	> 12.53	> 8.75	> 4.08	< 1.87
WISE J183058.56+454257.4	L9	14.81 ± 0.03	14.17 ± 0.04	> 13.17	> 9.67	0.65 ± 0.05	< 1.00
WISE J184124.73+700038.0	T5	16.59 ± 0.05	14.39 ± 0.03	13.67 ± 0.47	> 9.54	2.20 ± 0.06	0.71 ± 0.47
WISE J185215.76+353716.7	T7	16.55 ± 0.10	14.24 ± 0.05	12.55 ± 0.32	> 8.87	2.31 ± 0.11	1.69 ± 0.32
WISE J190624.74+450807.1	T6	16.09 ± 0.06	13.82 ± 0.04	13.03 ± 0.43	> 9.66	2.27 ± 0.07	0.79 ± 0.43
WISE J195246.65+724000.8	T4	14.22 ± 0.03	13.02 ± 0.03	12.05 ± 0.14	> 9.44	1.21 ± 0.04	0.96 ± 0.14
WISE J195905.65−333833.5	T8	16.44 ± 0.10	13.88 ± 0.05	> 12.14	> 8.76	2.56 ± 0.11	< 1.74
WISE J201824.97−742327.5	T7	16.54 ± 0.11	13.62 ± 0.04	> 12.52	> 9.22	2.92 ± 0.11	< 1.10
WISE J205628.91+145953.2	Y0	> 18.25	13.93 ± 0.04	12.00 ± 0.27	> 8.78	> 4.33	1.93 ± 0.27
WISE J213456.73−713744.5	T9 pec	> 17.74	13.99 ± 0.05	12.33 ± 0.31	> 9.02	> 3.75	1.66 ± 0.32
WISE J215751.35+265931.4	T7	17.13 ± 0.15	14.48 ± 0.06	> 11.91	> 8.58	2.65 ± 0.16	< 2.57
WISE J220922.11−273439.6	T7	16.50 ± 0.11	13.84 ± 0.05	> 12.28	> 9.12	2.66 ± 0.12	< 1.56
WISE J221354.68+091139.4	T7	16.69 ± 0.11	14.60 ± 0.07	> 12.34	> 9.04	2.10 ± 0.13	< 2.26
WISE J222623.05+044004.0	T8/8.5	17.29 ± 0.22	14.71 ± 0.09	> 12.24	> 9.08	2.58 ± 0.24	< 2.47
WISE J223729.52−061434.4	T5	> 17.49	14.73 ± 0.09	> 12.28	> 8.85	> 2.75	< 2.45
WISE J223937.55+161716.1	T3	14.67 ± 0.04	13.44 ± 0.03	12.14 ± 0.33	> 8.92	1.23 ± 0.05	1.30 ± 0.33
WISE J225540.75−311842.0	T8	16.92 ± 0.17	14.18 ± 0.06	> 12.20	> 9.09	2.74 ± 0.18	< 1.98
WISE J231336.38−803700.1	T8	16.30 ± 0.07	13.64 ± 0.03	12.40 ± 0.25	> 9.58	2.65 ± 0.07	1.24 ± 0.25
WISE J231939.14−184404.4	T7.5	17.15 ± 0.16	13.76 ± 0.05	> 12.06	9.07 ± 0.51	3.39 ± 0.17	< 1.70
WISE J232519.53−410535.0	T9 pec	17.60 ± 0.25	14.13 ± 0.06	> 12.49	> 9.04	3.47 ± 0.25	< 1.64
WISE J232728.74−273056.6	L9	14.05 ± 0.03	13.18 ± 0.03	11.82 ± 0.22	> 9.24	0.87 ± 0.05	1.36 ± 0.22
WISE J234026.61−074508.1	T7	15.95 ± 0.08	13.58 ± 0.04	> 12.37	> 9.00	2.37 ± 0.09	< 1.21
WISE J234351.20−741846.9	T6	15.74 ± 0.06	13.73 ± 0.04	> 12.43	> 9.37	2.01 ± 0.06	< 1.30
WISE J234446.23+103415.6	T9	> 18.03	15.11 ± 0.12	11.76 ± 0.25	> 8.56	> 2.92	3.35 ± 0.28
WISE J234841.10−102844.1	T7	16.89 ± 0.15	14.40 ± 0.06	> 12.56	> 9.09	2.49 ± 0.16	< 1.84
WISE J235941.07−733504.8	T6.5	15.25 ± 0.04	13.32 ± 0.03	11.57 ± 0.13	> 9.38	1.93 ± 0.05	1.75 ± 0.13

Note. — Scholz et al. (2011) independently discovered the T9 dwarf WISE J1741+2553, first announced in Gelino et al. (2011), and also noted WISE J0254+0223 as a proper motion object of presumably late type.

Table 2.   WISE All-Sky Photometry for Brown Dwarf Discoveries from This
Paper

Object Name (1)	W1 (mag) (2)	W2 (mag) (3)	W3 (mag) (4)	W4 (mag) (5)	W1 − W2 (mag) (6)	W2 − W3 (mag) (7)
WISE J000517.48+373720.5	16.88 ± 0.12	13.27 ± 0.03	11.99 ± 0.24	> 9.23	3.61 ± 0.12	1.28 ± 0.24
WISE J003829.05+275852.1	18.04 ± 0.29	14.38 ± 0.05	12.46 ± 0.31	> 8.78	3.67 ± 0.29	1.91 ± 0.32
WISE J003830.54+840517.7	17.53 ± 0.17	15.34 ± 0.09	> 13.18	> 9.53	2.19 ± 0.19	< 2.16
WISE J004024.88+090054.8	16.06 ± 0.08	13.92 ± 0.07	> 12.06	> 8.65	2.13 ± 0.11	< 1.87
WISE J004542.56+361139.1	15.34 ± 0.04	13.73 ± 0.03	12.61 ± 0.35	> 9.28	1.61 ± 0.05	1.12 ± 0.35
WISE J004945.61+215120.0	15.47 ± 0.04	12.97 ± 0.03	11.73 ± 0.17	> 9.21	2.50 ± 0.05	1.24 ± 0.17
WISE J013525.64+171503.4	17.19 ± 0.15	14.74 ± 0.07	> 12.73	> 8.86	2.45 ± 0.17	< 2.02
WISE J021010.25+400829.6	16.29 ± 0.09	14.74 ± 0.08	> 12.66	> 9.17	1.55 ± 0.12	< 2.08
WISE J023318.05+303030.5	16.59 ± 0.12	14.46 ± 0.07	> 12.25	> 9.06	2.13 ± 0.14	< 2.22
WISE J024512.62−345047.8	17.92 ± 0.31	14.56 ± 0.06	12.19 ± 0.27	> 9.20	3.36 ± 0.32	2.38 ± 0.27
WISE J024714.52+372523.5	> 18.37	14.70 ± 0.08	> 12.58	> 9.11	> 3.67	< 2.11
WISE J025934.00−034645.7	17.33 ± 0.14	15.10 ± 0.08	> 12.90	> 9.46	2.23 ± 0.16	< 2.20
WISE J031614.68+382008.0	14.72 ± 0.04	13.56 ± 0.04	12.37 ± 0.39	> 8.78	1.16 ± 0.06	1.19 ± 0.40
WISE J031624.35+430709.1	> 17.86	14.56 ± 0.07	> 12.82	> 9.18	> 3.30	< 1.74
WISE J032120.91−734758.8	> 19.19	15.60 ± 0.08	13.01 ± 0.32	> 9.19	> 3.59	2.59 ± 0.33
WISE J032517.69−385454.1	18.46 ± 0.31	14.98 ± 0.06	13.22 ± 0.46	> 9.66	3.47 ± 0.31	1.76 ± 0.46
WISE J032547.72+083118.2	15.44 ± 0.06	13.49 ± 0.04	> 11.66	> 8.80	1.95 ± 0.07	< 1.83
WISE J033515.01+431045.1	> 18.15	14.60 ± 0.08	> 12.42	> 8.95	> 3.55	< 2.18
WISE J033605.05−014350.4	> 17.96	14.54 ± 0.07	> 12.56	> 9.01	> 3.42	< 1.98
WISE J033651.90+282628.8	16.01 ± 0.08	14.44 ± 0.07	> 12.47	> 8.93	1.57 ± 0.11	< 1.97
WISE J041358.14−475039.3	> 19.39	15.69 ± 0.08	> 13.14	> 9.53	> 3.70	< 2.55
WISE J042417.94+072744.1	> 18.44	15.33 ± 0.13	> 12.68	> 9.02	> 3.11	< 2.65
WISE J043052.92+463331.6	> 18.08	14.40 ± 0.07	11.51 ± 0.18	> 8.69	> 3.69	2.88 ± 0.19
WISE J051208.66−300404.4	> 18.24	15.24 ± 0.10	12.53 ± 0.31	> 9.48	> 3.00	2.71 ± 0.32
WISE J054047.00+483232.4	> 18.25	15.07 ± 0.12	> 12.09	> 9.27	> 3.18	< 2.98
WISE J054601.19−095947.5	15.94 ± 0.07	13.96 ± 0.05	> 12.56	> 9.05	1.97 ± 0.08	< 1.40
WISE J061437.73+095135.0	16.92 ± 0.19	14.29 ± 0.07	> 12.04	8.90 ± 0.39	2.62 ± 0.20	< 2.25
WISE J062905.13+241804.9	14.36 ± 0.03	13.63 ± 0.04	11.83 ± 0.25	> 8.99	0.74 ± 0.06	1.80 ± 0.25
WISE J064205.58+410155.5	13.36 ± 0.03	12.55 ± 0.03	11.70 ± 0.31	> 8.76	0.81 ± 0.04	0.85 ± 0.31
WISE J070159.79+632129.2	14.20 ± 0.03	13.22 ± 0.03	12.48 ± 0.42	> 9.08	0.98 ± 0.05	0.74 ± 0.42
WISE J072312.44+340313.5	> 18.27	14.73 ± 0.08	> 12.21	> 8.92	> 3.54	< 2.52
WISE J073347.94+754439.2	17.16 ± 0.14	14.77 ± 0.07	12.20 ± 0.23	> 9.04	2.39 ± 0.15	2.57 ± 0.24
WISE J075430.95+790957.8	14.41 ± 0.03	13.73 ± 0.03	12.30 ± 0.26	> 9.52	0.67 ± 0.05	1.43 ± 0.26
WISE J081117.81−805141.3	17.29 ± 0.12	14.38 ± 0.04	11.85 ± 0.15	9.09 ± 0.30	2.91 ± 0.13	2.53 ± 0.15
WISE J081220.04+402106.2	18.24 ± 0.47	15.08 ± 0.10	> 12.76	> 9.06	3.16 ± 0.48	< 2.32
WISE J092055.40+453856.3[a]	13.06 ± 0.02	12.39 ± 0.03	11.29 ± 0.17	> 9.08	0.67 ± 0.04	1.10 ± 0.17
WISE J095047.32+011733.3[b]	18.05 ± 0.34	14.48 ± 0.06	> 12.85	> 9.20	3.56 ± 0.34	< 1.63
WISE J102557.72+030755.7	17.89 ± 0.38	14.10 ± 0.06	> 12.19	> 8.81	3.79 ± 0.38	< 1.90
WISE J103907.73−160002.9	16.65 ± 0.11	14.16 ± 0.05	12.73 ± 0.52	> 8.94	2.49 ± 0.12	1.43 ± 0.52
WISE J105047.90+505606.2	18.05 ± 0.34	14.94 ± 0.08	> 12.95	> 9.02	3.11 ± 0.35	< 1.99
WISE J105130.01−213859.7	17.17 ± 0.17	14.54 ± 0.06	> 12.69	> 9.17	2.62 ± 0.18	< 1.85
WISE J112438.12−042149.7	16.56 ± 0.12	14.05 ± 0.05	> 12.49	> 8.58	2.51 ± 0.13	< 1.56
WISE J114340.22+443123.8	18.51 ± 0.39	15.27 ± 0.08	> 13.00	> 9.70	3.25 ± 0.39	< 2.27
WISE J122152.28−313600.8	15.86 ± 0.06	13.85 ± 0.04	12.35 ± 0.35	> 9.14	2.01 ± 0.07	1.50 ± 0.35
WISE J122558.86−101345.0	16.34 ± 0.09	13.99 ± 0.05	12.11 ± 0.30	> 9.10	2.36 ± 0.10	1.88 ± 0.30
WISE J124629.65−313934.2[c]	13.33 ± 0.02	12.38 ± 0.02	11.41 ± 0.12	> 8.83	0.94 ± 0.03	0.98 ± 0.12
WISE J125015.56+262846.9	16.36 ± 0.09	14.58 ± 0.07	> 12.84	> 9.06	1.78 ± 0.11	< 1.74
WISE J125715.90+400854.2	16.74 ± 0.10	14.47 ± 0.05	> 12.40	> 8.76	2.28 ± 0.11	< 2.06
WISE J130141.62−030212.9	18.06 ± 0.38	14.95 ± 0.09	> 12.24	> 8.88	3.11 ± 0.39	< 2.72
WISE J131833.98−175826.5	18.10 ± 0.34	14.75 ± 0.07	> 12.43	> 9.47	3.35 ± 0.34	< 2.32
WISE J133750.46+263648.6	16.31 ± 0.08	14.62 ± 0.06	> 12.22	> 9.03	1.69 ± 0.10	< 2.39
WISE J134802.49−134412.0[d]	16.15 ± 0.07	14.18 ± 0.05	> 12.14	> 9.14	1.97 ± 0.08	< 2.03
WISE J140035.40−385013.5	15.34 ± 0.04	13.75 ± 0.03	> 12.78	> 9.47	1.60 ± 0.05	< 0.97
WISE J142320.84+011638.0[e]	18.01 ± 0.30	14.85 ± 0.07	> 12.66	> 9.41	3.16 ± 0.30	< 2.19
WISE J144901.85+114710.9[f]	17.39 ± 0.16	14.84 ± 0.07	> 12.40	> 9.44	2.55 ± 0.17	< 2.43
WISE J150502.39−285345.5[g]	14.02 ± 0.03	13.30 ± 0.04	11.76 ± 0.26	> 8.70	0.72 ± 0.05	1.53 ± 0.28
WISE J151721.13+052929.3	> 18.10	15.13 ± 0.08	> 13.13	> 9.52	> 2.97	< 2.01
WISE J152305.10+312537.6	17.91 ± 0.21	14.39 ± 0.04	> 13.32	> 9.62	3.52 ± 0.22	< 1.08
WISE J154214.00+223005.2	> 18.88	15.02 ± 0.06	> 12.88	> 9.51	> 3.86	< 2.15
WISE J154352.78−043909.5[h]	16.11 ± 0.08	14.39 ± 0.06	> 12.51	> 8.42	1.72 ± 0.10	< 1.89
WISE J154459.27+584204.5	18.39 ± 0.30	15.03 ± 0.06	> 13.42	> 9.75	3.36 ± 0.31	< 1.62
WISE J162541.36+152811.1[g]	16.90 ± 0.13	14.72 ± 0.07	> 12.50	> 9.15	2.18 ± 0.15	< 2.22
WISE J162918.56+033535.6[g]	13.40 ± 0.03	12.50 ± 0.03	11.32 ± 0.14	> 8.64	0.90 ± 0.04	1.18 ± 0.14
WISE J163236.47+032927.3	15.90 ± 0.07	14.34 ± 0.06	> 12.71	> 9.11	1.56 ± 0.09	< 1.63
WISE J163645.56−074325.1	16.20 ± 0.12	14.69 ± 0.09	> 12.40	> 8.81	1.51 ± 0.14	< 2.29

Table 2—Continued

Object Name	$W1$ (mag)	$W2$ (mag)	$W3$ (mag)	$W4$ (mag)	$W1 - W2$ (mag)	$W2 - W3$ (mag)
(1)	(2)	(3)	(4)	(5)	(6)	(7)
WISE J170745.85−174452.5	16.54 ± 0.15	13.68 ± 0.05	> 11.89	> 8.87	2.85 ± 0.16	< 1.79
WISE J172134.46+111739.4	15.90 ± 0.06	14.28 ± 0.06	> 12.27	> 8.86	1.62 ± 0.09	< 2.02
WISE J173035.99+420742.5	15.11 ± 0.03	14.61 ± 0.05	> 13.47	> 9.50	0.51 ± 0.06	< 1.13
WISE J173421.02+502349.9	15.41 ± 0.03	14.34 ± 0.04	> 13.48	> 9.85	1.07 ± 0.05	< 0.87
WISE J173623.03+605920.2	> 18.70	15.35 ± 0.07	13.29 ± 0.41	> 9.85	> 3.36	2.06 ± 0.42
WISE J173859.27+614242.1	14.06 ± 0.03	13.34 ± 0.03	12.20 ± 0.15	> 9.86	0.72 ± 0.04	1.14 ± 0.15
WISE J174113.12+132711.9	17.50 ± 0.29	14.73 ± 0.08	> 12.49	> 8.67	2.77 ± 0.30	< 2.24
WISE J174303.71+421150.0	15.40 ± 0.04	13.92 ± 0.04	12.38 ± 0.25	> 9.50	1.48 ± 0.05	1.54 ± 0.25
WISE J174556.65+645933.8	> 19.48	16.40 ± 0.09	> 14.22	> 10.54	> 3.08	< 2.18
WISE J174640.78−033818.0	> 18.02	14.79 ± 0.10	> 12.17	> 8.80	> 3.23	< 2.62
WISE J175510.28+180320.2	14.60 ± 0.03	13.74 ± 0.04	12.36 ± 0.31	> 9.28	0.87 ± 0.05	1.38 ± 0.32
WISE J175929.37+544204.7	> 18.55	15.51 ± 0.08	> 13.61	> 9.44	> 3.05	< 1.90
WISE J180901.07+383805.4[i]	> 18.00	15.19 ± 0.09	> 12.56	> 9.52	> 2.81	< 2.64
WISE J180952.53−044812.5	13.29 ± 0.03	12.73 ± 0.03	12.38 ± 0.48	> 8.98	0.56 ± 0.04	0.35 ± 0.48
WISE J181243.14+200746.4	> 18.55	15.35 ± 0.12	> 12.89	> 9.23	> 3.20	< 2.46
WISE J181329.40+283533.3	15.72 ± 0.06	14.07 ± 0.05	12.54 ± 0.35	> 9.38	1.65 ± 0.07	1.53 ± 0.35
WISE J184041.77+293229.2	> 18.53	15.12 ± 0.09	12.71 ± 0.40	> 9.37	> 3.41	2.41 ± 0.41
WISE J190903.16−520433.5	> 18.20	15.34 ± 0.13	12.56 ± 0.40	> 9.25	> 2.85	2.79 ± 0.42
WISE J191359.78+644456.6	17.37 ± 0.12	15.07 ± 0.05	> 12.90	> 9.63	2.30 ± 0.13	< 2.18
WISE J192841.35+235604.9	13.94 ± 0.04	12.11 ± 0.03	11.03 ± 0.13	> 8.91	1.83 ± 0.04	1.09 ± 0.13
WISE J195436.15+691541.3	17.35 ± 0.08	14.97 ± 0.04	> 13.84	> 9.51	2.38 ± 0.09	< 1.14
WISE J195500.42−254013.9	> 18.13	15.02 ± 0.11	> 12.34	> 8.51	> 3.12	< 2.67
WISE J200804.71−083428.5	16.25 ± 0.10	14.23 ± 0.06	> 12.64	> 8.86	2.02 ± 0.12	< 1.59
WISE J201404.13+042408.5	> 17.94	15.16 ± 0.12	> 12.30	> 8.95	> 2.78	< 2.87
WISEPC J201546.27+664645.1[j]	16.70 ± 0.09	14.68 ± 0.06	13.02 ± 0.45	> 9.14	2.02 ± 0.11	1.66 ± 0.46
WISE J201920.76−114807.5	17.29 ± 0.21	14.32 ± 0.06	> 12.20	> 9.03	2.96 ± 0.22	< 2.12
WISE J203042.79+074934.7	12.96 ± 0.03	12.12 ± 0.03	10.96 ± 0.11	> 8.96	0.83 ± 0.04	1.16 ± 0.11
WISE J204356.42+622048.9	13.90 ± 0.03	13.02 ± 0.03	12.12 ± 0.22	> 9.27	0.87 ± 0.04	0.90 ± 0.22
WISE J212321.92−261405.1	16.95 ± 0.13	14.52 ± 0.13	> 11.62	> 8.24	2.42 ± 0.19	< 2.90
WISE J214706.78−102924.0	> 17.60	15.06 ± 0.12	> 12.47	> 8.80	> 2.54	< 2.59
WISE J223617.59+510551.9	13.84 ± 0.03	12.48 ± 0.03	11.02 ± 0.08	> 9.32	1.36 ± 0.04	1.47 ± 0.09
WISE J223720.39+722833.8	15.67 ± 0.06	13.61 ± 0.04	12.62 ± 0.38	> 9.38	2.06 ± 0.07	0.99 ± 0.38
WISE J230133.32+021635.0	16.30 ± 0.08	14.34 ± 0.06	> 12.47	> 9.13	1.96 ± 0.10	< 1.88
WISE J230356.79+191432.9	16.50 ± 0.10	14.67 ± 0.07	> 12.66	> 8.74	1.83 ± 0.12	< 2.00
WISE J233543.79+422255.2	18.55 ± 0.51	15.31 ± 0.10	12.98 ± 0.49	> 9.36	3.24 ± 0.52	2.34 ± 0.50
WISE J234228.98+085620.2[f]	16.07 ± 0.08	13.97 ± 0.05	12.63 ± 0.53	9.08 ± 0.54	2.10 ± 0.09	1.34 ± 0.53
WISE J235716.49+122741.8	15.84 ± 0.06	13.99 ± 0.05	12.35 ± 0.40	> 9.16	1.85 ± 0.08	1.64 ± 0.40

[a] L dwarf candidate, Aberasturi et al. (2011)

[b] ULAS J095047.28+011734.3, Leggett et al. (2012)

[c] IR source, Andrei et al. (2011)

[d] LHS 2803B, Deacon et al. (2012)

[e] BD +01°2920B, Pinfield et al. (2012)

[f] T7 candidates, Scholz (2010)

[g] PSO J226.2599−28.8959, PSO J246.4222+15.4698, PSO J247.3273+03.5932, Deacon et al. (2011)

[h] VHS J154352.78−043909.6, Lodieu et al. (2012)

[i] WISE J180901.07+383805.4, Luhman et al. (2012)

[j] A nearby object caused source confusion in the pipeline used to generate the All-Sky Catalog, resulting in a non-detection of this object. The magnitudes reported here were taken from the first-pass processing operations co-add Source Working Database.

Table 3. Additional Follow-up 2MASS, MKO and IRAC Photometry for Discoveries from
Kirkpatrick et al. (2011)

Object Name	Obs. Ref.	Two Micron All-Sky Survey filter system			Mauna Kea Observatories filter system		*Spitzer*/IRAC observations		
		J	H	K_s	J	H	$ch1$	$ch2$	$ch1 - ch2$
		(mag)	(mag)	(mag)	(mag)	(mag)	(mag)	(mag)	(mag)
(1)	(2)	(3)	(4)	(5)	(6)	(7)	(8)	(9)	(10)
WISE J0448−1935	—	—	—	—	—	—	15.37 ± 0.02	14.16 ± 0.02	1.21 ± 0.03
WISE J0656+4205	—	—	—	—	—	—	13.64 ± 0.02	13.26 ± 0.02	0.38 ± 0.03
WISE J0744+5628	—	—	—	—	—	—	16.27 ± 0.03	14.55 ± 0.02	1.71 ± 0.04
WISE J0759−4904	3	—	—	—	17.38 ± 0.05	17.41 ± 0.04	—	—	—
WISE J0821+1443	—	—	—	—	—	—	15.59 ± 0.03	14.51 ± 0.02	1.08 ± 0.03
WISE J0836−1859	1	18.99 ± 0.22	18.79 ± 0.26	> 18.48	—	—	—	—	—
WISE J1018−2445	1	17.82 ± 0.12	18.00 ± 0.23	17.81 ± 0.31	—	—	—	—	—
WISE J1042−3842	4	—	—	—	18.98 ± 0.09	19.08 ± 0.11	—	—	—
WISE J1436−1814	2	17.52 ± 0.13	> 17.62	> 16.97	—	—	—	—	—
WISE J1612−3420	4	—	—	—	16.65 ± 0.03	16.96 ± 0.03	—	—	—
WISE J1812+2721	—	—	—	—	—	—	16.32 ± 0.03	14.17 ± 0.02	2.15 ± 0.04
WISE J1830+4542	—	—	—	—	—	—	14.29 ± 0.02	14.13 ± 0.02	0.16 ± 0.03
WISE J1906+4508	—	—	—	—	—	—	15.03 ± 0.02	13.82 ± 0.02	1.21 ± 0.03
WISE J1959−3338	—	—	—	—	—	—	15.36 ± 0.02	13.79 ± 0.02	1.58 ± 0.03
WISE J2018−7423	4	—	—	—	16.83 ± 0.03	17.17 ± 0.04	15.28 ± 0.02	13.55 ± 0.02	1.73 ± 0.03
WISE J2313−8037	—	—	—	—	—	—	15.29 ± 0.02	13.68 ± 0.02	1.61 ± 0.03
WISE J2343−7418	—	—	—	—	—	—	15.04 ± 0.02	13.75 ± 0.02	1.28 ± 0.03

Note. — Ref. for JHK instrument or catalog: 2MASS filter system: (1) Bigelow/2MASS, (2) PAIRITEL; MKO filter system: (3) Magellan/PANIC, (4) CTIO-4m/NEWFIRM

Table 4.   Follow-up 2MASS, MKO and IRAC Photometry for New Brown Dwarf Discoveries

| Object Name (1) | Obs. Ref. (2) | Two Micron All-Sky Survey filter system | | | Mauna Kea Observatories filter system | | *Spitzer*/IRAC observations | | |
		J (mag) (3)	H (mag) (4)	K_s (mag) (5)	J (mag) (6)	H (mag) (7)	$ch1$ (mag) (8)	$ch2$ (mag) (9)	$ch1 - ch2$ (mag) (10)
WISE J0005+3737	9	—	—	—	18.33 ± 0.12	18.10 ± 0.08	15.43 ± 0.02	13.28 ± 0.02	2.15 ± 0.03
WISE J0038+2758	5	—	—	—	18.61 ± 0.02	18.92 ± 0.04	16.45 ± 0.04	14.41 ± 0.02	2.04 ± 0.04
WISE J0038+8405	4	17.53 ± 0.06	17.06 ± 0.11	> 16.50	—	—	16.33 ± 0.04	14.99 ± 0.02	1.34 ± 0.04
WISE J0040+0900	1	16.50 ± 0.12	16.54 ± 0.27	> 15.74	—	—	15.07 ± 0.02	13.76 ± 0.02	1.31 ± 0.03
	7[a]	—	—	—	—	16.56 0.02	—	—	—
WISE J0045+3611	1	16.15 ± 0.08	16.04 ± 0.15	15.80 ± 0.20	—	—	14.68 ± 0.02	13.75 ± 0.02	0.94 ± 0.03
WISE J0049+2151	1	16.72 ± 0.16	> 16.51	> 15.86	—	—	15.01 ± 0.02	13.04 ± 0.02	1.97 ± 0.03
WISE J0135+1715	—	—	—	—	—	—	16.08 ± 0.03	14.57 ± 0.02	1.51 ± 0.04
WISE J0210+4008	2	16.77 ± 0.19	16.06 ± 0.18	> 15.88	—	—	—	—	—
WISE J0233+3030	1	16.85 ± 0.14	> 17.18	> 17.04	—	—	15.63 ± 0.03	14.35 ± 0.02	1.28 ± 0.03
WISE J0245−3450	9	—	—	—	17.77 ± 0.09	—	16.05 ± 0.03	14.59 ± 0.02	1.46 ± 0.04
WISE J0247+3725	3	18.44 ± 0.17	18.24 ± 0.19	18.37 ± 0.30	—	—	16.70 ± 0.04	14.56 ± 0.02	2.14 ± 0.05
WISE J0259−0346	—	—	—	—	—	—	16.22 ± 0.03	14.88 ± 0.02	1.34 ± 0.04
WISE J0316+3820	1	16.06 ± 0.09	15.44 ± 0.11	15.27 ± 0.15	—	—	14.10 ± 0.02	13.52 ± 0.02	0.58 ± 0.03
	3	16.21 ± 0.08	15.50 ± 0.08	15.33 ± 0.10	—	—	—	—	—
WISE J0316+4307	5	—	—	—	19.47 ± 0.04	19.70 ± 0.09	16.64 ± 0.04	14.58 ± 0.02	2.06 ± 0.05
WISE J0321−7347	9	—	—	—	19.13 ± 0.11	19.06 ± 0.12	17.28 ± 0.06	15.36 ± 0.02	1.92 ± 0.06
WISE J0325−3854	9*	—	—	—	∼ 19.40	∼ 19.30	17.12 ± 0.05	14.99 ± 0.02	2.14 ± 0.06
WISE J0325+0831	4	16.54 ± 0.07	16.15 ± 0.08	—	—	—	14.70 ± 0.02	13.59 ± 0.02	1.11 ± 0.03
WISE J0335+4310	3	> 19.73	> 19.18	> 18.56	—	—	16.60 ± 0.04	14.38 ± 0.02	2.21 ± 0.04
	5	—	—	—	20.07 ± 0.30	19.60 ± 0.26	—	—	—
WISE J0336−0143	4	> 19.00	> 18.25	—	—	—	17.26 ± 0.06	14.62 ± 0.02	2.64 ± 0.06
WISE J0336+2826	1	16.54 ± 0.12	16.53 ± 0.27	15.77 ± 0.24	—	—	15.31 ± 0.02	14.36 ± 0.02	0.95 ± 0.03
	7[b]	—	—	—	—	16.28 ± 0.03	—	—	—
WISE J0413−4750	9	—	—	—	20.29 ± 0.20	20.12 ± 0.20	17.80 ± 0.09	15.49 ± 0.02	2.32 ± 0.09
WISE J0424+0727	3	18.71 ± 0.16	18.76 ± 0.22	18.87 ± 0.40	—	—	16.75 ± 0.04	15.18 ± 0.02	1.56 ± 0.05
WISE J0430+4633	5	—	—	—	19.03 ± 0.05	19.25 ± 0.13	16.13 ± 0.03	14.22 ± 0.02	1.91 ± 0.04
WISE J0512−3004	5	—	—	—	19.21 ± 0.09	19.66 ± 0.41	17.64 ± 0.08	15.58 ± 0.02	2.06 ± 0.08
WISE J0540+4832	5	—	—	—	18.49 ± 0.02	18.62 ± 0.05	16.97 ± 0.05	14.77 ± 0.02	2.20 ± 0.05
WISE J0546−0959	1	16.18 ± 0.09	16.27 ± 0.22	> 15.47	—	—	15.01 ± 0.02	13.92 ± 0.02	1.09 ± 0.03
WISE J0614+0951	3	16.90 ± 0.08	16.82 ± 0.10	16.81 ± 0.14	—	—	15.49 ± 0.03	14.10 ± 0.02	1.39 ± 0.03
WISE J0629+2418	1	16.34 ± 0.13	15.47 ± 0.15	15.13 ± 0.15	—	—	—	—	—
	4	16.39 ± 0.05	15.58 ± 0.06	15.09 ± 0.07	—	—	—	—	—
WISE J0642+4101	1	16.16 ± 0.10	15.09 ± 0.07	14.28 ± 0.06	—	—	12.94 ± 0.02	12.65 ± 0.02	0.29 ± 0.02
WISE J0701+6321	1	15.79 ± 0.06	15.08 ± 0.07	14.88 ± 0.11	—	—	13.65 ± 0.02	13.24 ± 0.02	0.42 ± 0.03
WISE J0723+3403	4	18.21 ± 0.14	> 18.47	> 17.06	—	—	16.77 ± 0.04	14.68 ± 0.02	2.08 ± 0.05
WISE J0733+7544	2	17.20 ± 0.21	> 17.75	15.81 ± 0.27	—	—	16.00 ± 0.03	14.81 ± 0.02	1.19 ± 0.04
WISE J0754+7909	1	16.17 ± 0.11	15.44 ± 0.14	14.93 ± 0.12	—	—	13.81 ± 0.02	13.82 ± 0.02	-0.01 ± 0.03
	4	16.24 ± 0.05	15.27 ± 0.06	15.05 ± 0.08	—	—	—	—	—
WISE J0811−8051	9	—	—	—	19.90 ± 0.18	19.88 ± 0.21	16.82 ± 0.05	14.40 ± 0.02	2.42 ± 0.05
WISE J0812+4021	3	18.39 ± 0.16	18.30 ± 0.20	19.15 ± 0.51	—	—	16.93 ± 0.05	15.30 ± 0.02	1.63 ± 0.05
WISE J0920+4538	1	15.22 ± 0.05	14.16 ± 0.05	13.73 ± 0.05	—	—	—	—	—
	4	15.16 ± 0.04	14.13 ± 0.09	13.78 ± 0.06	—	—	—	—	—
WISE J0950+0117	5	—	—	—	18.09 ± 0.07	18.07 ± 0.08	16.31 ± 0.03	14.42 ± 0.02	1.88 ± 0.04
	7[c]	—	—	—	18.05 ± 0.04	18.24 ± 0.15	—	—	—
WISE J1025+0307	5	—	—	—	17.93 ± 0.03	18.36 ± 0.05	16.32 ± 0.03	14.19 ± 0.02	2.12 ± 0.04
	7[d]	—	—	—	17.84 ± 0.03	18.30 ± 0.12	—	—	—
WISE J1039−1600	3	17.26 ± 0.12	17.19 ± 0.20	> 17.13	—	—	15.79 ± 0.03	14.23 ± 0.02	1.55 ± 0.03

Table 4—Continued

Object Name	Obs. Ref.	Two Micron All-Sky Survey filter system			Mauna Kea Observatories filter system		Spitzer/IRAC observations		
		J	H	K_s	J	H	$ch1$	$ch2$	$ch1 - ch2$
		(mag)	(mag)	(mag)	(mag)	(mag)	(mag)	(mag)	(mag)
(1)	(2)	(3)	(4)	(5)	(6)	(7)	(8)	(9)	(10)
	4	17.34 ± 0.08	> 17.87	> 17.03	—	—	—	—	—
WISE J1050+5056	5	—	—	—	17.94 ± 0.02	18.31 ± 0.03	16.55 ± 0.04	14.90 ± 0.02	1.65 ± 0.04
WISE J1051−2138	9	—	—	—	18.93 ± 0.10	19.19 ± 0.39	16.43 ± 0.04	14.60 ± 0.02	1.83 ± 0.04
WISE J1124−0421	1	16.72 ± 0.13	> 16.32	> 16.37	—	—	15.37 ± 0.02	14.10 ± 0.02	1.27 ± 0.03
WISE J1143+4431	5	—	—	—	18.76 ± 0.04	19.04 ± 0.06	17.14 ± 0.06	15.16 ± 0.02	1.98 ± 0.06
WISE J1221−3136	1	16.38 ± 0.13	16.06 ± 0.18	> 15.63	—	—	15.09 ± 0.02	13.89 ± 0.02	1.20 ± 0.03
WISE J1225−1013	1	16.43 ± 0.10	16.30 ± 0.22	> 15.87	—	—	15.31 ± 0.02	13.96 ± 0.02	1.35 ± 0.03
	9	—	—	—	—	16.46 ± 0.15	—	—	—
WISE J1246−3139	1	15.02 ± 0.04	14.19 ± 0.03	13.97 ± 0.06	—	—	12.77 ± 0.02	12.45 ± 0.02	0.32 ± 0.02
WISE J1250+2628	2	16.93 ± 0.20	> 17.10	15.72 ± 0.21	—	—	—	—	—
WISE J1257+4008	3	17.23 ± 0.09	16.96 ± 0.13	17.00 ± 0.19	—	—	15.92 ± 0.03	14.49 ± 0.02	1.43 ± 0.04
WISE J1301−0302	5	—	—	—	18.00 ± 0.02	18.39 ± 0.06	16.64 ± 0.04	14.89 ± 0.02	1.74 ± 0.05
WISE J1318−1758	3	18.43 ± 0.19	17.71 ± 0.23	> 17.67	—	—	16.79 ± 0.05	14.73 ± 0.02	2.06 ± 0.05
WISE J1337+2636	1	16.67 ± 0.15	> 16.12	> 16.97	—	—	—	—	—
WISE J1348−1344	1	16.48 ± 0.12	16.09 ± 0.17	> 16.45	—	—	15.30 ± 0.03	14.10 ± 0.02	1.20 ± 0.03
	4	16.67 ± 0.10	16.67 ± 0.13	> 17.01	—	—	—	—	—
WISE J1400−3850	1	16.04 ± 0.10	15.82 ± 0.17	> 16.07	—	—	14.53 ± 0.02	13.85 ± 0.02	0.68 ± 0.03
WISE J1423+0116	5	—	—	—	18.55 ± 0.03	18.96 ± 0.07	16.73 ± 0.04	14.69 ± 0.02	2.03 ± 0.05
	7[e]	—	—	—	18.76 ± 0.12	—	—	—	—
WISE J1449+1147	4	> 17.96	> 17.32	> 16.64	—	—	16.11 ± 0.03	14.92 ± 0.02	1.19 ± 0.04
	7[f]	—	—	—	17.36 ± 0.02	17.73 ± 0.07	—	—	—
WISE J1505−2853	1	15.83 ± 0.07	15.24 ± 0.08	15.06 ± 0.13	—	—	13.56 ± 0.02	13.29 ± 0.02	0.27 ± 0.03
	4	15.97 ± 0.08	15.09 ± 0.10	14.69 ± 0.06	—	—	—	—	—
WISE J1517+0529	7[g]	—	—	—	18.54 ± 0.05	18.85 ± 0.15	16.85 ± 0.05	15.10 ± 0.02	1.74 ± 0.05
WISE J1523+3125	5	—	—	—	18.27 ± 0.07	18.69 ± 0.18	15.95 ± 0.03	14.28 ± 0.02	1.68 ± 0.04
WISE J1542+2230	5	—	—	—	20.25 ± 0.13	21.80 ± 0.80	17.26 ± 0.06	15.06 ± 0.02	2.20 ± 0.06
WISE J1543−0439	1	16.51 ± 0.13	> 15.98	> 16.34	—	—	15.43 ± 0.02	14.54 ± 0.02	0.89 ± 0.03
WISE J1544+5842	3	18.52 ± 0.17	18.34 ± 0.29	> 17.98	—	—	16.68 ± 0.04	14.95 ± 0.02	1.73 ± 0.05
WISE J1625+1528	3	17.14 ± 0.11	16.85 ± 0.14	16.98 ± 0.21	—	—	15.77 ± 0.03	14.75 ± 0.02	1.02 ± 0.04
WISE J1629+0335	1	15.29 ± 0.04	14.49 ± 0.04	14.18 ± 0.06	—	—	12.82 ± 0.02	12.57 ± 0.02	0.25 ± 0.02
	4	15.22 ± 0.05	14.43 ± 0.08	14.04 ± 0.03	—	—	—	—	—
WISE J1632+0329	1	16.75 ± 0.12	16.43 ± 0.19	> 16.63	—	—	15.28 ± 0.02	14.47 ± 0.02	0.81 ± 0.03
WISE J1636−0743	—	—	—	—	—	—	—	—	—
WISE J1707−1744	1	16.30 ± 0.12	> 15.45	> 15.85	—	—	14.98 ± 0.02	13.62 ± 0.02	1.35 ± 0.03
	5	—	—	—	16.35 ± 0.02	17.11 ± 0.03	—	—	—
	8	—	—	—	16.33 ± 0.02	16.58 ± 0.03	—	—	—
WISE J1721+1117	1	16.46 ± 0.15	> 16.24	> 16.12	—	—	15.24 ± 0.02	14.35 ± 0.02	0.89 ± 0.03
WISE J1730+4207	2	16.95 ± 0.18	16.00 ± 0.19	> 15.65	—	—	14.73 ± 0.02	14.56 ± 0.02	0.17 ± 0.03
WISE J1734+5023	1	16.34 ± 0.11	15.85 ± 0.14	> 15.37	—	—	15.23 ± 0.02	14.38 ± 0.02	0.84 ± 0.03
WISE J1736+6059	4	> 18.91	> 18.14	> 16.96	—	—	16.97 ± 0.05	15.37 ± 0.02	1.60 ± 0.05
WISE J1738+6142	2	—	16.32 ± 0.22	15.14 ± 0.16	—	—	13.56 ± 0.02	13.33 ± 0.02	0.23 ± 0.03
	4	17.82 ± 0.13	16.34 ± 0.08	15.27 ± 0.10	—	—	—	—	—
WISE J1741+1327	—	—	—	—	—	—	16.01 ± 0.03	14.67 ± 0.02	1.35 ± 0.04
WISE J1743+4211	1	15.84 ± 0.06	15.57 ± 0.14	15.43 ± 0.19	—	—	14.72 ± 0.02	13.93 ± 0.02	0.79 ± 0.03
	4	15.83 ± 0.06	15.73 ± 0.09	16.03 ± 0.22	—	—	—	—	—
WISE J1745+6459	—	—	—	—	—	—	17.41 ± 0.07	16.14 ± 0.03	1.27 ± 0.07
WISE J1746−0338	3	17.53 ± 0.17	17.57 ± 0.34	> 17.08	—	—	16.03 ± 0.03	14.44 ± 0.02	1.59 ± 0.04
	8	—	—	—	17.17 ± 0.03	17.45 ± 0.04	—	—	—

Table 4—Continued

Object Name	Obs. Ref.	Two Micron All-Sky Survey filter system			Mauna Kea Observatories filter system		Spitzer/IRAC observations		
		J	H	K_s	J	H	$ch1$	$ch2$	$ch1 - ch2$
		(mag)	(mag)	(mag)	(mag)	(mag)	(mag)	(mag)	(mag)
(1)	(2)	(3)	(4)	(5)	(6)	(7)	(8)	(9)	(10)
WISE J1755+1803	1	16.02 ± 0.09	15.22 ± 0.09	14.68 ± 0.13	—	—	14.09 ± 0.02	13.77 ± 0.02	0.32 ± 0.03
WISE J1759+5442	5	—	—	—	17.93 ± 0.01	18.26 ± 0.03	16.64 ± 0.04	15.12 ± 0.02	1.52 ± 0.05
WISE J1809+3838	—	—	—	—	—	—	16.49 ± 0.04	14.90 ± 0.02	1.59 ± 0.04
WISE J1809−0448	1	15.14 ± 0.05	14.28 ± 0.05	13.96 ± 0.06	—	—	—	—	—
WISE J1812+2007	5	—	—	—	18.54 ± 0.02	18.95 ± 0.06	16.96 ± 0.05	15.02 ± 0.02	1.93 ± 0.05
	8	—	—	—	18.75 ± 0.07	18.94 ± 0.09	—	—	—
WISE J1813+2835	—	—	—	—	—	—	15.82 ± 0.03	14.19 ± 0.02	1.63 ± 0.03
WISE J1840+2932	5	—	—	—	17.89 ± 0.01	18.12 ± 0.03	16.67 ± 0.04	15.20 ± 0.02	1.47 ± 0.05
WISE J1909−5204	6	—	—	—	17.35 ± 0.09	17.26 ± 0.06	16.37 ± 0.04	15.21 ± 0.02	1.17 ± 0.04
WISE J1913+6444	4	17.32 ± 0.10	16.89 ± 0.14	> 16.49	—	—	16.29 ± 0.03	14.99 ± 0.02	1.30 ± 0.04
WISE J1928+2356	2	14.34 ± 0.06	14.31 ± 0.06	14.09 ± 0.06	—	—	13.14 ± 0.02	12.06 ± 0.02	1.08 ± 0.02
WISE J1954+6915	4	17.73 ± 0.12	17.19 ± 0.16	17.06 ± 0.38	—	—	16.04 ± 0.03	14.83 ± 0.02	1.22 ± 0.04
WISE J1955−2540	5	—	—	—	17.58 ± 0.02	18.00 ± 0.05	16.61 ± 0.04	15.03 ± 0.02	1.58 ± 0.05
WISE J2008−0834	1	16.37 ± 0.12	16.69 ± 0.31	> 15.66	—	—	15.16 ± 0.02	14.11 ± 0.02	1.06 ± 0.03
WISE J2014+0424	3	18.76 ± 0.22	18.66 ± 0.30	17.84 ± 0.29	—	—	16.35 ± 0.04	14.77 ± 0.02	1.58 ± 0.04
WISE J2015+6646	4	16.91 ± 0.07	16.50 ± 0.09	> 16.43	—	—	16.33 ± 0.03	14.62 ± 0.02	1.71 ± 0.04
WISE J2019−1148	4	> 14.93	> 13.95	> 14.11	—	—	16.03 ± 0.03	14.25 ± 0.02	1.78 ± 0.04
	8	—	—	—	18.09 ± 0.06	18.23 ± 0.07	—	—	—
	9	—	—	—	18.54 ± 0.08	18.32 ± 0.11	—	—	—
WISE J2030+0749	1	14.23 ± 0.03	13.44 ± 0.03	13.32 ± 0.04	—	—	—	—	—
WISE J2043+6220	1	15.60 ± 0.07	14.70 ± 0.07	14.42 ± 0.07	—	—	—	—	—
WISE J2123−2614	2	17.44 ± 0.26	> 17.30	> 15.85	—	—	15.94 ± 0.03	14.45 ± 0.02	1.49 ± 0.04
WISE J2147−1029	3	17.66 ± 0.22	17.81 ± 0.36	> 17.12	—	—	16.55 ± 0.04	14.96 ± 0.02	1.59 ± 0.04
WISE J2236+5105	—	—	—	—	—	—	—	—	—
WISE J2237+7228	1	15.76 ± 0.07	15.94 ± 0.21	> 15.99	—	—	14.61 ± 0.02	13.56 ± 0.02	1.05 ± 0.03
WISE J2301+0216	1	16.71 ± 0.15	> 16.09	> 17.18	—	—	15.60 ± 0.03	14.37 ± 0.02	1.23 ± 0.03
	7[h]	—	—	—	16.36 ± 0.01	16.70 ± 0.03	—	—	—
WISE J2303+1914	1	16.86 ± 0.16	> 16.02	> 17.10	—	—	—	—	—
WISE J2335+4222	—	—	—	—	—	—	16.53 ± 0.04	15.30 ± 0.02	1.23 ± 0.05
WISE J2342+0856	2	16.73 ± 0.18	16.26 ± 0.23	> 15.94	—	—	15.29 ± 0.02	13.99 ± 0.02	1.30 ± 0.03
	7[i]	—	—	—	16.37 ± 0.01	16.73 ± 0.03	—	—	—
WISE J2357+1227	1	16.52 ± 0.14	> 15.75	> 16.12	—	—	15.26 ± 0.02	14.10 ± 0.02	1.16 ± 0.03
	7[j]	—	—	—	16.10 ± 0.01	16.49 ± 0.03	—	—	—

[*]Approximate magnitudes based on images with only three 2MASS sources available for photometric calibration.

[a]K=16.55 ± 0.05 (mag)

[b]Z=19.75 ± 0.09 (mag), Y=17.48 ± 0.02 (mag), K=16.40 ± 0.04 (mag)

[c]Y=18.96 ± 0.06 (mag)

[d]Y=18.92 ± 0.05 (mag)

[e]Y=19.51 ± 0.14 (mag)

[f]Y=18.35 ± 0.04 (mag), K=18.10 ± 0.15 (mag)

[g]Y=19.57 ± 0.07 (mag)

[h]Y=17.62 ±0.02 (mag), K=16.87 ± 0.05 (mag)

[i] Y=17.42 ± 0.02 (mag), K=16.98 ± 0.07 (mag)

[j] Y=17.34 ± 0.02 (mag), K=16.52 ± 0.04 (mag)

Note. — Ref. for JHK instrument or catalog: 2MASS filter system: (1) 2MASS All-Sky Point Source Catalog, (2) 2MASS Reject Table, (3) Bigelow/2MASS, (4) PAIRITEL; MKO filter system: (5) Palomar/WIRC, (6) Magellan/PANIC, (7) UKIDSS, (8) CTIO-4m/NEWFIRM, Other filter System: (9) SOAR/OSIRIS

Table 5.   Follow-up Near-IR Spectroscopy and Spectral Classifications for T
Dwarf Discoveries

Object Name and J2000 Coordinates (1)	NIR Sp. Type (2)	Spectrograph (3)	Int. Time (s) (4)	Tell. Corr. Star (5)	Obs. Date (UT) (6)
WISE J0005+3737	T9	Keck/NIRSPEC-J	2400	HD 9711	2011 Oct 07
WISE J0038+2758	T9	Keck/NIRSPEC-J	4800	HD 7215	2011 Sep 08
WISE J0038+8405	T6	Keck/NIRSPEC-J	3600	HD 33541	2011 Aug 09
WISE J0040+0900	T7	IRTF/SpeX	1200	HD 7215	2011 Nov 30
WISE J0045+3611	T5	IRTF/SpeX	1200	HD 9711	2011 Aug 25
WISE J0049+2151	T8.5	IRTF/SpeX	1200	HD 9711	2011 Aug 25
WISE J0135+1715	T6	IRTF/SpeX	1200	HD 19600	2011 Aug 25
WISE J0210+4008	T4.5	IRTF/SpeX	1200	HD 19600	2011 Nov 30
WISE J0233+3030	T6	IRTF/SpeX	1200	HD 19600	2011 Aug 25
WISE J0245−3450	T8	IRTF/SpeX	1200	HD 18735	2011 Aug 25
WISE J0247+3725	T8	Gemini/GNIRS	6000	HD 21038	2012 Jan 05
WISE J0259−0346	T5	Keck/NIRSPEC-J	1200	HD 18571	2011 Oct 09
WISE J0316+3820	T3	Palomar/TSpec	480	HD 20842	2011 Jul 13
WISE J0316+4307	T8	Keck/NIRSPEC-J	2400	HD 21038	2011 Sep 05
	T8	Keck/NIRSPEC-H	1800	HD 21038	2011 Sep 06
	T8	Keck/NIRSPEC-J	3600	HD 9711	2011 Oct 07
WISE J0321−7347	T8	Magellan/FIRE	1775	HD 80885	2012 Jan 05
WISE J0325−3854	T9	Keck/NIRSPEC-J	1200	HD 24966	2011 Sep 08
	T9	Keck/NIRSPEC-J	2400	HD 24966	2011 Oct 07
WISE J0325+0831	T7	IRTF/SpeX	1560	HD 22859	2011 Sep 11
WISE J0335+4310	T9	Keck/NIRSPEC-J	2400	HD 21038	2012 Sep 25
WISE J0336−0143	T8:	Keck/NIRSPEC-J	600	HD 18571	2011 Sep 08
WISE J0336+2826	T5	IRTF/SpeX	960	HD 202990	2011 Sep 11
WISE J0413−4750	T9	Magellan/FIRE	1775	HD 30252	2012 Jan 05
WISE J0424+0727	T7.5	Keck/NIRSPEC-J	2400	HD 31411	2012 Sep 24
WISE J0430+4633	T8	Keck/NIRSPEC-J	4200	HD 31069	2012 Sep 24
WISE J0512−3004	T8.5	Keck/NIRSPEC-J	2400	HD 36965	2012 Sep 25
WISE J0540+4832	T8.5	Keck/NIRSPEC-J	2400	HD 45105	2012 Sep 25
WISE J0546−0959	T5	IRTF/SpeX	1200	HD 37887	2012 Feb 01
WISE J0614+0951	T7	Palomar/TSpec	2700	HD 35036	2012 Jan 06
WISE J0629+2418	T2 sb	IRTF/SpeX	1200	HD 43607	2012 Feb 13
WISE J0642+4101	extremely red	Palomar/TSpec	1080	HD 45105	2012 Jan 07
WISE J0701+6321	T3	Palomar/TSpec	1440	HD 33654	2012 Jan 06
WISE J0723+3403	T9:	Keck/NIRSPEC-J	2400	HD 57208	2012 Apr 09
WISE J0733+7544	T6	Palomar/TSpec	3000	HD 43607	2012 Jan 06
WISE J0754+7909	extremely red	Palomar/TSpec	1440	HD 33541	2012 Jan 07
WISE J0811−8051	T9.5:	Magellan/FIRE	1268	HD 52364	2012 Jan 05
WISE J0812+4021	T8	Gemini/GNIRS	3000	HD 45105	2011 Mar 13
WISE J1025+0307	T8.5	Magellan/FIRE	960	HD 84920	2012 May 06
WISE J1039−1600	T7.5	IRTF/SpeX	1920	HD 88766	2012 Feb 13
WISE J1050+5056	T8	Keck/NIRSPEC-J	1800	HD 99966	2012 Jun 09
WISE J1051−2138	T9:	Palomar/TSpec	1800	HD 91398	2012 Jan 06
WISE J1124−0421	T7	IRTF/SpeX	1680	HD 93346	2012 Jan 31
WISE J1143+4431	T8.5	Keck/NIRSPEC-J	2100	HD 99966	2012 Jun 09

Table 5—Continued

Object Name and J2000 Coordinates (1)	NIR Sp. Type (2)	Spectrograph (3)	Int. Time (s) (4)	Tell. Corr. Star (5)	Obs. Date (UT) (6)
WISE J1221−3136	T6.5	IRTF/SpeX	1440	HD 112305	2012 May 13
WISE J1225−1013	T6	IRTF/SpeX	1200	HD 101122	2012 Jan 13
WISE J1250+2628	T6.5	Keck/NIRSPEC-J	1440	HD 122945	2012 Jun 08
WISE J1257+4008	T7	IRTF/SpeX	1200	HD 109615	2012 May 13
WISE J1301−0302	T8.5	Keck/NIRSPEC-J	1440	HD 118054	2012 Jun 09
WISE J1318−1758	T9:	Palomar/TSpec	2400	HD 114243	2012 Jan 06
WISE J1337+2636	T5	Keck/NIRSPEC-J	1440	HD 122945	2012 Jun 08
WISE J1400−3850	T4	IRTF/SpeX	1440	HD 120486	2012 Feb 13
WISE J1517+0529	T8	Keck/NIRSPEC-J	2400	HD 140775	2012 Apr 09
WISE J1523+3125	T6.5 pec	Gemini/GNIRS	2400	HD 136831	2011 Jul 04
WISE J1542+2230	T9.5	HST/WFC3	2012	—	2012 Mar 04
WISE J1544+5842	T7.5	Keck/NIRSPEC-J	900	HD 143187	2011 Aug 08
WISE J1632+0329	T5	IRTF/SpeX	1200	HD 145647	2011 Sep 11
WISE J1636−0743	T4.5	IRTF/SpeX	1200	HD 148968	2011 Aug 25
WISE J1707−1744	T5:	Palomar/TSpec	3600	HD 131951	2011 May 12
WISE J1721+1117	T6	IRTF/SpeX	960	HD 167163	2011 Aug 25
WISE J1730+4207	T0 sb	IRTF/SpeX	1200	HD 174567	2011 Jul 29
WISE J1734+5023	T4	IRTF/SpeX	1200	HD 184195	2011 Jul 29
WISE J1736+6059	T8	Keck/NIRSPEC-J	1800	HD 172728	2012 Sep 03
WISE J1738+6142	extremely red	Palomar/TSpec	1440	HD 143187	2011 Jul 13
	extremely red	IRTF/SpeX	1200	55 Dra	2012 Jul 23
WISE J1741+1327	T5	IRTF/SpeX	1200	HD 167163	2011 Aug 25
WISE J1743+4211	T4.5	Palomar/TSpec	1200	HD 158261	2011 May 12
WISE J1745+6459	T7	Keck/NIRSPEC-J	1800	HD 172728	2012 Jun 08
WISE J1746−0338	T6	Palomar/TSpec	3600	HD 161868	2011 May 13
WISE J1755+1803	T2	Palomar/TSpec	720	HD 165029	2011 Jul 13
WISE J1759+5442	T7	Keck/NIRSPEC-J	1440	HD 172728	2012 Jun 08
WISE J1809−0448	T0.5	IRTF/SpeX	960	HD 167163	2012 Jul 23
WISE J1812+2007	T9	Keck/NIRSPEC-J	1800	HD 199217	2012 Sep 03
WISE J1813+2835	T8	Keck/NIRSPEC-J	1800	HD 165029	2012 Jun 08
WISE J1840+2932	T6	Keck/NIRSPEC-J	1800	HD 165029	2012 Sep 03
WISE J1909−5204	T5.5	Magellan/FIRE	720	HD 182000	2012 Sep 05
WISE J1913+6444	T5:	Palomar/TSpec	1800	HD 184195	2011 Jul 13
WISE J1928+2356	T6	IRTF/SpeX	1200	HD 192538	2011 Sep 11
WISE J1954+6915	T5.5	Keck/NIRSPEC-J	1440	HD 172728	2012 Jun 09
WISE J1955−2540	T8	Keck/NIRSPEC-J	1440	HD 190285	2012 Jun 09
WISE J2008−0834	T5.5	IRTF/SpeX	1200	HD 202990	2011 Sep 11
WISE J2014+0424	T6.5 pec	Gemini/GNIRS	3600	HD 198070	2011 Aug 28
WISE J2015+6646	T8	Palomar/TSpec	2400	HD 214019	2011 Jul 14
WISE J2019−1148	T8:	Palomar/TSpec	2400	HD 202990	2011 Jul 14
WISE J2030+0749	T1.5	IRTF/SpeX	1200	HD 198070	2011 Sep 11
WISE J2043+6220	T1.5	IRTF/SpeX	720	HD 192538	2012 May 28
WISE J2123−2614	T5.5	IRTF/SpeX	1200	HD 202941	2011 Aug 25
WISE J2147−1029	T7.5	Keck/NIRSPEC-J	1400	HD 203769	2012 Jun 09

Table 5—Continued

Object Name and J2000 Coordinates (1)	NIR Sp. Type (2)	Spectrograph (3)	Int. Time (s) (4)	Tell. Corr. Star (5)	Obs. Date (UT) (6)
WISE J2236+5105	T5.5	Palomar/TSpec	1440	HD 223386	2012 Jan 06
WISE J2237+7228	T6	Keck/NIRSPEC-J	1200	HD 207636	2011 Sep 08
WISE J2301+0216	T6.5	IRTF/SpeX	1440	HD 215143	2011 Sep 11
WISE J2303+1914	T4:	Palomar/TSpec	1440	HD 209932	2012 Jan 07
WISE J2335+4222	T7	Keck/NIRSPEC-J	2400	HD 222749	2011 Sep 05
	T7	Keck/NIRSPEC-H	1200	HD 222749	2011 Sep 06
WISE J2357+1227	T6	IRTF/SpeX	1200	HD 210501	2011 Aug 25

Note. — Classification notes: 'pec' - peculiar, 'sb' - spectral binary, ':' - low SNR, 'extremely red' - discussed in §4.2.

Table 6.   New Near-IR Spectroscopy and Spectral Classifications for Other Brown Dwarfs from the Literature

Object Name (1)	NIR Sp. Type (2)	Spectrograph (3)	Int. Time (s) (4)	Tell. Corr. Star (5)	Obs. Date (UT) (6)	Published NIR Sp. Type (7)	Discovery Paper (8)
WISE J0920+4538	L9 sb?	Palomar/TSpec	1440	HD 89239	2012 Jan 07	L4/5 Candidate	Aberasturi et al. (2011)
ULAS J095047.28+011734.3	T8	Magellan/FIRE	1080	HD 75159	2012 May 05	T8	Leggett et al. (2012)
WISE J1246−3139	T1	Palomar/TSpec	1440	HD 109134	2012 Jan 07	IR Source	Andrei et al. (2011)
LHS 2803B	T5.5	IRTF/SpeX	1440	HD 134013	2012 May 13	T5.5	Deacon et al. (2012)
BD +01°2920B	T8	Magellan/FIRE	1440	HD 113147	2012 May 05	T8p	Pinfield et al. (2012)
WISE J1449+1147	T5 pec	Palomar/TSpec	3600	HD 131951	2011 May 12	T7 Candidate	Scholz (2010)
	T5 pec	Gemini/GNIRS	2400	HD 147295	2011 Jul 04	—	—
PSO J226.2599−28.8959	T2:	Palomar/TSpec	2400	HD 133652	2011 May 13	T1.5	Deacon et al. (2011)
VHS J154352.78−043909.6	T5:	IRTF/SpeX	720	HD 148968	2011 Aug 25	T4.5	Lodieu et al. (2012)
PSO J246.4222+15.4698	T4.5:	Palomar/TSpec	2400	HD 145122	2011 May 13	T4.5	Deacon et al. (2011)
PSO J247.3273+03.5932	T2	Palomar/TSpec	2400	HD 140775	2011 May 13	T2	Deacon et al. (2011)
WISE J1717+6129	T8	Gemini/GNIRS	2400	HD 199217	2011 Jun 14	T8:	Kirkpatrick et al. (2011)
WISE J1809+3838	T7.5	IRTF/SpeX	1800	HD 174567	2011 Jul 28	T7	Luhman et al. (2012)
WISE J2342+0856	T6.5	IRTF/SpeX	1920	HD 210501	2011 Sep 11	T7 Candidate	Scholz (2010)
WISE J2344+1034	T9	Gemini/GNIRS	6600	HD 222749	2011 Jun 15	T9:	Kirkpatrick et al. (2011)

Note. — Classification notes: 'pec' - peculiar, 'sb' - spectral binary, ':' - low SNR.

Table 7. Modified Spectral Indices Based on Median Fluxes

Object Name J2000 Coordinates (1)	Instrument (2)	NIR Sp. Type (3)	H_2O-J (4)	CH_4-J (5)	H_2O-H (6)	CH_4-H (7)	W_J (8)	NH_3-H (9)	J-narrow (10)
				T and Y Dwarf Standards					
SDSS J1207+0244	IRTF/SpeX[a]	T0	0.622 ± 0.005	0.847 ± 0.007	0.622 ± 0.008	0.958 ± 0.006	0.810 ± 0.016	0.864 ± 0.008	0.962 ± 0.008
SDSS J0151+1244	IRTF/SpeX[a]	T1	0.654 ± 0.008	0.714 ± 0.015	0.628 ± 0.013	0.954 ± 0.010	0.856 ± 0.020	0.864 ± 0.014	0.955 ± 0.012
SDSSp J1254−0122	IRTF/SpeX[a]	T2	0.477 ± 0.008	0.756 ± 0.012	0.476 ± 0.012	0.909 ± 0.010	0.752 ± 0.024	0.778 ± 0.016	0.930 ± 0.011
2MASS J1209−1004	IRTF/SpeX[a]	T3	0.415 ± 0.008	0.661 ± 0.014	0.436 ± 0.012	0.715 ± 0.011	0.688 ± 0.024	0.789 ± 0.017	0.897 ± 0.015
2MASSI J2254+3123	IRTF/SpeX[a]	T4	0.372 ± 0.005	0.628 ± 0.007	0.377 ± 0.007	0.587 ± 0.008	0.634 ± 0.008	0.766 ± 0.008	0.879 ± 0.006
2MASS J1503+2525	IRTF/SpeX[a]	T5	0.242 ± 0.003	0.443 ± 0.011	0.325 ± 0.010	0.412 ± 0.007	0.560 ± 0.012	0.773 ± 0.010	0.885 ± 0.005
SDSSp J1624+0029	IRTF/SpeX[a]	T6	0.155 ± 0.002	0.384 ± 0.010	0.278 ± 0.012	0.309 ± 0.007	0.478 ± 0.016	0.740 ± 0.014	0.884 ± 0.009
2MASSI J0727+1710	IRTF/SpeX[a]	T7	0.088 ± 0.004	0.304 ± 0.006	0.212 ± 0.014	0.191 ± 0.008	0.426 ± 0.012	0.670 ± 0.019	0.929 ± 0.013
2MASSI J0415−0935	IRTF/SpeX[a]	T8	0.042 ± 0.002	0.208 ± 0.004	0.172 ± 0.007	0.109 ± 0.004	0.296 ± 0.012	0.626 ± 0.009	0.904 ± 0.006
UGPS J0722−0540	IRTF/SpeX	T9	0.041 ± 0.027	0.156 ± 0.026	0.104 ± 0.040	0.086 ± 0.036	0.204 ± 0.052	0.556 ± 0.056	0.862 ± 0.040
WISEPA J1738+2732	HST/WFC3	Y0	0.039 ± 0.009	0.052 ± 0.010	0.050 ± 0.011	—	0.122 ± 0.028	0.320 ± 0.025	0.839 ± 0.027
				T Dwarf Discoveries from Kirkpatrick et al. (2011)					
WISE J0008−1739	Keck/NIRSPEC-J	T6	0.142 ± 0.033	0.402 ± 0.042	—	—	0.466 ± 0.028	—	0.877 ± 0.057
WISE J0123+4142	Keck/NIRSPEC-J	T7	0.038 ± 0.066	0.282 ± 0.066	—	—	0.418 ± 0.050	—	0.849 ± 0.100
WISE J0138−0322	IRTF/SpeX	T3	0.410 ± 0.008	0.570 ± 0.009	0.539 ± 0.014	0.756 ± 0.010	0.674 ± 0.012	0.858 ± 0.014	0.925 ± 0.012
WISE J0148−7202	Magellan/FIRE	T9.5	-0.016 ± 0.013	0.076 ± 0.013	0.073 ± 0.015	0.023 ± 0.015	0.124 ± 0.014	0.424 ± 0.024	0.829 ± 0.026
WISE J0150+3827	IRTF/SpeX	T0	0.665 ± 0.008	0.845 ± 0.010	0.675 ± 0.011	0.975 ± 0.007	0.818 ± 0.010	0.894 ± 0.011	0.927 ± 0.013
WISE J0221+3842	Palomar/TSpec	T6.5	0.106 ± 0.018	0.256 ± 0.022	0.213 ± 0.031	0.265 ± 0.017	0.346 ± 0.022	0.673 ± 0.034	0.797 ± 0.066
WISE J0223−2932	IRTF/SpeX	T7.5	0.041 ± 0.009	0.160 ± 0.011	0.139 ± 0.020	0.169 ± 0.014	0.372 ± 0.016	0.689 ± 0.031	0.931 ± 0.015
	Keck/NIRSPEC-H	T7	—	—	0.216 ± 0.048	0.178 ± 0.027	—	0.585 ± 0.038	—
WISE J0226−0211	Keck/NIRSPEC-H	T7	—	—	0.260 ± 0.063	0.104 ± 0.033	—	0.582 ± 0.045	—
WISE J0254+0223	IRTF/SpeX	T8	0.047 ± 0.004	0.209 ± 0.005	0.175 ± 0.012	0.114 ± 0.006	0.298 ± 0.006	0.627 ± 0.015	0.900 ± 0.008
WISE J0305+3954	Palomar/TSpec	T6	0.114 ± 0.011	0.351 ± 0.014	0.341 ± 0.016	0.245 ± 0.010	0.420 ± 0.012	0.724 ± 0.017	0.867 ± 0.023
WISE J0307+2904	IRTF/SpeX	T6.5	0.133 ± 0.043	0.361 ± 0.051	0.316 ± 0.070	0.227 ± 0.060	0.438 ± 0.040	0.822 ± 0.101	0.874 ± 0.057
WISE J0313+7807	Palomar/TSpec	T8.5	0.125 ± 0.017	0.108 ± 0.012	0.242 ± 0.020	0.147 ± 0.012	0.320 ± 0.012	0.598 ± 0.025	0.906 ± 0.026
WISE J0323−6025	Magellan/FIRE	T8.5	0.047 ± 0.018	0.170 ± 0.022	0.178 ± 0.021	0.120 ± 0.014	0.260 ± 0.018	0.587 ± 0.030	0.907 ± 0.025
WISE J0333−5856	SOAR/OSIRIS	T3	—	0.558 ± 0.034	0.520 ± 0.021	0.729 ± 0.021	—	0.714 ± 0.025	0.905 ± 0.078
WISE J0410+1411	IRTF/SpeX	T6	0.100 ± 0.036	0.351 ± 0.044	0.268 ± 0.067	0.288 ± 0.055	0.462 ± 0.042	0.742 ± 0.087	0.831 ± 0.048
WISE J0448−1935	IRTF/SpeX	T5 pec	0.206 ± 0.023	0.469 ± 0.028	0.368 ± 0.049	0.428 ± 0.037	0.588 ± 0.024	0.859 ± 0.059	0.908 ± 0.030
WISE J0458+6434	IRTF/SpeX	T8.5	0.038 ± 0.016	0.268 ± 0.023	0.136 ± 0.027	0.084 ± 0.026	0.238 ± 0.024	0.471 ± 0.044	0.846 ± 0.026
WISE J0500−1223	IRTF/SpeX	T8	0.045 ± 0.031	0.206 ± 0.033	0.121 ± 0.049	0.095 ± 0.040	0.332 ± 0.036	0.651 ± 0.070	0.946 ± 0.044
WISE J0513+0608	Palomar/TSpec	T6.5	0.125 ± 0.006	0.325 ± 0.010	0.282 ± 0.008	0.240 ± 0.007	0.414 ± 0.008	0.707 ± 0.013	0.821 ± 0.012
WISE J0525+6739	IRTF/SpeX	T6 pec	0.174 ± 0.012	0.368 ± 0.015	0.310 ± 0.032	0.316 ± 0.023	0.482 ± 0.018	0.808 ± 0.038	0.897 ± 0.018
WISE J0528−3308	Palomar/TSpec	T7 pec	0.009 ± 0.025	0.254 ± 0.019	0.230 ± 0.028	0.210 ± 0.017	0.350 ± 0.016	0.676 ± 0.032	0.842 ± 0.025
WISE J0539−1034	Palomar/TSpec	T5.5	0.195 ± 0.018	0.373 ± 0.023	0.408 ± 0.027	0.327 ± 0.018	0.484 ± 0.016	0.814 ± 0.029	0.906 ± 0.030
WISE J0542−1628	Palomar/TSpec	T6.5	0.143 ± 0.007	0.274 ± 0.010	0.230 ± 0.009	0.240 ± 0.008	0.398 ± 0.008	0.694 ± 0.013	0.852 ± 0.012
WISE J0611−0410	IRTF/SpeX	T0	0.586 ± 0.017	0.727 ± 0.022	0.604 ± 0.021	0.947 ± 0.018	0.776 ± 0.018	0.873 ± 0.020	0.911 ± 0.026
WISE J0612−4920	SOAR/OSIRIS	T3.5	—	0.510 ± 0.057	0.377 ± 0.040	0.684 ± 0.038	—	0.749 ± 0.050	0.882 ± 0.131
WISE J0612−3036	Palomar/TSpec	T6	0.108 ± 0.002	0.312 ± 0.005	0.291 ± 0.003	0.314 ± 0.002	0.446 ± 0.002	0.796 ± 0.005	0.874 ± 0.003
WISE J0614+3912	Palomar/TSpec	T6	0.137 ± 0.016	0.418 ± 0.020	0.346 ± 0.017	0.301 ± 0.013	0.462 ± 0.014	0.794 ± 0.025	0.889 ± 0.029
WISE J0623−0456	IRTF/SpeX	T8	0.015 ± 0.030	0.287 ± 0.035	0.178 ± 0.051	0.094 ± 0.039	0.380 ± 0.036	0.722 ± 0.065	0.880 ± 0.044
WISE J0625+5646	Palomar/TSpec	T6	0.182 ± 0.012	0.310 ± 0.015	0.316 ± 0.016	0.296 ± 0.010	0.418 ± 0.012	0.705 ± 0.018	0.854 ± 0.019
WISE J0627−1114	IRTF/SpeX	T6	0.162 ± 0.005	0.359 ± 0.007	0.294 ± 0.014	0.310 ± 0.010	0.462 ± 0.008	0.733 ± 0.018	0.871 ± 0.009
WISE J0656+4205	IRTF/SpeX	T3	0.467 ± 0.012	0.503 ± 0.016	0.491 ± 0.020	0.810 ± 0.018	0.758 ± 0.018	0.851 ± 0.024	0.907 ± 0.021

Table 7—Continued

Object Name J2000 Coordinates	Instrument	NIR Sp. Type	H$_2$O$-$J	CH$_4-$J	H$_2$O$-$H	CH$_4-$H	W$_J$	NH$_3-$H	J-narrow
(1)	(2)	(3)	(4)	(5)	(6)	(7)	(8)	(9)	(10)
WISE J0744+5628	Palomar/TSpec	T8	0.156 ± 0.028	0.256 ± 0.022	0.186 ± 0.038	0.069 ± 0.024	0.380 ± 0.020	0.630 ± 0.044	0.917 ± 0.040
WISE J0750+2725	Keck/NIRSPEC-JH	T8.5	-0.019 ± 0.016	0.117 ± 0.015	0.239 ± 0.027	0.066 ± 0.008	0.246 ± 0.012	0.576 ± 0.012	0.781 ± 0.021
WISE J0751−7634	Magellan/FIRE	T9	0.025 ± 0.029	0.119 ± 0.017	0.188 ± 0.041	0.121 ± 0.031	0.148 ± 0.020	0.510 ± 0.048	0.848 ± 0.035
WISE J0759−4904	Magellan/FIRE	T8	0.034 ± 0.004	0.160 ± 0.007	0.156 ± 0.008	0.122 ± 0.005	0.260 ± 0.008	0.608 ± 0.012	0.889 ± 0.010
WISE J0819−0335	IRTF/SpeX	T4	0.387 ± 0.006	0.553 ± 0.008	0.387 ± 0.012	0.663 ± 0.010	0.662 ± 0.010	0.781 ± 0.013	0.893 ± 0.011
WISE J0821+1443	IRTF/SpeX	T5.5	0.203 ± 0.013	0.401 ± 0.021	0.307 ± 0.025	0.385 ± 0.021	0.528 ± 0.022	0.715 ± 0.036	0.893 ± 0.026
WISE J0836−1859	Magellan/FIRE	T8 pec	0.045 ± 0.017	0.145 ± 0.017	0.154 ± 0.017	0.124 ± 0.012	0.322 ± 0.016	0.606 ± 0.025	0.905 ± 0.021
WISE J0857+5604	Palomar/TSpec	T8	0.069 ± 0.013	0.150 ± 0.013	0.125 ± 0.018	0.122 ± 0.011	0.296 ± 0.012	0.551 ± 0.023	0.892 ± 0.020
WISE J0906+4735	Palomar/TSpec	T8	0.065 ± 0.186	0.245 ± 0.092	0.234 ± 0.125	0.125 ± 0.057	0.348 ± 0.074	0.642 ± 0.105	0.912 ± 0.161
WISE J0929+0409	Palomar/TSpec	T6.5	0.082 ± 0.014	0.244 ± 0.018	0.273 ± 0.022	0.221 ± 0.014	0.364 ± 0.014	0.684 ± 0.026	0.880 ± 0.021
WISE J0952+1955	IRTF/SpeX	T6	0.159 ± 0.011	0.328 ± 0.014	0.285 ± 0.028	0.346 ± 0.022	0.476 ± 0.018	0.742 ± 0.038	0.915 ± 0.017
WISE J1018−2445	Magellan/FIRE	T8	0.037 ± 0.005	0.151 ± 0.010	0.163 ± 0.006	0.092 ± 0.004	0.282 ± 0.008	0.613 ± 0.015	0.887 ± 0.008
WISE J1019+6529	Palomar/TSpec	T6	0.134 ± 0.046	0.331 ± 0.029	0.293 ± 0.044	0.299 ± 0.024	0.472 ± 0.028	0.753 ± 0.045	0.877 ± 0.054
	IRTF/SpeX	T6	0.126 ± 0.015	0.307 ± 0.020	0.249 ± 0.033	0.326 ± 0.025	0.450 ± 0.022	0.773 ± 0.056	0.887 ± 0.032
WISE J1042−3842	Magellan/FIRE	T8.5	0.022 ± 0.012	0.147 ± 0.015	0.141 ± 0.014	0.116 ± 0.009	0.294 ± 0.016	0.561 ± 0.021	0.863 ± 0.020
WISE J1122+2550	IRTF/SpeX	T6	0.139 ± 0.014	0.350 ± 0.017	0.307 ± 0.031	0.234 ± 0.020	0.480 ± 0.022	0.770 ± 0.054	0.897 ± 0.032
WISE J1150+6302	Palomar/TSpec	T8	0.020 ± 0.013	0.191 ± 0.013	0.133 ± 0.015	0.119 ± 0.011	0.286 ± 0.010	0.604 ± 0.023	0.833 ± 0.019
WISE J1217+1626	Palomar/TSpec	T9	0.061 ± 0.017	0.083 ± 0.013	0.075 ± 0.022	0.099 ± 0.013	0.232 ± 0.012	0.539 ± 0.027	0.842 ± 0.026
WISE J1311+0122	Keck/NIRSPEC-H	T9:	—	—	0.127 ± 0.038	-0.123 ± 0.012	—	0.581 ± 0.015	—
WISE J1320+6034	IRTF/SpeX	T6.5	0.107 ± 0.009	0.101 ± 0.010	0.350 ± 0.028	0.202 ± 0.017	0.498 ± 0.018	0.842 ± 0.045	0.908 ± 0.017
WISE J1322−2340	IRTF/SpeX	T8	0.088 ± 0.014	0.293 ± 0.017	0.266 ± 0.026	0.208 ± 0.021	0.366 ± 0.020	0.705 ± 0.037	0.829 ± 0.024
WISE J1436−1814	Magellan/FIRE	T8 pec	0.061 ± 0.005	0.207 ± 0.009	0.238 ± 0.008	0.161 ± 0.006	0.292 ± 0.008	0.690 ± 0.014	0.855 ± 0.008
WISE J1457+5815	IRTF/SpeX	T7	0.102 ± 0.011	0.223 ± 0.014	0.257 ± 0.025	0.206 ± 0.017	0.412 ± 0.020	0.736 ± 0.036	0.931 ± 0.024
WISE J1506+7027	Palomar/TSpec	T6	0.139 ± 0.001	0.336 ± 0.004	0.271 ± 0.003	0.293 ± 0.002	0.436 ± 0.002	0.720 ± 0.005	0.842 ± 0.003
	Keck/NIRSPEC-H	T6	—	—	0.353 ± 0.016	0.276 ± 0.009	—	0.703 ± 0.014	—
WISE J1519+7009	Palomar/TSpec	T8	0.101 ± 0.200	0.210 ± 0.108	0.181 ± 0.145	0.102 ± 0.069	0.350 ± 0.086	0.654 ± 0.127	0.945 ± 0.178
WISE J1612−3420	Keck/NIRSPEC-H	T6.5	—	—	0.303 ± 0.022	0.227 ± 0.017	—	0.722 ± 0.023	—
WISE J1614+1739	Magellan/FIRE	T9	0.038 ± 0.031	0.116 ± 0.020	0.107 ± 0.037	0.094 ± 0.024	0.202 ± 0.034	0.513 ± 0.050	0.832 ± 0.032
WISE J1617+1807	Magellan/FIRE	T8	0.113 ± 0.241	0.167 ± 0.133	0.211 ± 0.110	0.104 ± 0.063	0.336 ± 0.132	0.594 ± 0.108	0.921 ± 0.211
WISE J1622−0959	IRTF/SpeX	T6	0.177 ± 0.006	0.410 ± 0.009	0.290 ± 0.018	0.328 ± 0.011	0.478 ± 0.012	0.743 ± 0.022	0.866 ± 0.013
WISE J1627+3255	IRTF/SpeX	T6	0.143 ± 0.005	0.386 ± 0.004	0.279 ± 0.012	0.289 ± 0.007	0.454 ± 0.006	0.746 ± 0.013	0.877 ± 0.006
	Keck/NIRSPEC-H	T6	—	—	0.372 ± 0.057	0.280 ± 0.035	—	0.733 ± 0.049	—
WISE J1653+4444	IRTF/SpeX	T8	0.035 ± 0.011	0.244 ± 0.016	0.175 ± 0.022	0.160 ± 0.015	0.276 ± 0.018	0.589 ± 0.038	0.867 ± 0.021
WISE J1711+3500	IRTF/SpeX	T8	-0.009 ± 0.018	0.260 ± 0.025	0.213 ± 0.034	0.181 ± 0.025	0.362 ± 0.026	0.700 ± 0.045	0.900 ± 0.046
WISE J1717+6129	Keck/NIRSPEC-JH	T8	0.094 ± 0.038	0.174 ± 0.039	0.192 ± 0.042	0.114 ± 0.024	0.288 ± 0.030	0.511 ± 0.030	0.904 ± 0.063
WISE J1728+5716	IRTF/SpeX	T6	0.136 ± 0.015	0.412 ± 0.021	0.265 ± 0.031	0.284 ± 0.022	0.444 ± 0.024	0.714 ± 0.040	0.871 ± 0.025
WISE J1741+2553	Magellan/FIRE	T9	0.023 ± 0.071	0.155 ± 0.045	0.123 ± 0.031	0.063 ± 0.019	0.230 ± 0.048	0.578 ± 0.047	0.907 ± 0.069
WISE J1804+3117	Keck/NIRSPEC-H	T9.5:	—	—	—	—	—	0.345 ± 0.042	—
WISE J1812+2721	Magellan/FIRE	T8.5:	0.042 ± 0.042	0.099 ± 0.033	0.128 ± 0.055	0.188 ± 0.061	0.202 ± 0.030	0.583 ± 0.097	0.930 ± 0.069
WISE J1841+7000	Palomar/TSpec	T5	0.237 ± 0.016	0.489 ± 0.020	0.436 ± 0.018	0.398 ± 0.010	0.564 ± 0.012	0.818 ± 0.018	0.919 ± 0.019
WISE J1852+3537	IRTF/SpeX	T7	0.070 ± 0.010	0.235 ± 0.011	0.219 ± 0.025	0.170 ± 0.012	0.382 ± 0.016	0.731 ± 0.029	0.868 ± 0.018
WISE J1906+4508	IRTF/SpeX	T6	0.184 ± 0.005	0.384 ± 0.006	0.316 ± 0.017	0.333 ± 0.010	0.516 ± 0.008	0.754 ± 0.019	0.907 ± 0.011
WISE J1952+7240	Palomar/TSpec	T4	0.350 ± 0.005	0.567 ± 0.009	0.384 ± 0.007	0.527 ± 0.006	0.620 ± 0.006	0.788 ± 0.009	0.878 ± 0.009
WISE J1959−3338	Palomar/TSpec	T8	0.049 ± 0.013	0.212 ± 0.011	0.245 ± 0.011	0.138 ± 0.005	0.308 ± 0.008	0.652 ± 0.013	0.894 ± 0.011
WISE J2018−7423	Magellan/FIRE	T7	0.086 ± 0.004	0.307 ± 0.009	0.227 ± 0.008	0.241 ± 0.005	0.384 ± 0.008	0.692 ± 0.018	0.879 ± 0.008
WISE J2134−7137	Magellan/FIRE	T9 pec	0.019 ± 0.015	0.094 ± 0.018	0.106 ± 0.020	0.070 ± 0.019	0.172 ± 0.016	0.452 ± 0.031	0.780 ± 0.020
WISE J2157+2659	Palomar/TSpec	T7	0.036 ± 0.004	0.231 ± 0.006	0.206 ± 0.004	0.185 ± 0.002	0.314 ± 0.004	0.670 ± 0.007	0.859 ± 0.006
WISE J2209−2734	Keck/NIRSPEC-H	T7	—	—	0.290 ± 0.055	0.240 ± 0.033	—	0.705 ± 0.044	—
WISE J2213+0911	IRTF/SpeX	T7	0.109 ± 0.006	0.313 ± 0.008	0.238 ± 0.016	0.219 ± 0.010	0.390 ± 0.012	0.690 ± 0.022	0.884 ± 0.011

Table 7—Continued

Object Name J2000 Coordinates	Instrument	NIR Sp. Type	H$_2$O$-$J	CH$_4-$J	H$_2$O$-$H	CH$_4-$H	W$_J$	NH$_3-$H	J-narrow
(1)	(2)	(3)	(4)	(5)	(6)	(7)	(8)	(9)	(10)
WISE J2226+0440	IRTF/SpeX	T8	0.053 ± 0.006	0.193 ± 0.008	0.217 ± 0.018	0.118 ± 0.009	0.352 ± 0.012	0.659 ± 0.024	0.923 ± 0.013
	Keck/NIRSPEC-JH	T8.5	0.062 ± 0.039	0.064 ± 0.042	0.314 ± 0.034	0.099 ± 0.018	0.456 ± 0.034	0.669 ± 0.027	1.018 ± 0.070
WISE J2237−0614	IRTF/SpeX	T5	0.206 ± 0.015	0.374 ± 0.018	0.403 ± 0.033	0.415 ± 0.024	0.602 ± 0.020	0.863 ± 0.036	0.917 ± 0.023
WISE J2239+1617	IRTF/SpeX	T3	0.417 ± 0.006	0.645 ± 0.007	0.510 ± 0.012	0.727 ± 0.007	0.682 ± 0.008	0.818 ± 0.013	0.932 ± 0.009
WISE J2255−3118	IRTF/SpeX	T8	0.037 ± 0.011	0.300 ± 0.015	0.159 ± 0.022	0.101 ± 0.014	0.254 ± 0.014	0.597 ± 0.033	0.894 ± 0.017
	Keck/NIRSPEC-H	T8	—	—	0.205 ± 0.033	0.097 ± 0.019	—	0.462 ± 0.024	—
WISE J2313−8037	Magellan/FIRE	T8	0.041 ± 0.004	0.163 ± 0.010	0.155 ± 0.007	0.136 ± 0.006	0.268 ± 0.012	0.555 ± 0.017	0.861 ± 0.009
WISE J2319−1844	IRTF/SpeX	T7.5	0.078 ± 0.019	0.309 ± 0.024	0.181 ± 0.038	0.122 ± 0.028	0.336 ± 0.024	0.587 ± 0.048	0.832 ± 0.026
WISE J2325−4105	Magellan/FIRE	T9 pec	0.011 ± 0.017	0.146 ± 0.024	0.062 ± 0.022	0.118 ± 0.019	0.184 ± 0.016	0.461 ± 0.027	0.799 ± 0.030
WISE J2340−0745	IRTF/SpeX	T7	0.115 ± 0.005	0.299 ± 0.007	0.255 ± 0.015	0.225 ± 0.008	0.422 ± 0.008	0.739 ± 0.017	0.883 ± 0.010
WISE J2343−7418	Magellan/FIRE	T6	0.184 ± 0.007	0.411 ± 0.014	0.289 ± 0.010	0.320 ± 0.008	0.492 ± 0.010	0.726 ± 0.018	0.818 ± 0.011
WISE J2344+1034	Keck/NIRSPEC-J	T9	-0.001 ± 0.023	0.119 ± 0.019	—	—	0.148 ± 0.016	—	0.944 ± 0.032
WISE J2348−1028	IRTF/SpeX	T7	0.079 ± 0.006	0.226 ± 0.008	0.213 ± 0.016	0.153 ± 0.011	0.388 ± 0.010	0.714 ± 0.023	0.883 ± 0.012
WISE J2359−7335	Magellan/FIRE	T6.5	0.074 ± 0.005	0.256 ± 0.010	0.260 ± 0.007	0.232 ± 0.005	0.346 ± 0.008	0.670 ± 0.015	0.846 ± 0.008
					New T Dwarf Discoveries				
WISE J0005+3737	Keck/NIRSPEC-J	T9	0.006 ± 0.019	0.130 ± 0.017	—	—	0.236 ± 0.014	—	0.884 ± 0.024
WISE J0038+2758	Keck/NIRSPEC-J	T9	-0.026 ± 0.010	0.097 ± 0.011	—	—	0.164 ± 0.010	—	0.869 ± 0.015
WISE J0038+8405	Keck/NIRSPEC-J	T6	0.155 ± 0.006	0.417 ± 0.020	—	—	0.452 ± 0.008	—	0.857 ± 0.011
WISE J0040+0900	IRTF/SpeX	T7	0.091 ± 0.005	0.295 ± 0.007	0.242 ± 0.016	0.233 ± 0.010	0.380 ± 0.010	0.678 ± 0.021	0.885 ± 0.012
WISE J0045+3611	IRTF/SpeX	T5	0.202 ± 0.004	0.382 ± 0.006	0.323 ± 0.013	0.405 ± 0.010	0.498 ± 0.008	0.716 ± 0.016	0.905 ± 0.010
WISE J0049+2151	IRTF/SpeX	T8.5	0.026 ± 0.005	0.166 ± 0.006	0.167 ± 0.013	0.093 ± 0.007	0.304 ± 0.008	0.569 ± 0.018	0.947 ± 0.011
WISE J0135+1715	IRTF/SpeX	T6	0.147 ± 0.015	0.353 ± 0.019	0.313 ± 0.033	0.284 ± 0.025	0.518 ± 0.024	0.737 ± 0.042	0.899 ± 0.028
WISE J0210+4008	IRTF/SpeX	T4.5	0.335 ± 0.008	0.473 ± 0.010	0.388 ± 0.019	0.491 ± 0.014	0.636 ± 0.012	0.809 ± 0.021	0.869 ± 0.013
WISE J0233+3030	IRTF/SpeX	T6	0.218 ± 0.010	0.382 ± 0.014	0.358 ± 0.024	0.332 ± 0.020	0.536 ± 0.018	0.750 ± 0.038	0.871 ± 0.021
WISE J0245−3450	IRTF/SpeX	T8	0.050 ± 0.017	0.208 ± 0.021	0.196 ± 0.032	0.133 ± 0.024	0.324 ± 0.024	0.637 ± 0.048	0.940 ± 0.025
WISE J0247+3725	Gemini/GNIRS	T8	0.025 ± 0.007	0.173 ± 0.010	0.154 ± 0.009	0.098 ± 0.008	0.272 ± 0.008	0.571 ± 0.022	0.870 ± 0.012
WISE J0259−0346	Keck/NIRSPEC-J	T5	0.210 ± 0.031	0.438 ± 0.036	—	—	0.526 ± 0.024	—	0.897 ± 0.045
WISE J0316+3820	Palomar/TSpec	T3	0.415 ± 0.017	0.570 ± 0.018	0.509 ± 0.012	0.676 ± 0.009	0.686 ± 0.016	0.821 ± 0.014	0.884 ± 0.021
WISE J0316+4307	Keck/NIRSPEC-JH	T8	-0.119 ± 0.025	0.214 ± 0.017	0.179 ± 0.043	0.074 ± 0.030	0.230 ± 0.012	0.575 ± 0.036	0.840 ± 0.018
WISE J0321−7347	Magellan/FIRE	T8	0.052 ± 0.013	0.166 ± 0.012	0.163 ± 0.014	0.101 ± 0.009	0.216 ± 0.010	0.685 ± 0.013	0.933 ± 0.015
WISE J0325−3854	Keck/NIRSPEC-J	T9	0.019 ± 0.041	0.135 ± 0.025	—	—	0.228 ± 0.018	—	0.861 ± 0.036
WISE J0325+0831	IRTF/SpeX	T7	0.097 ± 0.007	0.260 ± 0.009	0.295 ± 0.015	0.240 ± 0.012	0.412 ± 0.012	0.687 ± 0.026	0.897 ± 0.012
WISE J0335+4310	Keck/NIRSPEC-J	T9	0.051 ± 0.013	0.138 ± 0.015	—	—	0.231 ± 0.011	—	0.820 ± 0.019
WISE J0336−0143	Keck/NIRSPEC-J	T8:	—	0.055 ± 0.022	—	—	0.216 ± 0.044	—	0.947 ± 0.248
WISE J0336+2826	IRTF/SpeX	T5	0.311 ± 0.011	0.464 ± 0.016	0.371 ± 0.020	0.487 ± 0.021	0.588 ± 0.018	0.784 ± 0.030	0.867 ± 0.020
WISE J0413−4750	Magellan/FIRE	T9	0.007 ± 0.009	0.034 ± 0.027	0.123 ± 0.059	0.015 ± 0.015	0.154 ± 0.052	0.564 ± 0.038	0.943 ± 0.020
WISE J0424+0727	Keck/NIRSPEC-J	T7.5	0.048 ± 0.009	0.225 ± 0.016	—	—	0.356 ± 0.010	—	0.911 ± 0.015
WISE J0430+4633	Keck/NIRSPEC-J	T8	0.045 ± 0.008	0.210 ± 0.017	—	—	0.278 ± 0.008	—	0.839 ± 0.013
WISE J0512−3004	Keck/NIRSPEC-J	T8.5	0.092 ± 0.015	0.106 ± 0.014	—	—	0.231 ± 0.013	—	0.918 ± 0.021
WISE J0540+4832	Keck/NIRSPEC-J	T8.5	0.078 ± 0.008	0.144 ± 0.010	—	—	0.249 ± 0.007	—	0.877 ± 0.011
WISE J0546−0959	IRTF/SpeX	T5	0.234 ± 0.008	0.550 ± 0.013	0.355 ± 0.022	0.402 ± 0.015	0.602 ± 0.014	0.763 ± 0.029	0.973 ± 0.019
WISE J0614+0951	Palomar/TSpec	T7	0.109 ± 0.001	0.287 ± 0.002	0.285 ± 0.002	0.212 ± 0.002	0.348 ± 0.002	0.712 ± 0.003	0.826 ± 0.003
WISE J0629+2418	IRTF/SpeX	T2 sb	0.451 ± 0.013	0.691 ± 0.019	0.561 ± 0.021	0.839 ± 0.017	0.662 ± 0.022	0.852 ± 0.024	0.925 ± 0.020
WISE J0642+4101	Palomar/TSpec	extr. red	0.539 ± 0.003	0.881 ± 0.003	0.606 ± 0.002	1.202 ± 0.003	0.738 ± 0.002	0.834 ± 0.002	0.949 ± 0.003
WISE J0701+6321	Palomar/TSpec	T3	0.390 ± 0.001	0.685 ± 0.002	0.475 ± 0.001	0.790 ± 0.001	0.646 ± 0.002	0.819 ± 0.002	0.914 ± 0.002
WISE J0723+3403	Keck/NIRSPEC-J	T9:	—	—	—	—	0.142 ± 0.063	—	0.885 ± 0.101
WISE J0733+7544	Palomar/TSpec	T6	0.141 ± 0.002	0.366 ± 0.003	0.309 ± 0.003	0.323 ± 0.003	0.444 ± 0.002	0.746 ± 0.004	0.845 ± 0.004

Table 7—Continued

Object Name J2000 Coordinates	Instrument	NIR Sp. Type	H$_2$O$-$J	CH$_4$$-$J	H$_2$O$-$H	CH$_4$$-$H	W$_J$	NH$_3$$-$H	J-narrow
(1)	(2)	(3)	(4)	(5)	(6)	(7)	(8)	(9)	(10)
WISE J0754+7909	Palomar/TSpec	extr. red	0.476 ± 0.003	0.800 ± 0.004	0.443 ± 0.003	1.081 ± 0.002	0.774 ± 0.002	0.815 ± 0.003	0.978 ± 0.003
WISE J0811−8051	Magellan/FIRE	T9.5:	0.034 ± 0.058	0.037 ± 0.030	-0.198 ± 0.067	-0.072 ± 0.047	0.146 ± 0.024	0.584 ± 0.071	0.900 ± 0.052
WISE J0812+4021	Gemini/GNIRS	T8	0.054 ± 0.005	0.204 ± 0.009	0.221 ± 0.009	0.118 ± 0.008	0.308 ± 0.008	0.671 ± 0.016	0.881 ± 0.011
WISE J1025+0307	Magellan/FIRE	T8.5	0.025 ± 0.003	0.118 ± 0.004	0.111 ± 0.003	0.079 ± 0.002	0.242 ± 0.004	0.547 ± 0.005	0.877 ± 0.006
WISE J1039−1600	IRTF/SpeX	T7.5	0.090 ± 0.015	0.296 ± 0.021	0.180 ± 0.032	0.141 ± 0.022	0.314 ± 0.024	0.637 ± 0.046	0.865 ± 0.026
WISE J1050+5056	Keck/NIRSPEC-J	T8	0.041 ± 0.013	0.210 ± 0.017	—	—	0.321 ± 0.010	—	0.842 ± 0.017
WISE J1051−2138	Palomar/TSpec	T9:	0.138 ± 0.012	0.122 ± 0.008	0.223 ± 0.012	0.081 ± 0.007	0.282 ± 0.006	0.543 ± 0.014	0.941 ± 0.014
WISE J1124−0421	IRTF/SpeX	T7	0.108 ± 0.006	0.324 ± 0.008	0.235 ± 0.018	0.229 ± 0.011	0.366 ± 0.010	0.623 ± 0.023	0.862 ± 0.011
WISE J1143+4431	Keck/NIRSPEC-J	T8.5	0.071 ± 0.034	0.165 ± 0.024	—	—	0.238 ± 0.019	—	0.839 ± 0.038
WISE J1221−3136	IRTF/SpeX	T6.5	0.139 ± 0.008	0.341 ± 0.011	0.285 ± 0.026	0.262 ± 0.016	0.424 ± 0.016	0.633 ± 0.034	0.830 ± 0.016
WISE J1225−1013	IRTF/SpeX	T6	0.161 ± 0.006	0.417 ± 0.008	0.276 ± 0.016	0.303 ± 0.012	0.466 ± 0.010	0.744 ± 0.023	0.875 ± 0.011
WISE J1250+2628	Keck/NIRSPEC-J	T6.5	0.131 ± 0.004	0.349 ± 0.010	—	—	0.412 ± 0.008	—	0.802 ± 0.008
WISE J1257+4008	IRTF/SpeX	T7	0.100 ± 0.013	0.390 ± 0.019	0.217 ± 0.029	0.188 ± 0.020	0.385 ± 0.021	0.668 ± 0.044	0.801 ± 0.022
WISE J1301−0302	Keck/NIRSPEC-J	T8.5	-0.002 ± 0.024	0.194 ± 0.022	—	—	0.265 ± 0.015	—	0.861 ± 0.026
WISE J1318−1758	Palomar/TSpec	T9:	0.080 ± 0.006	0.115 ± 0.005	0.146 ± 0.007	0.121 ± 0.005	0.236 ± 0.006	0.652 ± 0.010	0.906 ± 0.009
WISE J1337+2636	Keck/NIRSPEC-J	T5	0.182 ± 0.007	0.407 ± 0.013	—	—	0.518 ± 0.010	—	0.870 ± 0.012
WISE J1400−3850	IRTF/SpeX	T4	0.402 ± 0.018	0.614 ± 0.022	0.439 ± 0.026	0.553 ± 0.021	0.708 ± 0.020	0.867 ± 0.028	0.910 ± 0.022
WISE J1517+0529	Keck/NIRSPEC-J	T8	0.079 ± 0.032	0.177 ± 0.026	—	—	0.297 ± 0.018	—	0.870 ± 0.036
WISE J1523+3125	Gemini/GNIRS	T6.5 pec	0.084 ± 0.010	0.334 ± 0.020	0.219 ± 0.014	0.280 ± 0.020	0.380 ± 0.012	0.669 ± 0.027	0.881 ± 0.017
WISE J1542+2230	HST/WFC3	T9.5	0.015 ± 0.016	0.100 ± 0.017	0.108 ± 0.016	0.116 ± 0.017	0.166 ± 0.022	0.419 ± 0.031	0.782 ± 0.034
WISE J1544+5842	Keck/NIRSPEC-J	T7.5	0.086 ± 0.038	0.205 ± 0.037	—	—	0.370 ± 0.028	—	0.975 ± 0.060
WISE J1632+0329	IRTF/SpeX	T5	0.222 ± 0.017	0.421 ± 0.022	0.243 ± 0.031	0.452 ± 0.030	0.536 ± 0.024	0.795 ± 0.050	0.894 ± 0.041
WISE J1636−0743	IRTF/SpeX	T4.5	0.390 ± 0.024	0.670 ± 0.029	0.363 ± 0.037	0.601 ± 0.030	0.694 ± 0.028	0.794 ± 0.050	0.947 ± 0.037
WISE J1707−1744	Palomar/TSpec	T5:	0.228 ± 0.014	0.393 ± 0.019	0.307 ± 0.017	0.425 ± 0.013	0.540 ± 0.014	0.789 ± 0.022	0.891 ± 0.023
WISE J1721+1117	IRTF/SpeX	T6	0.149 ± 0.019	0.435 ± 0.026	0.240 ± 0.039	0.294 ± 0.032	0.444 ± 0.026	0.688 ± 0.058	0.876 ± 0.034
WISE J1730+4207	IRTF/SpeX	T0 sb	0.551 ± 0.011	0.758 ± 0.016	0.636 ± 0.017	0.832 ± 0.013	0.754 ± 0.016	0.869 ± 0.019	0.890 ± 0.019
WISE J1734+5023	IRTF/SpeX	T4	0.398 ± 0.007	0.392 ± 0.006	0.449 ± 0.013	0.528 ± 0.010	0.678 ± 0.010	0.840 ± 0.014	0.892 ± 0.011
WISE J1736+6059	Keck/NIRSPEC-J	T8	0.075 ± 0.010	0.195 ± 0.015	—	—	0.274 ± 0.009	—	0.803 ± 0.016
WISE J1738+6142	Palomar/TSpec	extr. red	0.553 ± 0.040	0.882 ± 0.045	0.647 ± 0.017	1.139 ± 0.016	0.700 ± 0.036	0.829 ± 0.017	0.955 ± 0.066
	IRTF/SpeX	extr. red	0.572 ± 0.026	0.892 ± 0.036	0.632 ± 0.024	1.087 ± 0.023	0.847 ± 0.031	0.822 ± 0.024	0.992 ± 0.038
WISE J1741+1327	IRTF/SpeX	T5	0.249 ± 0.020	0.486 ± 0.024	0.362 ± 0.036	0.366 ± 0.030	0.564 ± 0.024	0.726 ± 0.047	0.884 ± 0.029
WISE J1743+4211	Palomar/TSpec	T4.5	0.380 ± 0.006	0.562 ± 0.011	0.392 ± 0.007	0.511 ± 0.006	0.614 ± 0.008	0.768 ± 0.010	0.871 ± 0.011
WISE J1745+6459	Keck/NIRSPEC-J	T7	0.155 ± 0.020	0.297 ± 0.023	—	—	0.393 ± 0.015	—	0.854 ± 0.026
WISE J1746−0338	Palomar/TSpec	T6	0.180 ± 0.012	0.348 ± 0.016	0.337 ± 0.015	0.303 ± 0.011	0.470 ± 0.012	0.764 ± 0.020	0.893 ± 0.017
WISE J1755+1803	Palomar/TSpec	T2	0.531 ± 0.009	0.720 ± 0.012	0.526 ± 0.008	0.857 ± 0.006	0.706 ± 0.010	0.835 ± 0.008	0.906 ± 0.014
WISE J1759+5442	Keck/NIRSPEC-J	T7	0.111 ± 0.016	0.247 ± 0.019	—	—	0.363 ± 0.012	—	0.894 ± 0.021
WISE J1809−0448	IRTF/SpeX	T0.5	0.622 ± 0.008	0.781 ± 0.009	0.607 ± 0.012	0.948 ± 0.010	0.826 ± 0.010	0.878 ± 0.012	0.925 ± 0.010
WISE J1812+2007	Keck/NIRSPEC-J	T9	0.014 ± 0.023	0.135 ± 0.021	—	—	0.204 ± 0.016	—	0.900 ± 0.035
WISE J1813+2835	Keck/NIRSPEC-J	T8	0.044 ± 0.005	0.170 ± 0.010	—	—	0.267 ± 0.007	—	0.859 ± 0.009
WISE J1840+2932	Keck/NIRSPEC-J	T6	0.194 ± 0.018	0.339 ± 0.027	—	—	0.467 ± 0.015	—	0.895 ± 0.028
WISE J1909−5204	Magellan/FIRE	T5.5	0.222 ± 0.007	0.484 ± 0.011	0.330 ± 0.009	0.329 ± 0.007	0.504 ± 0.009	0.761 ± 0.012	0.841 ± 0.011
WISE J1913+6444	Palomar/TSpec	T5:	0.296 ± 0.023	0.509 ± 0.027	0.367 ± 0.027	0.426 ± 0.020	0.538 ± 0.020	0.837 ± 0.033	0.911 ± 0.033
WISE J1928+2356	IRTF/SpeX	T6	0.175 ± 0.001	0.431 ± 0.002	0.294 ± 0.003	0.357 ± 0.003	0.520 ± 0.002	0.695 ± 0.004	0.912 ± 0.003
WISE J1954+6915	Keck/NIRSPEC-J	T5.5	0.189 ± 0.011	0.473 ± 0.018	—	—	0.500 ± 0.010	—	0.895 ± 0.015
WISE J1955−2540	Keck/NIRSPEC-J	T8	0.005 ± 0.013	0.151 ± 0.015	—	—	0.266 ± 0.010	—	0.875 ± 0.017
WISE J2008−0834	IRTF/SpeX	T5.5	0.205 ± 0.006	0.318 ± 0.007	0.344 ± 0.022	0.364 ± 0.013	0.552 ± 0.012	0.835 ± 0.025	0.904 ± 0.013
WISE J2014+0424	Gemini/GNIRS	T6.5 pec	0.083 ± 0.006	0.291 ± 0.013	0.202 ± 0.010	0.275 ± 0.010	0.400 ± 0.008	0.726 ± 0.018	0.919 ± 0.013
WISE J2015+6646	Palomar/TSpec	T8	0.072 ± 0.013	0.191 ± 0.014	0.167 ± 0.015	0.156 ± 0.010	0.324 ± 0.012	0.604 ± 0.020	0.839 ± 0.019
WISE J2019−1148	Palomar/TSpec	T8:	0.062 ± 0.036	0.122 ± 0.021	0.162 ± 0.030	0.135 ± 0.020	0.234 ± 0.020	0.649 ± 0.037	0.924 ± 0.042

Table 7—Continued

Object Name J2000 Coordinates	Instrument	NIR Sp. Type	H_2O-J	CH_4-J	H_2O-H	CH_4-H	W_J	NH_3-H	J-narrow
(1)	(2)	(3)	(4)	(5)	(6)	(7)	(8)	(9)	(10)
WISE J2030+0749	IRTF/SpeX	T1.5	0.603 ± 0.003	0.787 ± 0.003	0.580 ± 0.003	0.885 ± 0.003	0.806 ± 0.004	0.863 ± 0.004	0.916 ± 0.004
WISE J2043+6220	IRTF/SpeX	T1.5	0.561 ± 0.012	0.639 ± 0.014	0.545 ± 0.017	0.923 ± 0.014	0.800 ± 0.017	0.890 ± 0.020	0.943 ± 0.017
WISE J2123−2614	IRTF/SpeX	T5.5	0.230 ± 0.022	0.452 ± 0.027	0.266 ± 0.051	0.334 ± 0.040	0.542 ± 0.030	0.840 ± 0.061	0.930 ± 0.031
WISE J2147−1029	Keck/NIRSPEC-J	T7.5	0.071 ± 0.011	0.212 ± 0.016	—	—	0.339 ± 0.010	—	0.888 ± 0.015
WISE J2236+5105	Palomar/TSpec	T5.5	0.186 ± 0.001	0.406 ± 0.001	0.296 ± 0.001	0.439 ± 0.001	0.474 ± 0.000	0.712 ± 0.002	0.826 ± 0.001
WISE J2237+7228	Keck/NIRSPEC-J	T6	0.172 ± 0.006	0.389 ± 0.014	—	—	0.478 ± 0.010	—	0.881 ± 0.012
WISE J2301+0216	IRTF/SpeX	T6.5	0.135 ± 0.008	0.308 ± 0.012	0.309 ± 0.021	0.256 ± 0.014	0.440 ± 0.014	0.766 ± 0.029	0.867 ± 0.018
WISE J2303+1914	Palomar/TSpec	T4:	0.409 ± 0.004	0.557 ± 0.005	0.372 ± 0.005	0.538 ± 0.003	0.664 ± 0.004	0.847 ± 0.005	0.906 ± 0.007
WISE J2335+4222	Keck/NIRSPEC-JH	T7	0.101 ± 0.011	0.275 ± 0.020	0.295 ± 0.018	0.215 ± 0.014	0.384 ± 0.012	0.674 ± 0.019	0.891 ± 0.019
WISE J2357+1227	IRTF/SpeX	T6	0.145 ± 0.007	0.452 ± 0.010	0.257 ± 0.017	0.267 ± 0.012	0.408 ± 0.010	0.682 ± 0.025	0.838 ± 0.013
T Dwarfs from Table 6									
WISE J0920+4538	Palomar/TSpec	L9 sb?	0.603 ± 0.001	0.865 ± 0.002	0.613 ± 0.002	0.998 ± 0.001	0.774 ± 0.002	0.876 ± 0.002	0.949 ± 0.002
ULAS J0950+0117	Magellan/FIRE	T8	0.050 ± 0.003	0.220 ± 0.006	0.159 ± 0.003	0.160 ± 0.003	0.344 ± 0.005	0.592 ± 0.007	0.936 ± 0.007
WISE J1246−3139	Palomar/TSpec	T1	0.542 ± 0.002	0.791 ± 0.002	0.548 ± 0.002	0.905 ± 0.001	0.784 ± 0.002	0.877 ± 0.002	0.939 ± 0.002
LHS 2803B	IRTF/SpeX	T5.5	0.168 ± 0.009	0.308 ± 0.012	0.285 ± 0.029	0.432 ± 0.021	0.540 ± 0.017	0.726 ± 0.037	0.920 ± 0.019
BD +01°2920B	Magellan/FIRE	T8	0.052 ± 0.007	0.206 ± 0.007	0.218 ± 0.010	0.156 ± 0.008	0.321 ± 0.007	0.686 ± 0.016	0.862 ± 0.009
WISE J1449+1147	Gemini/GNIRS	T5 pec	0.223 ± 0.006	0.436 ± 0.012	0.292 ± 0.008	0.415 ± 0.010	0.552 ± 0.010	0.781 ± 0.015	0.915 ± 0.012
	Palomar/TSpec	T5 pec	0.236 ± 0.015	0.392 ± 0.019	0.310 ± 0.018	0.423 ± 0.013	0.550 ± 0.014	0.792 ± 0.023	0.893 ± 0.023
PSOJ226.25−28.89	Palomar/TSpec	T2:	0.687 ± 0.014	0.736 ± 0.015	0.571 ± 0.009	0.847 ± 0.007	0.798 ± 0.010	0.842 ± 0.009	0.926 ± 0.012
VHS J1543−0439	IRTF/SpeX	T5:	0.325 ± 0.024	0.477 ± 0.029	0.372 ± 0.040	0.486 ± 0.037	0.624 ± 0.034	0.681 ± 0.051	0.876 ± 0.050
PSOJ246.42+15.46	Palomar/TSpec	T4.5:	0.315 ± 0.014	0.500 ± 0.017	0.396 ± 0.014	0.465 ± 0.011	0.602 ± 0.012	0.818 ± 0.018	0.883 ± 0.019
PSOJ247.32+03.59	Palomar/TSpec	T2	0.443 ± 0.004	0.684 ± 0.007	0.449 ± 0.003	0.909 ± 0.004	0.684 ± 0.004	0.764 ± 0.005	0.935 ± 0.005
WISE J1717+6128	Gemini/GNIRS	T8	0.036 ± 0.014	0.198 ± 0.017	0.203 ± 0.015	0.134 ± 0.018	0.306 ± 0.014	0.655 ± 0.033	0.912 ± 0.026
WISE J1809+3838	IRTF/SpeX	T7.5	0.069 ± 0.018	0.266 ± 0.025	0.199 ± 0.032	0.154 ± 0.024	0.348 ± 0.026	0.582 ± 0.053	0.892 ± 0.036
WISE J2342+0856	IRTF/SpeX	T6.5	0.115 ± 0.006	0.380 ± 0.009	0.221 ± 0.016	0.276 ± 0.010	0.408 ± 0.010	0.672 ± 0.023	0.885 ± 0.012
WISE J2344+1034	Gemini/GNIRS	T9	0.028 ± 0.009	0.095 ± 0.010	0.144 ± 0.012	0.070 ± 0.014	0.196 ± 0.010	0.522 ± 0.027	0.857 ± 0.020
Y Dwarfs from Cushing et al. (2011) and Kirkpatrick et al. (2012)									
WISE J0146+4234	Keck/NIRSPEC-JH	Y0	-0.115 ± 0.032	0.070 ± 0.021	-0.019 ± 0.081	-0.032 ± 0.038	0.150 ± 0.014	0.185 ± 0.037	0.805 ± 0.030
WISE J0350−5658	HST/WFC3	Y1	-0.055 ± 0.071	0.068 ± 0.049	0.118 ± 0.054	—	0.116 ± 0.096	0.401 ± 0.068	0.676 ± 0.095
WISE J0359−5401	HST/WFC3	Y0	-0.020 ± 0.055	0.068 ± 0.037	0.144 ± 0.055	0.101 ± 0.058	0.170 ± 0.040	0.483 ± 0.067	0.801 ± 0.074
WISE J0410+1502	Magellan/FIRE	Y0	-0.002 ± 0.082	0.026 ± 0.040	-0.065 ± 0.424	-0.160 ± 0.375	0.126 ± 0.042	0.349 ± 0.732	0.822 ± 0.074
WISE J0713−2917	Keck/NIRSPEC-J	Y0	-0.029 ± 0.035	0.016 ± 0.019	—	—	0.046 ± 0.014	—	0.724 ± 0.024
WISE J0734−7157	Magellan/FIRE	Y0	-0.042 ± 0.044	0.037 ± 0.020	0.298 ± 0.047	0.020 ± 0.024	0.162 ± 0.024	0.484 ± 0.040	0.821 ± 0.034
WISE J1405+5534	HST/WFC3	Y0 (pec?)	-0.056 ± 0.035	-0.008 ± 0.023	0.001 ± 0.020	0.121 ± 0.029	0.068 ± 0.028	0.356 ± 0.040	0.696 ± 0.037
WISE J1541−2250	Magellan/FIRE	Y0.5	-0.024 ± 0.422	0.061 ± 0.238	0.075 ± 0.276	0.034 ± 0.199	0.088 ± 0.212	0.289 ± 0.246	0.747 ± 0.393
WISE J1828+2650	HST/WFC3	≥Y2	0.337 ± 0.198	0.254 ± 0.130	0.101 ± 0.123	0.114 ± 0.133	0.522 ± 0.142	0.469 ± 0.154	0.872 ± 0.289
WISE J2056+1459	HST/WFC3	Y0	0.052 ± 0.009	0.096 ± 0.010	0.186 ± 0.011	0.223 ± 0.010	0.130 ± 0.014	0.481 ± 0.024	0.755 ± 0.016
WISE J2220−3628	Keck/NIRSPEC-H	Y0	—	—	0.154 ± 0.032	0.015 ± 0.025	—	0.420 ± 0.031	0.742 ± 0.046

[a]Spectra from Adam Burgasser's SpeX Prism Spectral Library.

Table 8.　Average Median-Flux Spectral Indices for Each Half Spectral Type

NIR Sp. Type (1)	H_2O-J (2)	CH_4-J (3)	H_2O-H (4)	CH_4-H (5)	W_J (6)	NH_3-H (7)	J-narrow (8)	Y/J (9)	H/J (10)	K/J (11)
T0	0.647 ± 0.054	0.841 ± 0.063	0.651 ± 0.036	0.970 ± 0.054	0.803 ± 0.030	0.884 ± 0.021	0.928 ± 0.024	0.579 ± 0.033	0.846 ± 0.051	0.496 ± 0.060
T0.5	0.581 ± 0.087	0.802 ± 0.050	0.591 ± 0.074	1.035 ± 0.100	0.790 ± 0.036	0.850 ± 0.039	0.934 ± 0.028	0.567 ± 0.040	0.854 ± 0.037	0.554 ± 0.121
T1	0.572 ± 0.079	0.772 ± 0.064	0.582 ± 0.041	0.912 ± 0.068	0.766 ± 0.080	0.853 ± 0.018	0.922 ± 0.028	0.557 ± 0.076	0.814 ± 0.033	0.445 ± 0.053
T1.5	0.537 ± 0.068	0.728 ± 0.067	0.518 ± 0.045	0.924 ± 0.059	0.777 ± 0.040	0.840 ± 0.051	0.937 ± 0.017	0.585 ± 0.051	0.734 ± 0.023	0.344 ± 0.033
T2	0.490 ± 0.071	0.707 ± 0.077	0.522 ± 0.052	0.861 ± 0.064	0.712 ± 0.055	0.828 ± 0.045	0.916 ± 0.030	0.532 ± 0.039	0.732 ± 0.035	0.370 ± 0.060
T2.5	0.457 ± 0.037	0.679 ± 0.055	0.490 ± 0.033	0.813 ± 0.059	0.697 ± 0.040	0.813 ± 0.032	0.914 ± 0.007	0.537 ± 0.023	0.687 ± 0.030	0.314 ± 0.026
T3	0.410 ± 0.035	0.625 ± 0.061	0.485 ± 0.038	0.722 ± 0.047	0.685 ± 0.048	0.802 ± 0.042	0.911 ± 0.019	0.563 ± 0.053	0.660 ± 0.030	0.281 ± 0.046
T3.5	0.368 ± 0.096	0.604 ± 0.071	0.390 ± 0.042	0.702 ± 0.042	0.621 ± 0.072	0.759 ± 0.038	0.900 ± 0.026	0.510 ± 0.018	0.611 ± 0.027	0.233 ± 0.032
T4	0.378 ± 0.026	0.558 ± 0.075	0.393 ± 0.031	0.571 ± 0.045	0.648 ± 0.034	0.801 ± 0.039	0.894 ± 0.022	0.481 ± 0.062	0.583 ± 0.041	0.208 ± 0.029
T4.5	0.325 ± 0.041	0.557 ± 0.054	0.376 ± 0.023	0.503 ± 0.059	0.623 ± 0.036	0.788 ± 0.027	0.894 ± 0.032	0.476 ± 0.031	0.533 ± 0.030	0.191 ± 0.029
T5	0.238 ± 0.037	0.462 ± 0.047	0.336 ± 0.041	0.416 ± 0.038	0.552 ± 0.039	0.764 ± 0.050	0.887 ± 0.027	0.495 ± 0.054	0.476 ± 0.028	0.152 ± 0.038
T5.5	0.197 ± 0.040	0.427 ± 0.087	0.313 ± 0.037	0.365 ± 0.053	0.512 ± 0.050	0.738 ± 0.054	0.888 ± 0.028	0.444 ± 0.048	0.480 ± 0.041	0.160 ± 0.036
T6	0.155 ± 0.024	0.379 ± 0.039	0.297 ± 0.031	0.303 ± 0.028	0.467 ± 0.029	0.739 ± 0.030	0.877 ± 0.026	0.458 ± 0.047	0.461 ± 0.021	0.135 ± 0.035
T6.5	0.117 ± 0.023	0.320 ± 0.075	0.260 ± 0.044	0.250 ± 0.023	0.398 ± 0.062	0.706 ± 0.058	0.864 ± 0.038	0.448 ± 0.063	0.472 ± 0.018	0.137 ± 0.049
T7	0.090 ± 0.032	0.290 ± 0.048	0.241 ± 0.030	0.200 ± 0.033	0.387 ± 0.028	0.676 ± 0.042	0.880 ± 0.033	0.424 ± 0.062	0.477 ± 0.030	0.148 ± 0.026
T7.5	0.063 ± 0.017	0.243 ± 0.047	0.183 ± 0.023	0.157 ± 0.026	0.344 ± 0.023	0.637 ± 0.050	0.899 ± 0.037	0.450 ± 0.066	0.489 ± 0.025	0.111 ± 0.044
T8	0.056 ± 0.060	0.200 ± 0.047	0.182 ± 0.034	0.126 ± 0.033	0.303 ± 0.044	0.625 ± 0.054	0.890 ± 0.036	0.429 ± 0.089	0.498 ± 0.047	0.118 ± 0.038
T8.5	0.051 ± 0.035	0.188 ± 0.056	0.183 ± 0.045	0.122 ± 0.035	0.295 ± 0.047	0.610 ± 0.059	0.884 ± 0.044	0.432 ± 0.082	0.503 ± 0.045	0.116 ± 0.039
T9	0.032 ± 0.037	0.117 ± 0.030	0.127 ± 0.045	0.068 ± 0.067	0.203 ± 0.038	0.539 ± 0.054	0.879 ± 0.053	0.448 ± 0.095	0.555 ± 0.030	0.100 ± 0.032
T9.5	0.011 ± 0.025	0.071 ± 0.032	0.100 ± 0.253	-0.021 ± 0.116	0.145 ± 0.021	0.443 ± 0.101	0.865 ± 0.071	0.357 ± 0.008	0.504 ± 0.080	0.033 ± 0.083
Y0	-0.022 ± 0.050	0.045 ± 0.031	0.116 ± 0.132	0.066 ± 0.133	0.117 ± 0.043	0.385 ± 0.105	0.778 ± 0.050	0.423 ± 0.131	0.467 ± 0.061	0.063 ± 0.031

Table 9.   WISE All-Sky Photometry for Interloper Sources

Object Name	W1 (mag)	W2 (mag)	W3 (mag)	W4 (mag)	W1 − W2 (mag)	W2 − W3 (mag)
(1)	(2)	(3)	(4)	(5)	(6)	(7)
WISE J004733.81+671834.8	17.00 ± 0.15	14.21 ± 0.06	> 12.01	> 8.82	2.79 ± 0.16	< 2.20
WISE J014837.57−104803.0	16.54 ± 0.09	14.56 ± 0.06	12.67 ± 0.40	> 9.38	1.98 ± 0.11	1.89 ± 0.41
WISE J020110.08+483633.7	17.41 ± 0.22	14.67 ± 0.07	12.05 ± 0.27	> 9.13	2.74 ± 0.23	2.62 ± 0.28
WISE J022058.58+620236.4	> 17.42	13.04 ± 0.03	> 11.88	7.18 ± 0.12	> 4.39	< 1.16
WISE J022116.78+590337.7	16.14 ± 0.09	14.07 ± 0.06	11.01 ± 0.10	8.06 ± 0.17	2.07 ± 0.10	3.06 ± 0.11
WISE J040450.69+261825.1	14.23 ± 0.03	13.32 ± 0.04	> 12.65	8.07 ± 0.22	0.91 ± 0.05	< 0.66
WISE J042102.74+372125.2	13.72 ± 0.03	13.30 ± 0.04	11.63 ± 0.27	8.59 ± 0.45	0.42 ± 0.05	1.67 ± 0.27
WISE J044627.93−072611.6	16.09 ± 0.06	14.22 ± 0.05	—	—	1.87 ± 0.08	—
WISE J054319.50+465312.9	16.96 ± 0.19	13.67 ± 0.04	10.61 ± 0.08	8.59 ± 0.32	3.29 ± 0.19	3.06 ± 0.09
WISE J054647.84+263946.4	13.11 ± 0.03	12.61 ± 0.03	> 12.47	> 8.43	0.50 ± 0.04	< 0.15
WISE J055439.47+245728.8	16.40 ± 0.11	14.20 ± 0.06	11.14 ± 0.14	7.91 ± 0.17	2.21 ± 0.12	3.06 ± 0.15
WISE J062748.89−140155.0	13.94 ± 0.03	13.36 ± 0.04	11.49 ± 0.15	8.04 ± 0.14	0.59 ± 0.05	1.87 ± 0.15
WISE J071429.04−121239.5	15.67 ± 0.06	13.57 ± 0.04	> 12.56	8.31 ± 0.23	2.11 ± 0.07	< 1.01
WISE J082009.59−761323.1	15.38 ± 0.04	14.50 ± 0.04	12.91 ± 0.34	> 9.76	0.89 ± 0.05	1.59 ± 0.34
WISE J120854.51−484423.2	17.07 ± 0.13	14.49 ± 0.05	11.33 ± 0.09	8.98 ± 0.27	2.58 ± 0.14	3.16 ± 0.10
WISE J150119.95−045329.7	13.87 ± 0.03	13.32 ± 0.03	12.18 ± 0.26	> 9.51	0.55 ± 0.04	1.14 ± 0.26
WISE J153015.18−261753.5	18.11 ± 0.49	14.23 ± 0.06	10.47 ± 0.09	> 8.97	3.89 ± 0.50	3.76 ± 0.11
WISE J154500.53−843159.0	17.59 ± 0.19	14.81 ± 0.07	11.16 ± 0.09	8.63 ± 0.26	2.78 ± 0.20	3.65 ± 0.11
WISE J164312.53+371535.4	16.56 ± 0.08	13.72 ± 0.04	10.85 ± 0.07	> 8.74	2.84 ± 0.09	2.88 ± 0.08
WISE J165031.12−001417.8	16.42 ± 0.10	13.88 ± 0.05	9.78 ± 0.05	8.03 ± 0.20	2.54 ± 0.11	4.10 ± 0.06
WISE J172256.74+555031.7	16.34 ± 0.05	14.17 ± 0.04	10.85 ± 0.05	> 9.27	2.17 ± 0.06	3.32 ± 0.06
WISE J175443.93+323332.5	17.22 ± 0.14	15.54 ± 0.12	12.17 ± 0.23	> 8.72	1.69 ± 0.19	3.37 ± 0.26
WISE J185916.88+362732.5	> 18.42	14.53 ± 0.06	11.44 ± 0.12	9.30 ± 0.48	> 3.89	3.09 ± 0.13
WISE J223204.75+384703.8	17.22 ± 0.16	14.82 ± 0.07	12.28 ± 0.27	9.37 ± 0.52	2.40 ± 0.18	2.55 ± 0.28
WISE J224245.85−201511.0	> 18.32	15.15 ± 0.13	11.73 ± 0.24	> 9.02	> 3.16	3.42 ± 0.27
WISE J224416.22+433724.7	15.89 ± 0.07	14.36 ± 0.05	12.57 ± 0.39	> 9.29	1.54 ± 0.09	1.79 ± 0.39
WISE J225144.24+243034.9	16.40 ± 0.10	14.89 ± 0.09	> 12.54	> 9.05	1.51 ± 0.13	< 2.35
WISE J233555.92+650621.2	17.44 ± 0.19	14.30 ± 0.05	> 13.01	8.67 ± 0.20	3.15 ± 0.20	< 1.28
WISE J234847.41+335104.9	14.38 ± 0.03	13.24 ± 0.03	11.74 ± 0.15	> 8.82	1.14 ± 0.04	1.50 ± 0.16
WISE J235135.76+735746.9	18.43 ± 0.50	14.97 ± 0.08	12.12 ± 0.26	> 9.33	3.46 ± 0.51	2.84 ± 0.28
WISE J235329.88+801604.3	18.34 ± 0.37	15.26 ± 0.08	> 13.09	> 9.10	3.08 ± 0.38	< 2.18

Table 10.   *Spitzer*/IRAC Photometry for
Interloper Sources

Object Name	$ch1$ (mag)	$ch2$ (mag)	$ch1 - ch2$ (mag)
(1)	(2)	(3)	(4)
WISE J0148−1048	16.47 ± 0.04	14.63 ± 0.02	1.84 ± 0.04
WISE J0201+4836	16.54 ± 0.04	14.70 ± 0.02	1.84 ± 0.04
WISE J0220+6202	14.79 ± 0.02	13.05 ± 0.02	1.75 ± 0.03
WISE J0221+5903	15.06 ± 0.02	13.93 ± 0.02	1.13 ± 0.03
WISE J0446−0726	15.59 ± 0.03	14.35 ± 0.02	1.25 ± 0.03
WISE J0543+4653	15.91 ± 0.03	13.64 ± 0.02	2.27 ± 0.03
WISE J0546+2639	12.88 ± 0.02	12.67 ± 0.02	0.21 ± 0.02
WISE J0554+2457	14.94 ± 0.02	14.10 ± 0.02	0.84 ± 0.03
WISE J0714−1212	15.51 ± 0.03	13.89 ± 0.02	1.63 ± 0.03
WISE J0820−7613	15.24 ± 0.02	14.63 ± 0.02	0.61 ± 0.03
WISE J1208−4844	15.98 ± 0.03	14.43 ± 0.02	1.55 ± 0.04
WISE J1501−0453	13.84 ± 0.02	13.49 ± 0.02	0.35 ± 0.03
WISE J1530−2617	16.11 ± 0.03	14.24 ± 0.02	1.87 ± 0.04
WISE J1545−8431	16.54 ± 0.04	14.83 ± 0.02	1.71 ± 0.04
WISE J1754+3233	16.68 ± 0.04	15.51 ± 0.02	1.17 ± 0.05
WISE J1859+3627	16.50 ± 0.04	14.49 ± 0.02	2.01 ± 0.04
WISE J2232+3847	15.87 ± 0.03	14.39 ± 0.02	1.47 ± 0.03
WISE J2242−2015	17.48 ± 0.07	15.11 ± 0.02	2.37 ± 0.07
WISE J2244+4337	15.21 ± 0.02	14.33 ± 0.02	0.88 ± 0.03
WISE J2335+6506	15.62 ± 0.03	13.89 ± 0.02	1.73 ± 0.03
WISE J2351+7357	16.90 ± 0.05	14.93 ± 0.02	1.97 ± 0.05
WISE J2353+8016	16.40 ± 0.04	15.13 ± 0.02	1.26 ± 0.04

Table 11.   Follow-up Near-IR Spectroscopy for Interloper Sources

Object Name J2000 Coordinates (1)	Spectrograph (2)	Obs. Date (UT) (3)	Description of Spectrum (4)
WISE J0047+6718	Keck/NIRSPEC-H	2010 Jul 18	Faint continuum throughout the H band
WISE J0148−1048	Keck/NIRSPEC-J	2011 Aug 09	Faint continuum; cluster of *Spitzer* sources within $0''\!.5$
WISE J0201+4836	Keck/NIRSPEC-J	2011 Oct 08/09	Faint continuum; two blended *Spitzer* sources
WISE J0220+6202	Palomar/TSpec	2012 Jan 07	Faint K-band continuum
WISE J0221+5903	Palomar/TSpec	2011 Nov 08	Faint K-band continuum; no motion between WISE and *Spitzer* epochs
WISE J0404+2618	Palomar/TSpec	2012 Jan 06	K-band and faint H-band continuum
WISE J0421+3721	IRTF/SpeX	2012 Feb 01	YSO with high SNR hump throughout NIR; peak flux near 1.8 μm (Figure 26)
WISE J0446−0726	Palomar/TSpec	2012 Jan 07	Faint H and K-band continuum; no motion between WISE and *Spitzer* epochs
WISE J0543+4653	Gemini/GNIRS	2012 Jan 03	Faint continuum throughout near-IR, flux decreases as wavelength increases
WISE J0546+2639	IRTF/SpeX	2012 Jan 31	YSO with high SNR hump throughout NIR; peak flux near 1.9 μm (Figure 26)
WISE J0554+2457	Palomar/TSpec	2011 Nov 08	Faint K-band continuum
WISE J0627−1401	IRTF/SpeX	2012 Feb 13	Extended object in the guider camera; very faint K-band flux
WISE J0714−1212	IRTF/SpeX	2010 Dec 18	Reddened star in Galactic plane - Upper Canis Major
WISE J0820−7613	Magellan/FIRE	2010 Dec 23	No near-IR flux measured; no motion between WISE and *Spitzer* epochs
WISE J1208−4844	HST/WFC2	2011 May 19	Extended source in HST image
WISE J1501−0453	IRTF/SpeX	2012 Feb 13	Faint continuum throughout near-IR
WISE J1530−2617	Keck/NIRSPEC-J	2012 Mar 30	AGN with Hα at 1.3136 μm, z$\sim$1.00 (Figure 27)
WISE J1545−8431	HST/WFC3	2011 May 12	Extended source in HST image
WISE J1643+3715	IRTF/SpeX	2010 May 27	No near-IR flux measured
WISE J1650−0014	IRTF/SpeX	2010 May 26	No near-IR flux measured
WISE J1722+5550	IRTF/SpeX	2010 May 26	No near-IR flux measured
WISE J1754+3233	HST/WFC3	2011 Mar 19/20	Hβ and [OIII] (500.7 nm) at 1.4192 and 1.4611 μm for z$\sim$1.92 AGN (Figure 28)
WISE J1859+3627	Keck/NIRSPEC-J	2011 Aug 08	Faint continuum; no motion between WISE and *Spitzer* epochs
WISE J2232+3847	HST/WFC3	2011 Sep 21/22	Continuum throughout near-IR; no motion between WISE and *Spitzer* epochs
WISE J2242−2015	Keck/NIRSPEC-J	2012 Sep 25	Faint continuum throughout the J band
WISE J2244+4337	Palomar/TSpec	2012 Jan 07	Faint continuum throughout near-IR
WISE J2251+2430	Keck/NIRSPEC-J	2012 Jun 09	Faint continuum; broad emission hump at 1.167 μm
WISE J2335+6506	Keck/NIRSPEC-J	2011 Oct 09	Faint continuum; no motion between WISE and *Spitzer* epochs
WISE J2348+3351	IRTF/SpeX	2010 Sep 14	Faint continuum throughout near-IR
WISE J2351+7357	Keck/NIRSPEC-J	2012 Sep 25	Faint continuum throughout the J band
WISE J2353+8016	Keck/NIRSPEC-J	2012 Sep 25	Faint continuum throughout the J band

Table A1.   Appendix: Spectral Indices using Integrated (not Median) Fluxes

Object Name J2000 Coordinates (1)	Instrument (2)	NIR Sp. Type (3)	H$_2$O$-$J (4)	CH$_4-$J (5)	H$_2$O$-$H (6)	CH$_4-$H (7)	W$_J$ (8)	NH$_3-$H (9)
				T Dwarf Discoveries from Kirkpatrick et al. (2011)				
WISE J0008$-$1739	Keck/NIRSPEC-J	T6	0.141 ± 0.025	0.393 ± 0.028	—	—	0.463 ± 0.021	—
WISE J0123+4142	Keck/NIRSPEC-J	T7	—	0.285 ± 0.051	—	—	0.419 ± 0.041	—
WISE J0138$-$0322	IRTF/SpeX	T3	0.409 ± 0.006	0.502 ± 0.004	0.536 ± 0.006	0.831 ± 0.007	0.655 ± 0.005	0.846 ± 0.008
WISE J0148$-$7202	Magellan/FIRE	T9.5	-0.017 ± 0.011 [a]	0.076 ± 0.006 [a]	0.070 ± 0.013 [a]	0.016 ± 0.012 [a]	0.152 ± 0.006 [a]	0.431 ± 0.015 [a]
WISE J0150+3827	IRTF/SpeX	T0	0.665 ± 0.006	0.908 ± 0.006	0.675 ± 0.004	0.979 ± 0.005	0.976 ± 0.006	0.891 ± 0.006
WISE J0221+3842	Palomar/TSpec	T6.5	0.129 ± 0.019	0.247 ± 0.016	0.179 ± 0.035	0.255 ± 0.022	0.349 ± 0.020	0.660 ± 0.039
WISE J0223$-$2932	IRTF/SpeX	T7.5	0.040 ± 0.007	0.156 ± 0.004	0.165 ± 0.012	0.163 ± 0.010	0.383 ± 0.005	0.696 ± 0.016
	Keck/NIRSPEC-H	T7	—	—	—	0.177 ± 0.022	—	0.580 ± 0.027
WISE J0226$-$0211	Keck/NIRSPEC-H	T7	—	—	—	0.104 ± 0.028	—	0.574 ± 0.032
WISE J0254+0223	IRTF/SpeX	T8	0.047 ± 0.003	0.188 ± 0.002	0.167 ± 0.004	0.111 ± 0.004	0.295 ± 0.002	0.572 ± 0.005
WISE J0305+3954	Palomar/TSpec	T6	0.111 ± 0.012	0.334 ± 0.008	0.355 ± 0.018	0.225 ± 0.012	0.435 ± 0.009	0.719 ± 0.019
WISE J0307+2904	IRTF/SpeX	T6.5	0.142 ± 0.042	0.389 ± 0.029	0.302 ± 0.060	0.217 ± 0.045	0.486 ± 0.026	0.821 ± 0.079
WISE J0313+7807	Palomar/TSpec	T8.5	0.121 ± 0.021	0.114 ± 0.010	0.251 ± 0.030	0.097 ± 0.019	0.341 ± 0.011	0.608 ± 0.029
WISE J0323$-$6025	Magellan/FIRE	T8.5	0.052 ± 0.016	0.166 ± 0.008	0.179 ± 0.021	0.121 ± 0.013	0.283 ± 0.008	0.554 ± 0.018
WISE J0333$-$5856	SOAR/OSIRIS	T3	—	0.511 ± 0.021	0.515 ± 0.018	0.714 ± 0.016		0.711 ± 0.020
WISE J0410+1411	IRTF/SpeX	T6	0.083 ± 0.030	0.313 ± 0.022	0.247 ± 0.049	0.269 ± 0.042	0.416 ± 0.020	0.669 ± 0.055
WISE J0448$-$1935	IRTF/SpeX	T5 pec	0.196 ± 0.017	0.398 ± 0.013	0.324 ± 0.029	0.417 ± 0.029	0.532 ± 0.012	0.765 ± 0.039
WISE J0458+6434	IRTF/SpeX	T8.5	0.039 ± 0.015	0.281 ± 0.013	0.125 ± 0.019	0.080 ± 0.018	0.289 ± 0.009	0.477 ± 0.026
WISE J0500$-$1223	IRTF/SpeX	T8	0.034 ± 0.026	0.200 ± 0.018	0.112 ± 0.037	0.106 ± 0.034	0.315 ± 0.016	0.576 ± 0.045
WISE J0513+0608	Palomar/TSpec	T6.5	0.159 ± 0.006	0.315 ± 0.004	0.287 ± 0.009	0.232 ± 0.006	0.420 ± 0.004	0.698 ± 0.010
WISE J0525+6739	IRTF/SpeX	T6 pec	0.171 ± 0.009	0.323 ± 0.006	0.291 ± 0.017	0.314 ± 0.016	0.455 ± 0.006	0.722 ± 0.022
WISE J0528$-$3308	Palomar/TSpec	T7 pec	-0.002 ± 0.039	0.272 ± 0.014	0.183 ± 0.048	0.233 ± 0.029	0.377 ± 0.013	0.631 ± 0.044
WISE J0539$-$1034	Palomar/TSpec	T5.5	0.177 ± 0.022	0.335 ± 0.013	0.426 ± 0.037	0.302 ± 0.023	0.485 ± 0.014	0.827 ± 0.038
WISE J0542$-$1628	Palomar/TSpec	T6.5	0.144 ± 0.009	0.266 ± 0.005	0.215 ± 0.012	0.226 ± 0.008	0.406 ± 0.004	0.686 ± 0.012
WISE J0611$-$0410	IRTF/SpeX	T0	0.583 ± 0.013	0.590 ± 0.010	0.657 ± 0.012	1.043 ± 0.014	0.760 ± 0.011	0.985 ± 0.015
WISE J0612$-$4920	SOAR/OSIRIS	T3.5	—	0.474 ± 0.039	0.357 ± 0.035	0.683 ± 0.030		0.755 ± 0.042
WISE J0612$-$3036	Palomar/TSpec	T6	0.117 ± 0.001	0.311 ± 0.001	0.317 ± 0.001	0.315 ± 0.001	0.443 ± 0.001	0.793 ± 0.001
WISE J0614+3912	Palomar/TSpec	T6	0.140 ± 0.023	0.401 ± 0.012	0.334 ± 0.023	0.273 ± 0.016	0.465 ± 0.012	0.789 ± 0.026
WISE J0623$-$0456	IRTF/SpeX	T8	0.002 ± 0.028	0.293 ± 0.020	0.166 ± 0.039	0.082 ± 0.032	0.425 ± 0.019	0.721 ± 0.052
WISE J0625+5646	Palomar/TSpec	T6	0.182 ± 0.012	0.312 ± 0.007	0.330 ± 0.020	0.275 ± 0.013	0.425 ± 0.007	0.686 ± 0.020
WISE J0627$-$1114	IRTF/SpeX	T6	0.163 ± 0.004	0.315 ± 0.003	0.277 ± 0.005	0.339 ± 0.005	0.454 ± 0.003	0.654 ± 0.007
WISE J0656+4205	IRTF/SpeX	T3	0.466 ± 0.010	0.436 ± 0.007	0.489 ± 0.011	0.792 ± 0.012	0.738 ± 0.008	0.836 ± 0.014
WISE J0744+5628	Palomar/TSpec	T8	0.156 ± 0.031	0.266 ± 0.018	0.196 ± 0.061	-0.054 ± 0.041	0.404 ± 0.018	0.695 ± 0.061
WISE J0750+2725	Keck/NIRSPEC-JH	T8.5	0.036 ± 0.008	0.118 ± 0.008	—	0.039 ± 0.004	0.231 ± 0.006	0.578 ± 0.005
WISE J0751$-$7634	Magellan/FIRE	T9	0.010 ± 0.023	0.132 ± 0.013	0.224 ± 0.042	0.117 ± 0.029	0.178 ± 0.012	0.511 ± 0.042
WISE J0759$-$4904	Magellan/FIRE	T8	0.036 ± 0.003	0.160 ± 0.002	0.154 ± 0.004	0.116 ± 0.004	0.279 ± 0.002	0.615 ± 0.006
WISE J0819$-$0335	IRTF/SpeX	T4	0.384 ± 0.004	0.474 ± 0.003	0.395 ± 0.005	0.654 ± 0.005	0.642 ± 0.003	0.761 ± 0.006
WISE J0821+1443	IRTF/SpeX	T5.5	0.199 ± 0.011	0.352 ± 0.009	0.317 ± 0.016	0.383 ± 0.015	0.506 ± 0.009	0.714 ± 0.020
WISE J0836$-$1859	Magellan/FIRE	T8 pec	0.046 ± 0.014	0.148 ± 0.005	0.153 ± 0.015	0.118 ± 0.010	0.310 ± 0.007	0.609 ± 0.014
WISE J0857+5604	Palomar/TSpec	T8	0.065 ± 0.015	0.171 ± 0.008	0.095 ± 0.025	0.094 ± 0.017	0.311 ± 0.008	0.534 ± 0.025
WISE J0906+4735	Palomar/TSpec	T8	0.048 ± 0.165	0.235 ± 0.072	0.220 ± 0.113	0.124 ± 0.044	0.336 ± 0.062	0.620 ± 0.081
WISE J0929+0409	Palomar/TSpec	T6.5	0.074 ± 0.017	0.252 ± 0.010	0.317 ± 0.031	0.190 ± 0.019	0.380 ± 0.009	0.666 ± 0.033
WISE J0952+1955	IRTF/SpeX	T6	0.156 ± 0.008	0.294 ± 0.006	0.260 ± 0.017	0.332 ± 0.016	0.444 ± 0.006	0.669 ± 0.021
WISE J1018$-$2445	Magellan/FIRE	T8	0.037 ± 0.004	0.158 ± 0.002	0.163 ± 0.004	0.084 ± 0.003	0.302 ± 0.002	0.625 ± 0.005
WISE J1019+6529	Palomar/TSpec	T6	0.131 ± 0.038	0.328 ± 0.021	0.280 ± 0.036	0.297 ± 0.019	0.472 ± 0.023	0.745 ± 0.033

Table A1—Continued

Object Name J2000 Coordinates (1)	Instrument (2)	NIR Sp. Type (3)	H$_2$O−J (4)	CH$_4$−J (5)	H$_2$O−H (6)	CH$_4$−H (7)	W$_J$ (8)	NH$_3$−H (9)
	IRTF/SpeX	T6	0.122 ± 0.012	0.259 ± 0.008	0.269 ± 0.024	0.352 ± 0.022	0.443 ± 0.010	0.849 ± 0.034
WISE J1042−3842	Magellan/FIRE	T8.5	0.026 ± 0.010	0.155 ± 0.005	0.146 ± 0.011	0.108 ± 0.007	0.297 ± 0.006	0.558 ± 0.011
WISE J1122+2550	IRTF/SpeX	T6	0.135 ± 0.011	0.304 ± 0.008	0.299 ± 0.025	0.261 ± 0.018	0.448 ± 0.009	0.767 ± 0.028
WISE J1150+6302	Palomar/TSpec	T8	0.017 ± 0.015	0.202 ± 0.008	0.161 ± 0.023	0.148 ± 0.015	0.308 ± 0.007	0.591 ± 0.026
WISE J1217+1626	Palomar/TSpec	T9	0.066 ± 0.020	0.103 ± 0.010	0.032 ± 0.030	0.054 ± 0.019	0.247 ± 0.010	0.542 ± 0.030
WISE J1311+0122	Keck/NIRSPEC-H	T9:	—	—	—	-0.084 ± 0.005	—	0.610 ± 0.007
WISE J1320+6034	IRTF/SpeX	T6.5	0.105 ± 0.008	0.108 ± 0.004	0.347 ± 0.015	0.212 ± 0.013	0.487 ± 0.006	0.805 ± 0.021
WISE J1322−2340	IRTF/SpeX	T8	0.084 ± 0.011	0.240 ± 0.007	0.256 ± 0.018	0.202 ± 0.015	0.349 ± 0.008	0.708 ± 0.024
WISE J1436−1814	Magellan/FIRE	T8 pec	0.062 ± 0.003	0.202 ± 0.002	0.244 ± 0.004	0.157 ± 0.003	0.318 ± 0.002	0.670 ± 0.005
WISE J1457+5815	IRTF/SpeX	T7	0.100 ± 0.010	0.197 ± 0.005	0.282 ± 0.019	0.218 ± 0.015	0.411 ± 0.007	0.819 ± 0.024
WISE J1506+7027	Palomar/TSpec	T6	0.140 ± 0.001	0.315 ± 0.001	0.280 ± 0.001	0.271 ± 0.001	0.443 ± 0.001	0.718 ± 0.002
	Keck/NIRSPEC-H	T6	—	—	—	0.271 ± 0.006	—	0.705 ± 0.009
WISE J1519+7009	Palomar/TSpec	T8	0.081 ± 0.167	0.198 ± 0.085	0.152 ± 0.138	0.105 ± 0.053	0.341 ± 0.069	0.626 ± 0.098
WISE J1612−3420	Keck/NIRSPEC-H	T6.5				0.217 ± 0.013		0.719 ± 0.016
WISE J1614+1739	Magellan/FIRE	T9	0.037 ± 0.022	0.107 ± 0.009	0.124 ± 0.033	0.106 ± 0.022	0.187 ± 0.016	0.508 ± 0.037
WISE J1617+1807	Magellan/FIRE	T8	0.020 ± 0.004 [b]	0.170 ± 0.003 [b]	0.159 ± 0.007 [b]	0.108 ± 0.006 [b]	0.275 ± 0.003 [b]	0.724 ± 0.101
WISE J1622−0959	IRTF/SpeX	T6	0.176 ± 0.005	0.353 ± 0.004	0.278 ± 0.007	0.325 ± 0.007	0.468 ± 0.004	0.649 ± 0.009
WISE J1627+3255	IRTF/SpeX	T6	0.143 ± 0.003	0.332 ± 0.002	0.261 ± 0.004	0.277 ± 0.003	0.425 ± 0.002	0.756 ± 0.006
	Keck/NIRSPEC-H	T6	—	—	—	0.278 ± 0.028	—	0.744 ± 0.039
WISE J1653+4444	IRTF/SpeX	T8	0.030 ± 0.009	0.213 ± 0.007	0.168 ± 0.012	0.153 ± 0.012	0.271 ± 0.006	0.602 ± 0.018
WISE J1711+3500	IRTF/SpeX	T8	-0.023 ± 0.017	0.255 ± 0.013	0.222 ± 0.022	0.173 ± 0.020	0.456 ± 0.015	0.698 ± 0.031
WISE J1717+6129	Keck/NIRSPEC-JH	T8	0.092 ± 0.029	0.173 ± 0.030	—	0.116 ± 0.018	0.292 ± 0.023	0.507 ± 0.023
WISE J1728+5716	IRTF/SpeX	T6	0.132 ± 0.012	0.353 ± 0.009	0.268 ± 0.018	0.276 ± 0.018	0.400 ± 0.008	0.703 ± 0.027
WISE J1741+2553	Magellan/FIRE	T9	0.021 ± 0.060	0.157 ± 0.029	0.136 ± 0.028	0.073 ± 0.018	0.274 ± 0.030	0.566 ± 0.025
WISE J1804+3117	Keck/NIRSPEC-H	T9.5:	—	—	—	-0.133 ± 0.029	—	0.313 ± 0.030
WISE J1812+2721	Magellan/FIRE	T8.5:	0.040 ± 0.050 [b]	0.120 ± 0.030 [b]	0.140 ± 0.130 [b]	0.290 ± 0.110 [b]	0.220 ± 0.040 [b]	0.631 ± 0.104
WISE J1841+7000	Palomar/TSpec	T5	0.236 ± 0.013	0.467 ± 0.009	0.423 ± 0.015	0.394 ± 0.008	0.556 ± 0.008	0.805 ± 0.013
WISE J1852+3537	IRTF/SpeX	T7	0.068 ± 0.007	0.207 ± 0.005	0.253 ± 0.012	0.184 ± 0.010	0.379 ± 0.005	0.825 ± 0.017
WISE J1906+4508	IRTF/SpeX	T6	0.183 ± 0.004	0.332 ± 0.003	0.324 ± 0.007	0.330 ± 0.006	0.495 ± 0.003	0.754 ± 0.010
WISE J1952+7240	Palomar/TSpec	T4	0.352 ± 0.006	0.480 ± 0.004	0.384 ± 0.007	0.502 ± 0.005	0.614 ± 0.004	0.776 ± 0.007
WISE J1959−3338	Palomar/TSpec	T8	0.049 ± 0.013	0.207 ± 0.006	0.233 ± 0.010	0.137 ± 0.004	0.318 ± 0.004	0.649 ± 0.007
WISE J2018−7423	Magellan/FIRE	T7	0.086 ± 0.006 [b]	0.198 ± 0.004 [b]	0.224 ± 0.011 [b]	0.231 ± 0.010 [b]	0.420 ± 0.005 [b]	0.681 ± 0.006
WISE J2134−7137	Magellan/FIRE	T9 pec	0.017 ± 0.014	0.100 ± 0.007	0.108 ± 0.018	0.055 ± 0.017	0.197 ± 0.008	0.436 ± 0.020
WISE J2157+2659	Palomar/TSpec	T7	0.029 ± 0.003	0.255 ± 0.002	0.193 ± 0.002	0.185 ± 0.001	0.329 ± 0.001	0.658 ± 0.002
WISE J2209−2734	Keck/NIRSPEC-H	T7	—	—	—	0.240 ± 0.025	—	0.692 ± 0.034
WISE J2213+0911	IRTF/SpeX	T7	0.108 ± 0.005	0.274 ± 0.003	0.229 ± 0.008	0.210 ± 0.007	0.370 ± 0.003	0.708 ± 0.011
WISE J2226+0440	IRTF/SpeX	T8	0.052 ± 0.005	0.172 ± 0.003	0.237 ± 0.009	0.125 ± 0.008	0.347 ± 0.004	0.757 ± 0.012
	Keck/NIRSPEC-JH	T8.5	0.060 ± 0.032	0.063 ± 0.034	—	0.099 ± 0.015	0.461 ± 0.027	0.660 ± 0.020
WISE J2237−0614	IRTF/SpeX	T5	0.200 ± 0.012	0.314 ± 0.008	0.435 ± 0.023	0.439 ± 0.021	0.576 ± 0.009	0.948 ± 0.031
WISE J2239+1617	IRTF/SpeX	T3	0.498 ± 0.005	0.677 ± 0.004	0.511 ± 0.005	0.725 ± 0.004	0.792 ± 0.004	0.813 ± 0.006
WISE J2255−3118	IRTF/SpeX	T8	0.031 ± 0.008	0.263 ± 0.006	0.164 ± 0.014	0.108 ± 0.012	0.260 ± 0.005	0.662 ± 0.017
	Keck/NIRSPEC-H	T8	—	—	—	0.099 ± 0.016	—	0.456 ± 0.017
WISE J2313−8037	Magellan/FIRE	T8	0.044 ± 0.008 [b]	0.116 ± 0.004 [b]	0.174 ± 0.012 [b]	0.142 ± 0.011 [b]	0.324 ± 0.005 [b]	0.561 ± 0.005
WISE J2319−1844	IRTF/SpeX	T7.5	0.072 ± 0.015	0.268 ± 0.010	0.167 ± 0.023	0.106 ± 0.021	0.308 ± 0.008	0.599 ± 0.033
WISE J2325−4105	Magellan/FIRE	T9 pec	0.011 ± 0.014	0.153 ± 0.009	0.047 ± 0.020	0.100 ± 0.015	0.222 ± 0.009	0.450 ± 0.021
WISE J2340−0745	IRTF/SpeX	T7	0.114 ± 0.004	0.253 ± 0.003	0.295 ± 0.007	0.242 ± 0.006	0.411 ± 0.003	0.827 ± 0.009
WISE J2343−7418	Magellan/FIRE	T6	0.184 ± 0.005	0.371 ± 0.003	0.297 ± 0.006	0.306 ± 0.005	0.489 ± 0.003	0.697 ± 0.007
WISE J2344+1034	Keck/NIRSPEC-J	T9	—	0.126 ± 0.013	—	—	0.169 ± 0.009	—
WISE J2348−1028	IRTF/SpeX	T7	0.078 ± 0.005	0.198 ± 0.003	0.252 ± 0.009	0.169 ± 0.008	0.373 ± 0.004	0.817 ± 0.012

Object Name J2000 Coordinates (1)	Instrument (2)	NIR Sp. Type (3)	H_2O-J (4)	CH_4-J (5)	H_2O-H (6)	CH_4-H (7)	W_J (8)	NH_3-H (9)
WISE J2359−7335	Magellan/FIRE	T6.5	0.206 ± 0.008 [b]	0.261 ± 0.004 [b]	0.343 ± 0.011 [b]	0.315 ± 0.008 [b]	0.549 ± 0.005 [b]	0.653 ± 0.005
			T Dwarf Discoveries from This Paper					
WISE J0005+3737	Keck/NIRSPEC-J	T9	—	0.130 ± 0.016	—	—	0.238 ± 0.019	—
WISE J0038+2758	Keck/NIRSPEC-J	T9	-0.080 ± 0.020	0.102 ± 0.006	—	—	0.174 ± 0.004	—
WISE J0038+8405	Keck/NIRSPEC-J	T6	—	—	—	—	0.464 ± 0.003	—
WISE J0040+0900	IRTF/SpeX	T7	0.090 ± 0.004	0.259 ± 0.003	0.246 ± 0.008	0.231 ± 0.006	0.372 ± 0.003	0.661 ± 0.009
WISE J0045+3611	IRTF/SpeX	T5	0.201 ± 0.003	0.332 ± 0.002	0.304 ± 0.005	0.389 ± 0.005	0.468 ± 0.003	0.631 ± 0.006
WISE J0049+2151	IRTF/SpeX	T8.5	0.027 ± 0.004	0.179 ± 0.003	0.173 ± 0.006	0.088 ± 0.005	0.379 ± 0.003	0.607 ± 0.008
WISE J0135+1715	IRTF/SpeX	T6	0.170 ± 0.014	0.360 ± 0.010	0.313 ± 0.021	0.277 ± 0.018	0.570 ± 0.011	0.735 ± 0.028
WISE J0210+4008	IRTF/SpeX	T4.5	0.334 ± 0.006	0.409 ± 0.004	0.366 ± 0.008	0.535 ± 0.007	0.619 ± 0.005	0.705 ± 0.009
WISE J0233+3030	IRTF/SpeX	T6	0.216 ± 0.009	0.335 ± 0.006	0.331 ± 0.014	0.319 ± 0.012	0.504 ± 0.006	0.672 ± 0.017
WISE J0245−3450	IRTF/SpeX	T8	0.042 ± 0.013	0.185 ± 0.009	0.182 ± 0.021	0.126 ± 0.018	0.316 ± 0.009	0.577 ± 0.025
WISE J0247+3725	Gemini/GNIRS	T8	0.030 ± 0.007	0.164 ± 0.004	0.152 ± 0.008	0.089 ± 0.007	0.289 ± 0.004	0.574 ± 0.012
WISE J0259−0346	Keck/NIRSPEC-J	T5	—	0.414 ± 0.022	—	—	0.526 ± 0.018	—
WISE J0316+3820	Palomar/TSpec	T3	0.410 ± 0.015	0.516 ± 0.009	0.511 ± 0.012	0.669 ± 0.009	0.680 ± 0.011	0.817 ± 0.013
WISE J0316+4307	Keck/NIRSPEC-JH	T8	—	0.192 ± 0.013	—	0.070 ± 0.023	0.233 ± 0.009	0.564 ± 0.027
WISE J0321−7347	Magellan/FIRE	T8	0.072 ± 0.013	0.148 ± 0.007	0.192 ± 0.006	0.058 ± 0.003	0.302 ± 0.004	0.643 ± 0.005
WISE J0325−3854	Keck/NIRSPEC-J	T9	—	0.128 ± 0.022	—	—	0.245 ± 0.013	—
WISE J0325+0831	IRTF/SpeX	T7	0.096 ± 0.005	0.234 ± 0.004	0.279 ± 0.008	0.235 ± 0.008	0.406 ± 0.004	0.707 ± 0.012
WISE J0335+4310	Keck/NIRSPEC-J	T9	—	0.138 ± 0.009	—	—	0.226 ± 0.016	—
WISE J0336−0143	Keck/NIRSPEC-J	T8:	—	0.147 ± 0.034	—	—	0.344 ± 0.054	—
WISE J0336+2826	IRTF/SpeX	T5	0.309 ± 0.009	0.403 ± 0.007	0.350 ± 0.011	0.474 ± 0.012	0.546 ± 0.007	0.789 ± 0.018
WISE J0413−4750	Magellan/FIRE	T9	0.033 ± 0.036	0.102 ± 0.041	0.193 ± 0.069	0.017 ± 0.027	0.284 ± 0.072	0.584 ± 0.235
WISE J0424+0727	Keck/NIRSPEC-J	T7.5	—	0.220 ± 0.006	—	—	0.355 ± 0.005	—
WISE J0430+4633	Keck/NIRSPEC-J	T8	—	0.229 ± 0.006	—	—	0.281 ± 0.004	—
WISE J0512−3004	Keck/NIRSPEC-J	T8.5	—	0.110 ± 0.009	—	—	0.243 ± 0.007	—
WISE J0540+4832	Keck/NIRSPEC-J	T8.5	—	0.161 ± 0.004	—	—	0.278 ± 0.003	—
WISE J0546−0959	IRTF/SpeX	T5	0.232 ± 0.006	0.484 ± 0.006	0.347 ± 0.012	0.434 ± 0.012	0.571 ± 0.005	0.771 ± 0.016
WISE J0614+0951	Palomar/TSpec	T7	0.130 ± 0.001	0.278 ± 0.001	0.300 ± 0.001	0.209 ± 0.001	0.347 ± 0.001	0.699 ± 0.001
WISE J0629+2418	IRTF/SpeX	T2 sb	0.447 ± 0.011	0.626 ± 0.009	0.512 ± 0.011	0.832 ± 0.013	0.607 ± 0.008	0.739 ± 0.014
WISE J0642+4101	Palomar/TSpec	extr. red	0.544 ± 0.001	0.793 ± 0.001	0.613 ± 0.001	1.197 ± 0.001	0.737 ± 0.001	0.844 ± 0.001
WISE J0701+6321	Palomar/TSpec	T3	0.385 ± 0.001	0.583 ± 0.001	0.494 ± 0.001	0.777 ± 0.001	0.641 ± 0.001	0.814 ± 0.001
WISE J0723+3403	Keck/NIRSPEC-J	T9:	—	—	—	—	0.081 ± 0.027	—
WISE J0733+7544	Palomar/TSpec	T6	0.139 ± 0.001	0.330 ± 0.001	0.322 ± 0.002	0.301 ± 0.001	0.452 ± 0.001	0.741 ± 0.001
WISE J0754+7909	Palomar/TSpec	extr. red	0.472 ± 0.001	0.651 ± 0.001	0.469 ± 0.002	1.071 ± 0.001	0.757 ± 0.001	0.792 ± 0.005
WISE J0811−8051	Magellan/FIRE	T9.5:	0.026 ± 0.041	0.054 ± 0.014	-0.449 ± 0.035	-0.293 ± 0.018	0.201 ± 0.013	0.596 ± 0.026
WISE J0812+4021	Gemini/GNIRS	T8	0.065 ± 0.006	0.183 ± 0.003	0.207 ± 0.008	0.110 ± 0.007	0.322 ± 0.004	0.649 ± 0.013
WISE J1025+0307	Magellan/FIRE	T8.5	0.030 ± 0.002	0.112 ± 0.001	0.113 ± 0.001	0.069 ± 0.001	0.308 ± 0.001	0.551 ± 0.001
WISE J1039−1600	IRTF/SpeX	T7.5	0.084 ± 0.012	0.250 ± 0.009	0.175 ± 0.020	0.135 ± 0.019	0.308 ± 0.008	0.572 ± 0.025
WISE J1050+5056	Keck/NIRSPEC-J	T8	—	0.224 ± 0.007	—	—	0.332 ± 0.005	—
WISE J1051−2138	Palomar/TSpec	T9:	0.113 ± 0.026	0.132 ± 0.003	0.262 ± 0.008	0.075 ± 0.006	0.254 ± 0.002	0.412 ± 0.007
WISE J1124−0421	IRTF/SpeX	T7	0.108 ± 0.005	0.269 ± 0.003	0.259 ± 0.010	0.252 ± 0.008	0.366 ± 0.003	0.692 ± 0.012
WISE J1143+4431	Keck/NIRSPEC-J	T8.5	—	0.170 ± 0.018	—	—	0.248 ± 0.014	—
WISE J1221−3136	IRTF/SpeX	T6.5	0.136 ± 0.007	0.298 ± 0.005	0.268 ± 0.013	0.258 ± 0.013	0.399 ± 0.005	0.579 ± 0.016
WISE J1225−1013	IRTF/SpeX	T6	0.160 ± 0.004	0.358 ± 0.004	0.289 ± 0.008	0.301 ± 0.007	0.454 ± 0.003	0.717 ± 0.011
WISE J1250+2628	Keck/NIRSPEC-J	T6.5	—	0.312 ± 0.003	—	—	0.422 ± 0.002	—
WISE J1257+4008	IRTF/SpeX	T7	0.097 ± 0.010	0.337 ± 0.008	0.206 ± 0.018	0.177 ± 0.016	0.386 ± 0.007	0.670 ± 0.025

Object Name J2000 Coordinates	Instrument	NIR Sp. Type	H$_2$O−J	CH$_4$−J	H$_2$O−H	CH$_4$−H	W$_J$	NH$_3$−H
(1)	(2)	(3)	(4)	(5)	(6)	(7)	(8)	(9)
WISE J1301−0302	Keck/NIRSPEC-J	T8.5	—	0.191 ± 0.015	—	—	0.273 ± 0.009	—
WISE J1318−1758	Palomar/TSpec	T9:	0.072 ± 0.020	0.122 ± 0.002	0.113 ± 0.006	0.133 ± 0.004	0.285 ± 0.002	0.637 ± 0.005
WISE J1337+2636	Keck/NIRSPEC-J	T5	—	0.366 ± 0.004	—	—	0.524 ± 0.003	—
WISE J1400−3850	IRTF/SpeX	T4	0.399 ± 0.013	0.520 ± 0.010	0.437 ± 0.018	0.604 ± 0.017	0.677 ± 0.011	0.850 ± 0.021
WISE J1517+0529	Keck/NIRSPEC-J	T8	—	0.175 ± 0.027	—	—	0.294 ± 0.013	—
WISE J1523+3125	Gemini/GNIRS	T6.5 pec	0.090 ± 0.011	0.298 ± 0.008	0.222 ± 0.013	0.256 ± 0.020	0.401 ± 0.007	0.652 ± 0.025
WISE J1542+2230	HST/WFC3	T9.5	0.008 ± 0.014	0.092 ± 0.009	0.106 ± 0.013	0.136 ± 0.017	0.182 ± 0.009	0.539 ± 0.019
WISE J1544+5842	Keck/NIRSPEC-J	T7.5	—	0.210 ± 0.027	—	—	0.367 ± 0.021	—
WISE J1632+0329	IRTF/SpeX	T5	0.216 ± 0.013	0.365 ± 0.011	0.239 ± 0.024	0.439 ± 0.021	0.513 ± 0.013	0.741 ± 0.032
WISE J1636−0743	IRTF/SpeX	T4.5	0.448 ± 0.020	0.698 ± 0.019	0.366 ± 0.024	0.591 ± 0.023	0.807 ± 0.020	0.789 ± 0.035
WISE J1707−1744	Palomar/TSpec	T5:	0.226 ± 0.016	0.352 ± 0.009	0.301 ± 0.025	0.391 ± 0.018	0.535 ± 0.010	0.794 ± 0.028
WISE J1721+1117	IRTF/SpeX	T6	0.144 ± 0.015	0.372 ± 0.011	0.236 ± 0.031	0.279 ± 0.026	0.425 ± 0.011	0.688 ± 0.040
WISE J1730+4207	IRTF/SpeX	T0 sb	0.549 ± 0.008	0.679 ± 0.008	0.622 ± 0.008	0.831 ± 0.008	0.751 ± 0.008	0.870 ± 0.010
WISE J1734+5023	IRTF/SpeX	T4	0.389 ± 0.004	0.339 ± 0.003	0.498 ± 0.005	0.543 ± 0.005	0.650 ± 0.004	0.936 ± 0.007
WISE J1736+6059	Keck/NIRSPEC-J	T8	—	0.196 ± 0.006	—	—	0.295 ± 0.005	—
WISE J1738+6142	Palomar/TSpec	extr. red	0.527 ± 0.038	0.792 ± 0.035	0.629 ± 0.020	1.148 ± 0.019	0.719 ± 0.033	0.844 ± 0.022
	IRTF/SpeX	extr. red	0.676 ± 0.026	0.998 ± 0.025	0.635 ± 0.015	1.095 ± 0.017	1.008 ± 0.024	0.821 ± 0.018
WISE J1741+1327	IRTF/SpeX	T5	0.244 ± 0.015	0.425 ± 0.011	0.334 ± 0.026	0.357 ± 0.023	0.511 ± 0.011	0.643 ± 0.030
WISE J1743+4211	Palomar/TSpec	T4.5	0.381 ± 0.007	0.493 ± 0.005	0.397 ± 0.007	0.491 ± 0.006	0.610 ± 0.005	0.759 ± 0.008
WISE J1745+6459	Keck/NIRSPEC-J	T7	—	0.298 ± 0.012	—	—	0.400 ± 0.010	—
WISE J1746−0338	Palomar/TSpec	T6	0.181 ± 0.015	0.338 ± 0.008	0.369 ± 0.022	0.305 ± 0.014	0.465 ± 0.008	0.755 ± 0.023
WISE J1755+1803	Palomar/TSpec	T2	0.630 ± 0.009	0.610 ± 0.006	0.533 ± 0.006	0.847 ± 0.006	0.696 ± 0.007	0.827 ± 0.007
WISE J1759+5442	Keck/NIRSPEC-J	T7	—	0.252 ± 0.009	—	—	0.379 ± 0.007	—
WISE J1809−0448	IRTF/SpeX	T0.5	0.619 ± 0.006	0.694 ± 0.005	0.556 ± 0.005	0.950 ± 0.006	0.757 ± 0.004	0.765 ± 0.006
WISE J1812+2007	Keck/NIRSPEC-J	T9	—	0.138 ± 0.015	—	—	0.216 ± 0.011	—
WISE J1813+2835	Keck/NIRSPEC-J	T8	—	0.172 ± 0.003	—	—	0.287 ± 0.002	—
WISE J1840+2932	Keck/NIRSPEC-J	T6	—	0.325 ± 0.013	—	—	0.465 ± 0.010	—
WISE J1909−5204	Magellan/FIRE	T5.5	0.292 ± 0.005	0.335 ± 0.002	0.337 ± 0.003	0.270 ± 0.002	0.550 ± 0.003	0.737 ± 0.004
WISE J1913+6444	Palomar/TSpec	T5:	0.362 ± 0.028	0.481 ± 0.016	0.338 ± 0.034	0.418 ± 0.027	0.550 ± 0.017	0.834 ± 0.039
WISE J1928+2356	IRTF/SpeX	T6	0.210 ± 0.001	0.447 ± 0.001	0.300 ± 0.001	0.344 ± 0.001	0.605 ± 0.001	0.701 ± 0.001
WISE J1954+6915	Keck/NIRSPEC-J	T5.5	—	0.404 ± 0.007	—	—	0.494 ± 0.005	—
WISE J1955−2540	Keck/NIRSPEC-J	T8	—	0.166 ± 0.007	—	—	0.288 ± 0.005	—
WISE J2008−0834	IRTF/SpeX	T5.5	0.205 ± 0.005	0.277 ± 0.003	0.351 ± 0.009	0.357 ± 0.008	0.543 ± 0.004	0.829 ± 0.012
WISE J2014+0424	Gemini/GNIRS	T6.5 pec	0.096 ± 0.006	0.268 ± 0.004	0.214 ± 0.009	0.253 ± 0.009	0.409 ± 0.004	0.715 ± 0.014
WISE J2015+6646	Palomar/TSpec	T8	0.071 ± 0.015	0.207 ± 0.008	0.138 ± 0.019	0.149 ± 0.014	0.350 ± 0.008	0.594 ± 0.020
WISE J2019−1148	Palomar/TSpec	T8:	0.063 ± 0.041	0.137 ± 0.018	0.141 ± 0.040	0.122 ± 0.026	0.245 ± 0.018	0.675 ± 0.040
WISE J2030+0749	IRTF/SpeX	T1.5	0.714 ± 0.002	0.828 ± 0.002	0.585 ± 0.001	0.889 ± 0.001	0.949 ± 0.002	0.854 ± 0.002
WISE J2043+6220	IRTF/SpeX	T1.5	0.561 ± 0.009	0.520 ± 0.006	0.610 ± 0.011	1.009 ± 0.011	0.793 ± 0.008	0.995 ± 0.013
WISE J2123−2614	IRTF/SpeX	T5.5	0.223 ± 0.018	0.383 ± 0.012	0.244 ± 0.035	0.297 ± 0.030	0.496 ± 0.013	0.745 ± 0.044
WISE J2147−1029	Keck/NIRSPEC-J	T7.5	—	0.214 ± 0.006	—	—	0.356 ± 0.004	—
WISE J2236+5105	Palomar/TSpec	T5.5	0.185 ± 0.001	0.374 ± 0.001	0.312 ± 0.001	0.423 ± 0.001	0.477 ± 0.001	0.708 ± 0.001
WISE J2237+7228	Keck/NIRSPEC-J	T6	0.170 ± 0.004	0.345 ± 0.005	—	—	0.484 ± 0.004	—
WISE J2301+0216	IRTF/SpeX	T6.5	0.133 ± 0.006	0.266 ± 0.005	0.343 ± 0.012	0.276 ± 0.010	0.421 ± 0.005	0.844 ± 0.016
WISE J2303+1914	Palomar/TSpec	T4:	0.412 ± 0.002	0.467 ± 0.001	0.405 ± 0.003	0.525 ± 0.002	0.666 ± 0.001	0.841 ± 0.003
WISE J2335+4222	Keck/NIRSPEC-JH	T7	—	0.274 ± 0.008	—	0.208 ± 0.009	0.390 ± 0.010	0.671 ± 0.013
WISE J2357+1227	IRTF/SpeX	T6	0.143 ± 0.005	0.384 ± 0.004	0.245 ± 0.009	0.295 ± 0.008	0.387 ± 0.004	0.593 ± 0.010

T Dwarfs from Table 6

Object Name J2000 Coordinates	Instrument	NIR Sp. Type	H_2O-J	CH_4-J	H_2O-H	CH_4-H	W_J	NH_3-H
(1)	(2)	(3)	(4)	(5)	(6)	(7)	(8)	(9)
WISE J0920+4538	Palomar/TSpec	L9 sb?	0.588 ± 0.001	0.745 ± 0.001	0.618 ± 0.001	1.003 ± 0.001	0.774 ± 0.001	0.872 ± 0.001
ULAS J0950+0117	Magellan/FIRE	T8	0.066 ± 0.002	0.187 ± 0.001	0.189 ± 0.001	0.142 ± 0.001	0.394 ± 0.001	0.705 ± 0.002
WISE J1246−3139	Palomar/TSpec	T1	0.529 ± 0.001	0.682 ± 0.001	0.553 ± 0.001	0.909 ± 0.001	0.776 ± 0.001	0.868 ± 0.001
LHS 2803B	IRTF/SpeX	T5.5	0.168 ± 0.007	0.270 ± 0.005	0.297 ± 0.015	0.415 ± 0.014	0.534 ± 0.006	0.711 ± 0.019
BD +01°2920B	Magellan/FIRE	T8	0.070 ± 0.006	0.182 ± 0.002	0.236 ± 0.004	0.125 ± 0.002	0.393 ± 0.003	0.720 ± 0.004
WISE J1449+1147	Gemini/GNIRS	T5 pec	0.268 ± 0.006	0.378 ± 0.004	0.301 ± 0.006	0.394 ± 0.009	0.559 ± 0.005	0.767 ± 0.011
	Palomar/TSpec	T5 pec	0.232 ± 0.016	0.350 ± 0.009	0.303 ± 0.026	0.387 ± 0.017	0.543 ± 0.011	0.796 ± 0.029
PSOJ226.25−28.89	Palomar/TSpec	T2:	0.699 ± 0.018	0.649 ± 0.008	0.561 ± 0.011	0.831 ± 0.008	0.799 ± 0.008	0.827 ± 0.010
VHS J1543−0439	IRTF/SpeX	T5:	0.321 ± 0.019	0.381 ± 0.014	0.396 ± 0.034	0.523 ± 0.028	0.621 ± 0.020	0.750 ± 0.040
PSOJ246.42+15.46	Palomar/TSpec	T4.5:	0.319 ± 0.014	0.441 ± 0.009	0.373 ± 0.019	0.438 ± 0.013	0.604 ± 0.010	0.787 ± 0.019
PSOJ247.32+03.59	Palomar/TSpec	T2	0.442 ± 0.002	0.589 ± 0.002	0.456 ± 0.002	0.898 ± 0.002	0.677 ± 0.002	0.751 ± 0.003
WISE J1717+6128	Gemini/GNIRS	T8	0.026 ± 0.017	0.201 ± 0.009	0.207 ± 0.019	0.115 ± 0.018	0.316 ± 0.008	0.651 ± 0.028
WISE J1809+3838	IRTF/SpeX	T7.5	0.063 ± 0.014	0.232 ± 0.011	0.198 ± 0.024	0.148 ± 0.019	0.345 ± 0.010	0.609 ± 0.031
WISE J2342+0856	IRTF/SpeX	T6.5	0.114 ± 0.004	0.328 ± 0.004	0.213 ± 0.007	0.274 ± 0.007	0.380 ± 0.003	0.596 ± 0.009
WISE J2344+1034	Gemini/GNIRS	T9	0.037 ± 0.012	0.107 ± 0.005	0.149 ± 0.015	0.062 ± 0.017	0.233 ± 0.005	0.538 ± 0.025

[a]Cushing et al. (2011)

[b]Burgasser et al. (2011)
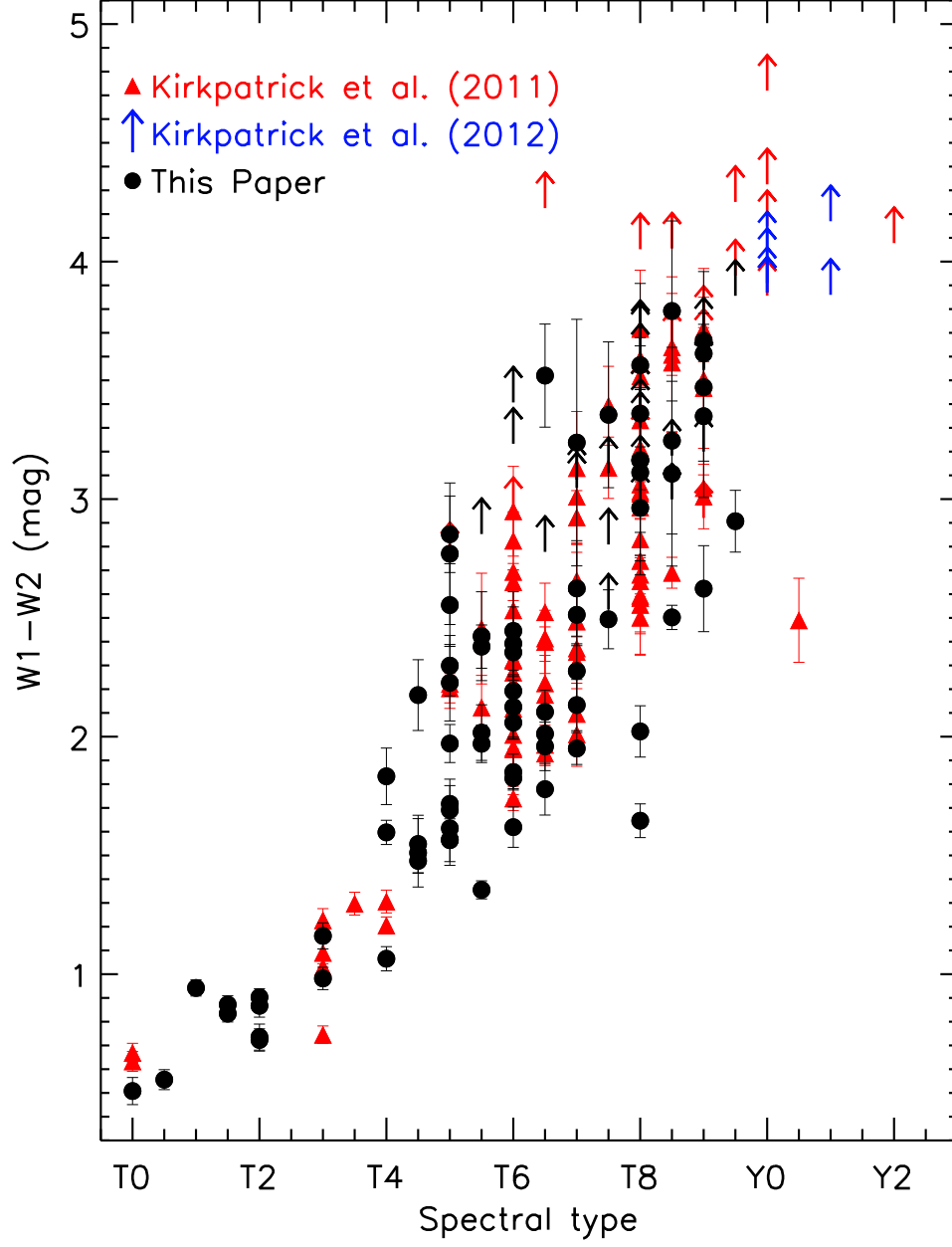
Fig. 1.— WISE $W1 - W2$ color versus spectral type. Objects from Kirkpatrick et al. (2011) (including those announced by Mainzer et al. (2011), Cushing et al. (2011), and Burgasser et al. (2011)) are marked with red triangles and limit arrows. The Y dwarfs from Kirkpatrick et al. (2012) are marked with blue squares and limit arrows. T dwarfs announced in this paper are marked with black circles and limit arrows.
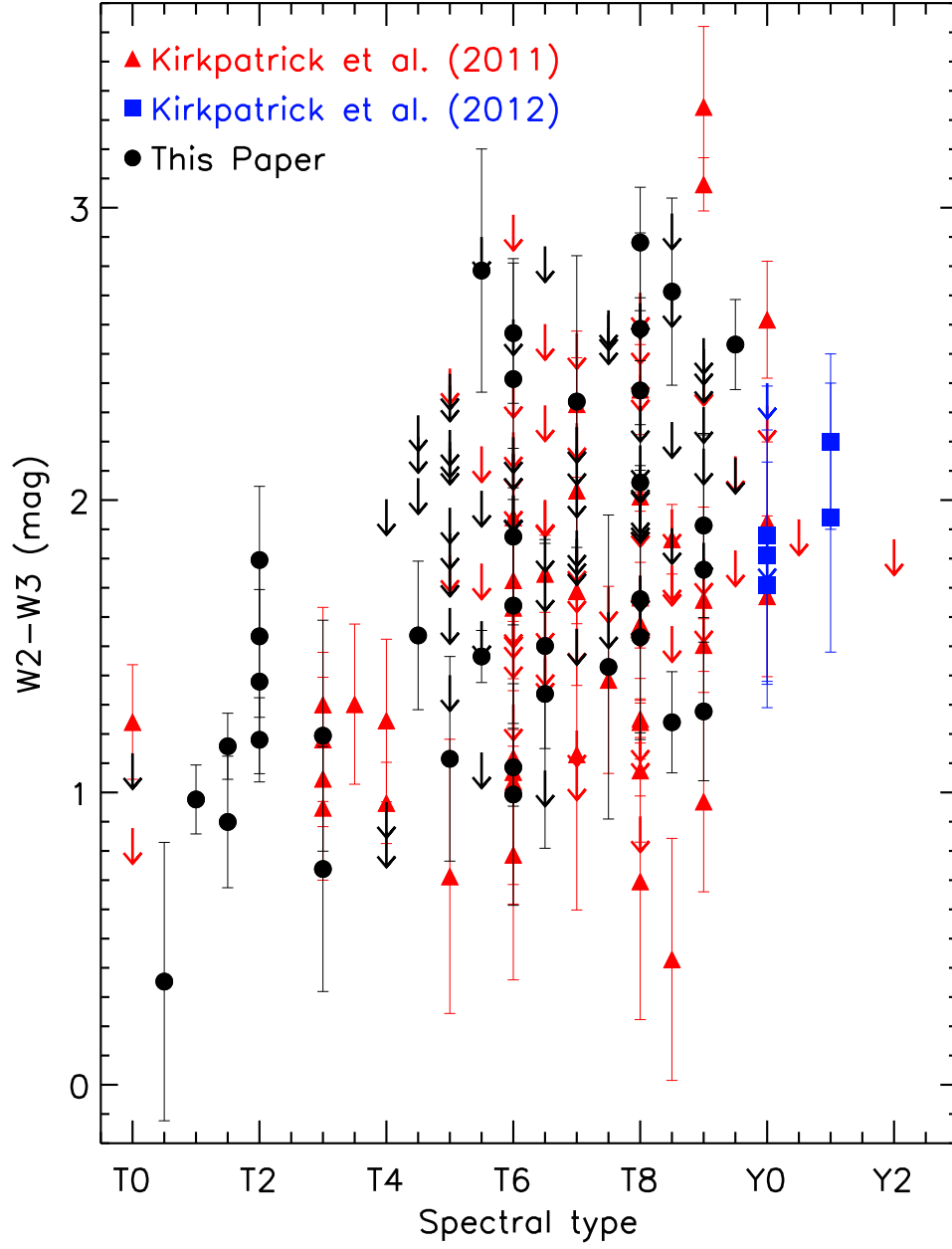
Fig. 2.— WISE $W2 - W3$ color versus spectral type. Same symbols as in Figure 1.
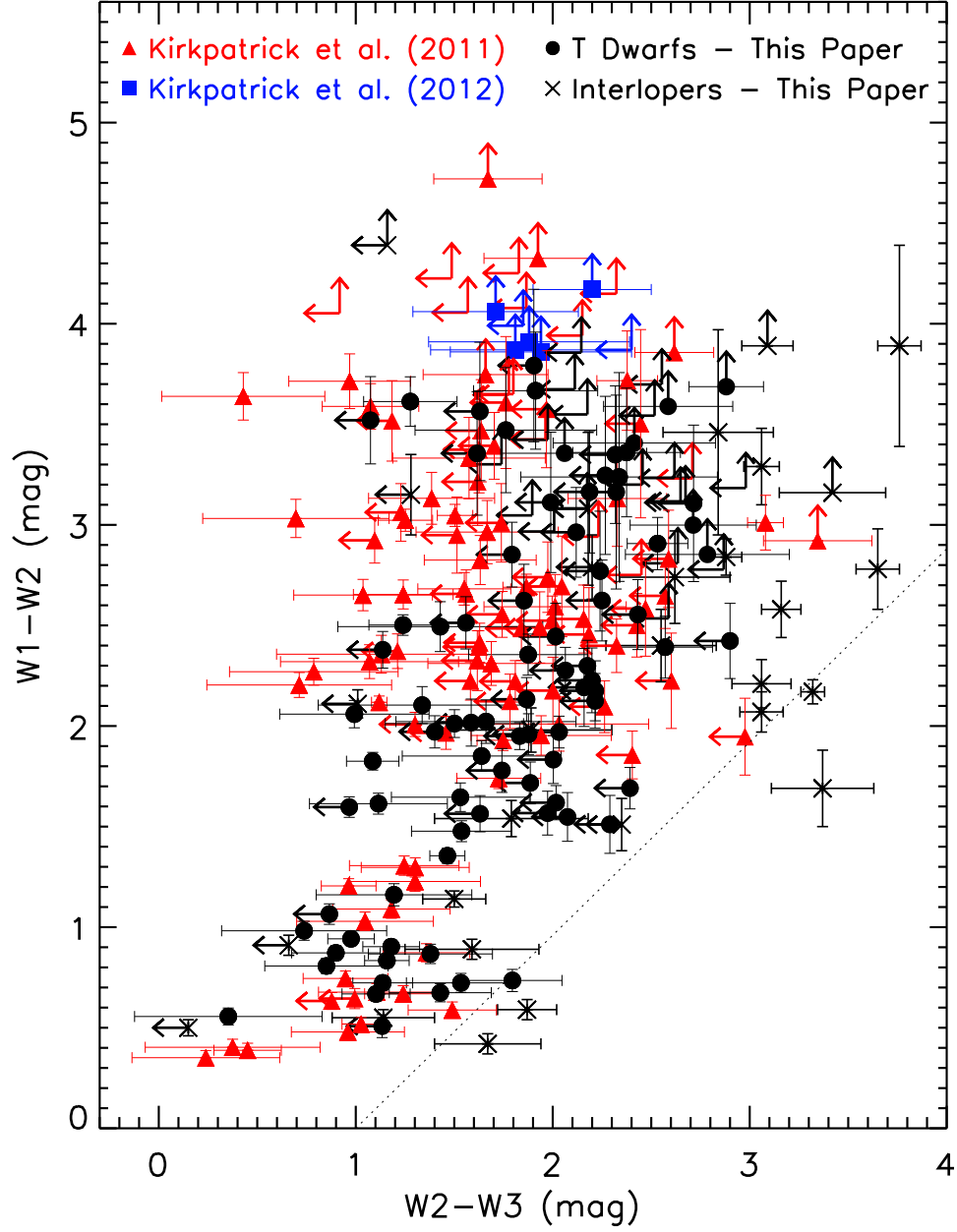
Fig. 3.— WISE $W1 - W2$ versus $W2 - W3$ color-color diagram. Same symbols as in Figure 1. Interlopers are marked by black x's and limits. The dotted line identifies our $W1 - W2 > 0.96(W2 - W3) - 0.96$ selection criterion.
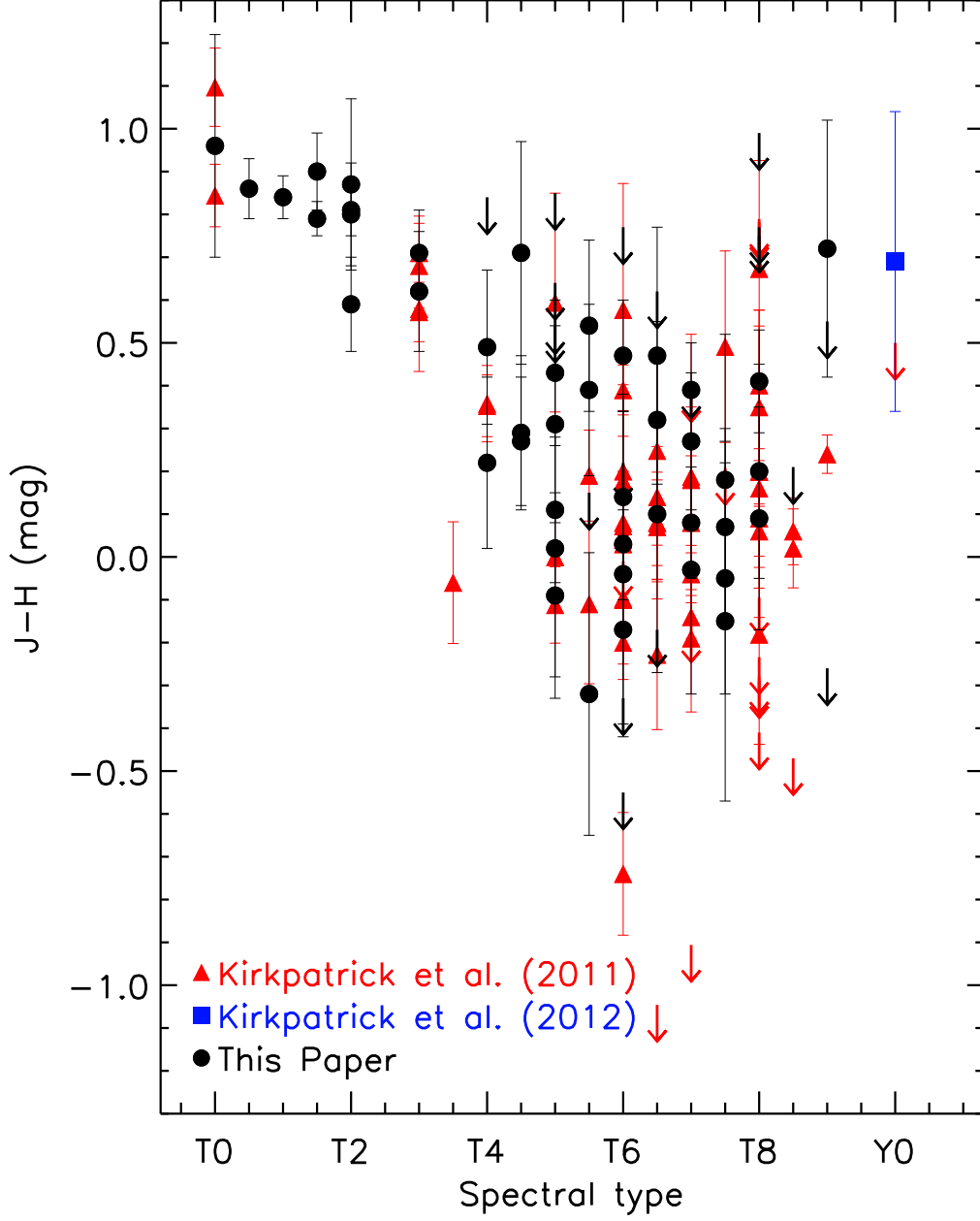
Fig. 4.— $J - H$ color versus spectral type. Same symbols as in Figure 1. A turnaround in the $J - H$ color at T7±1 is seen here, but it is tentative based on the large dispersion and uncertainties in our photometry.

Fig. 5.— $J - W2$ color versus spectral type. Same symbols as in Figure 1.
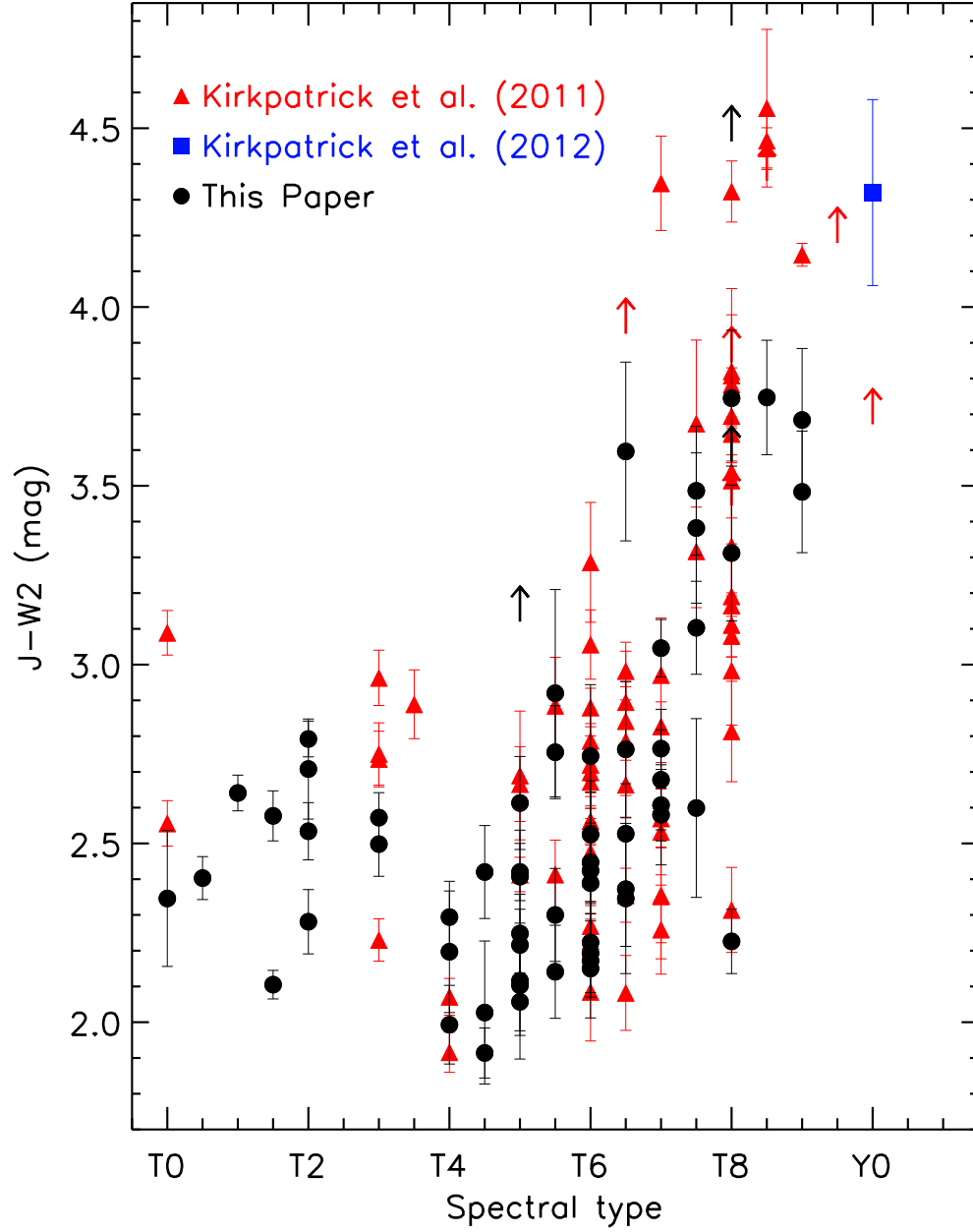
Fig. 6.— $H - W2$ color versus spectral type. Same symbols as in Figure 1.
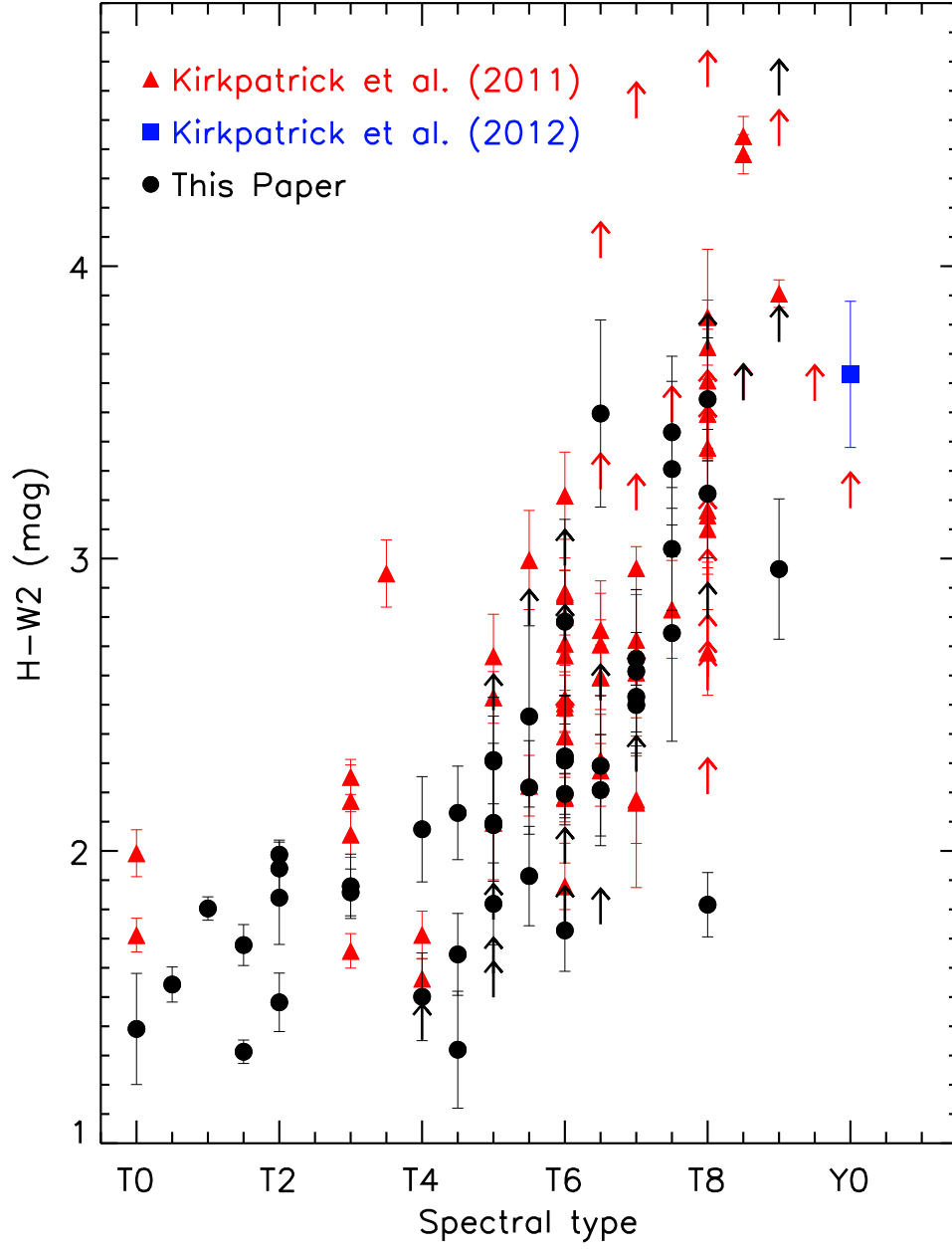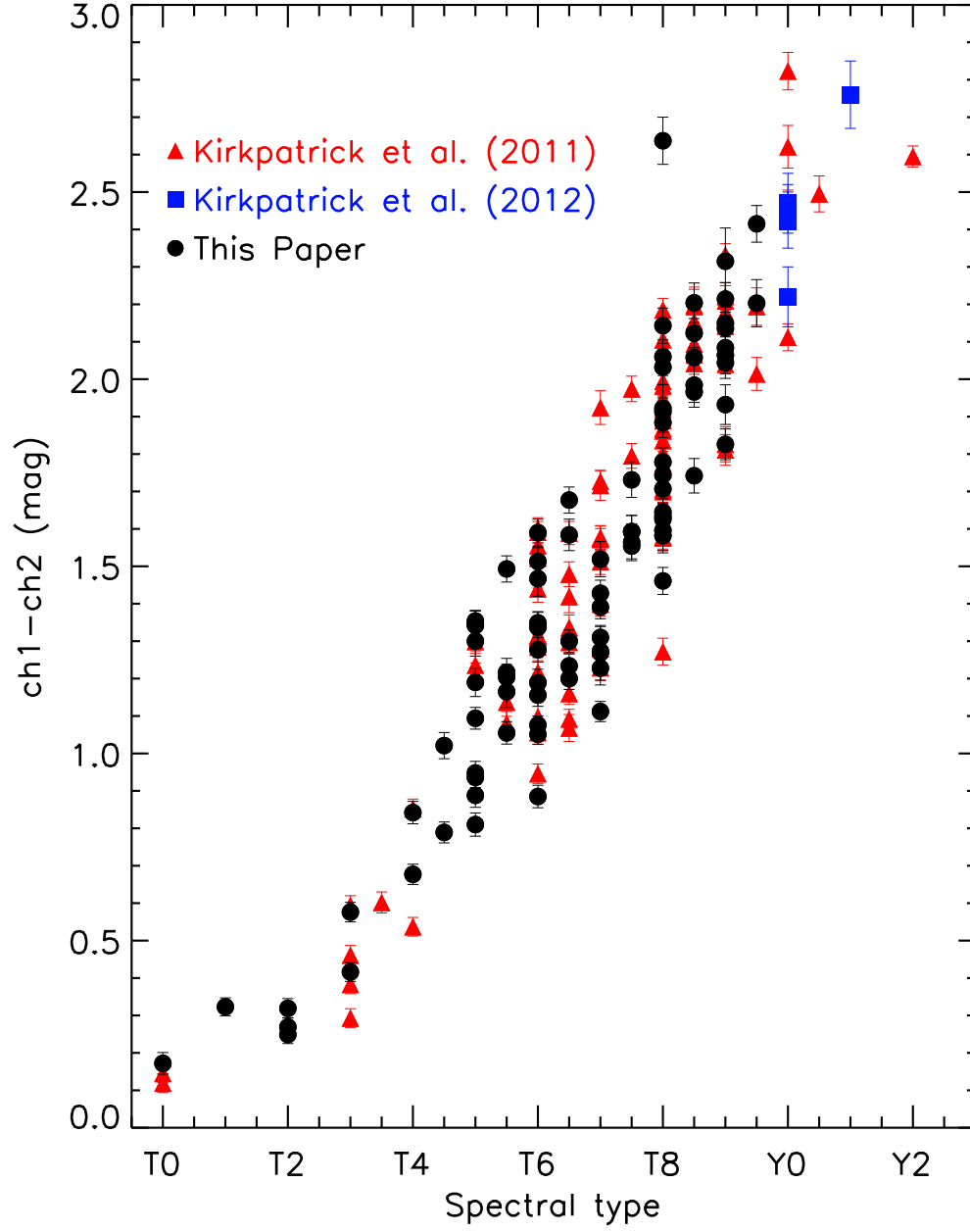
Fig. 7.— *Spitzer ch1 − ch2* versus spectral type. Same symbols as in Figure 1. These colors can nearly be fit by a straight line, but the early-type T dwarfs are all bluer than the fit.
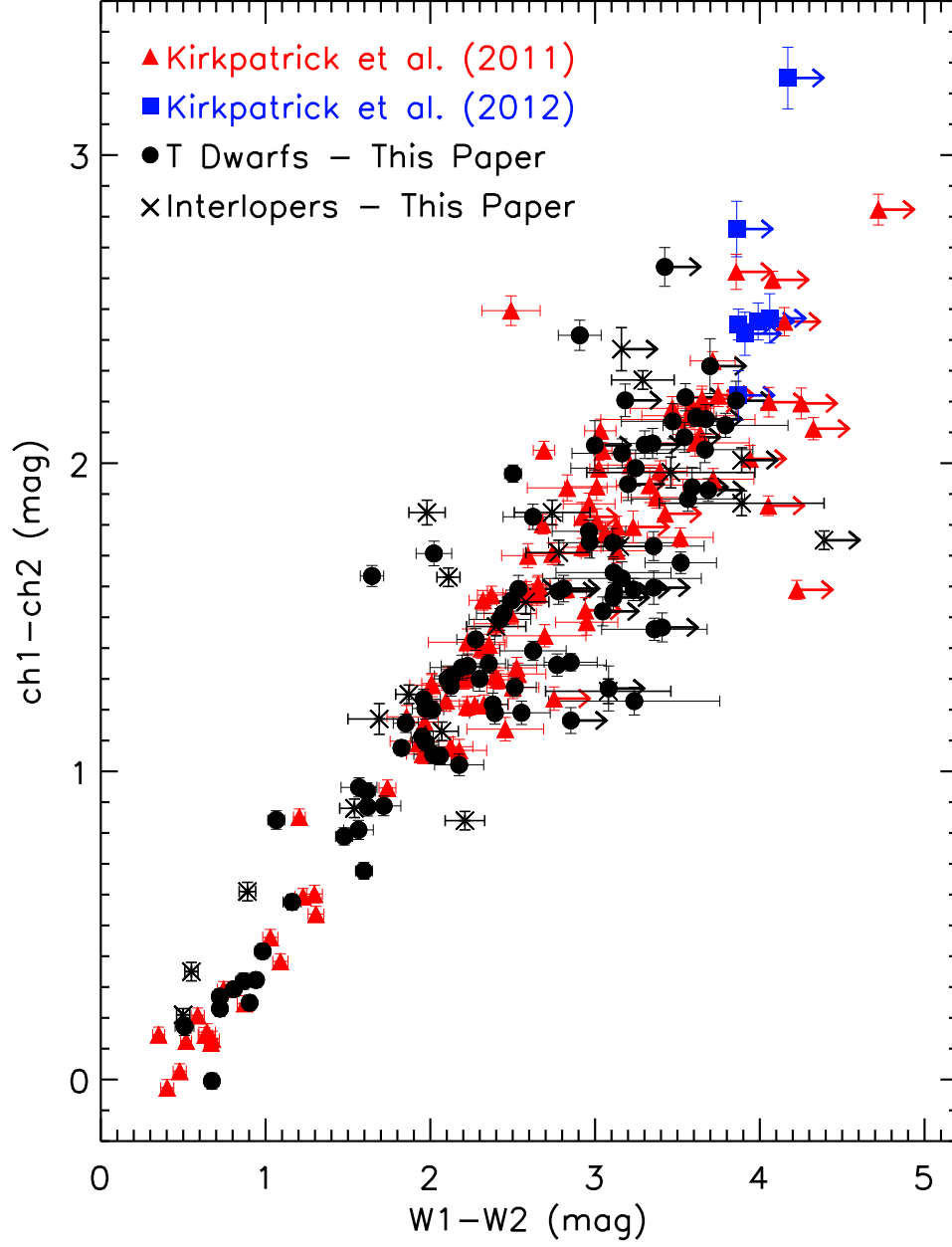
Fig. 8.— *Spitzer ch*1 − *ch*2 versus WISE *W*1 − *W*2 color-color diagram. Same symbols as in Figure 1. Interlopers are marked by black x's and limits.
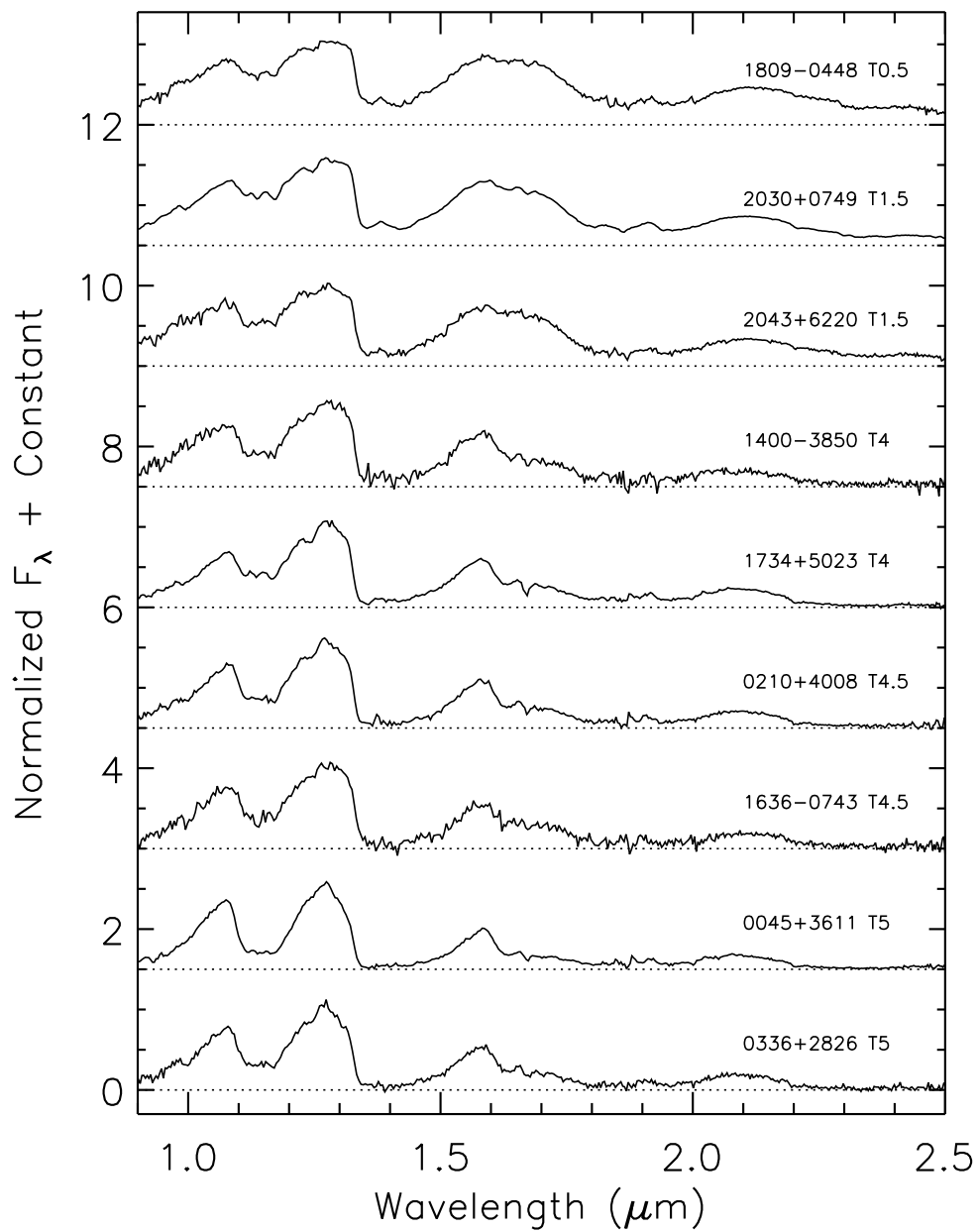
Fig. 9.— IRTF/SpeX spectra of confirmed WISE brown dwarfs with spectral types from T0.5 to T8.5. Spectra have been normalized at 1.27μm and offset vertically.
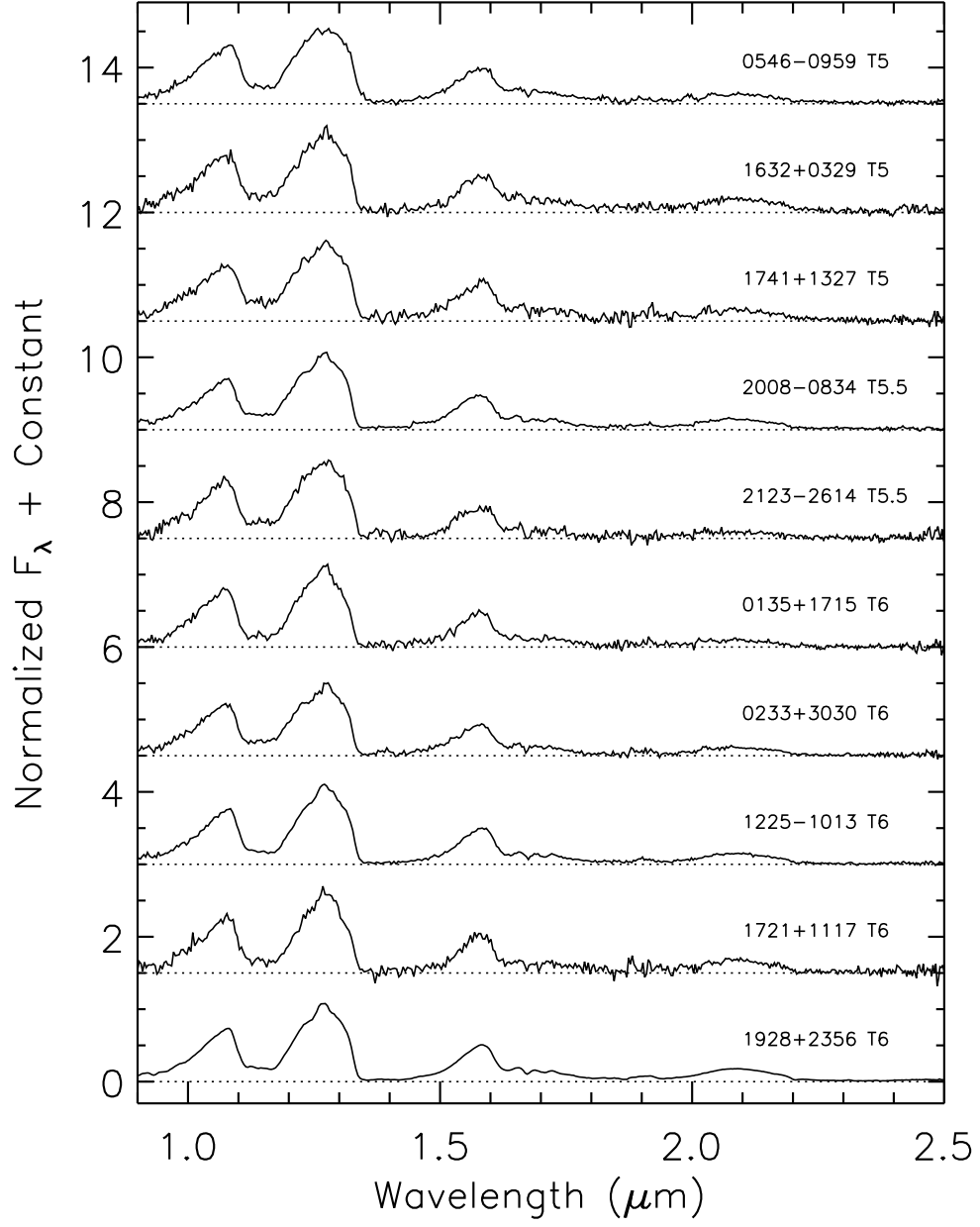
Fig. 9b.— Continued.
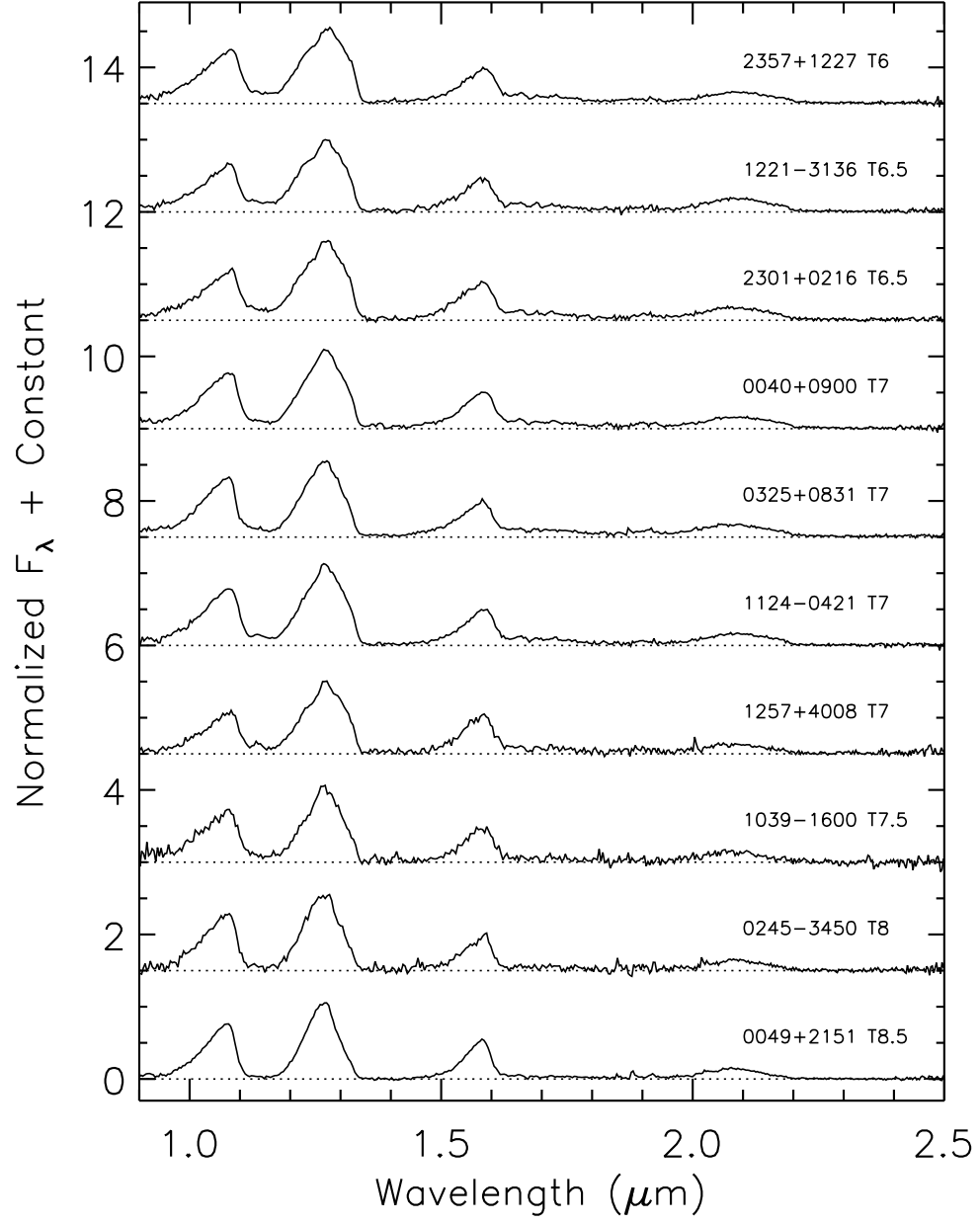
Fig. 9c.— Continued.
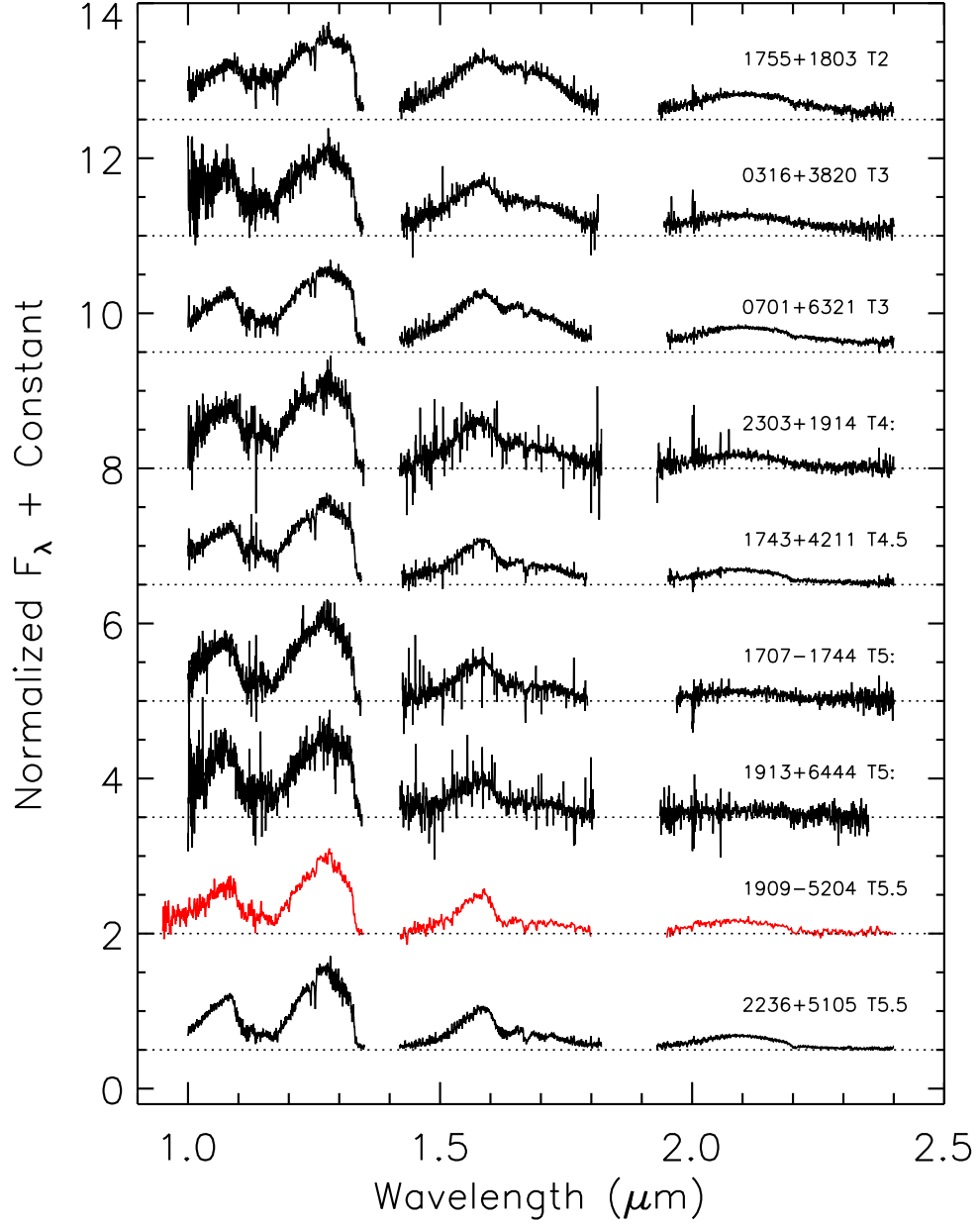
Fig. 10.— Other spectra of confirmed WISE brown dwarfs with spectral types from T2 to T9.5. Spectra have been normalized at 1.27μm and offset vertically. Palomar/TSpec spectra are shown in black, Magellan/FIRE spectra in red, and Gemini/GNIRS spectra in blue.
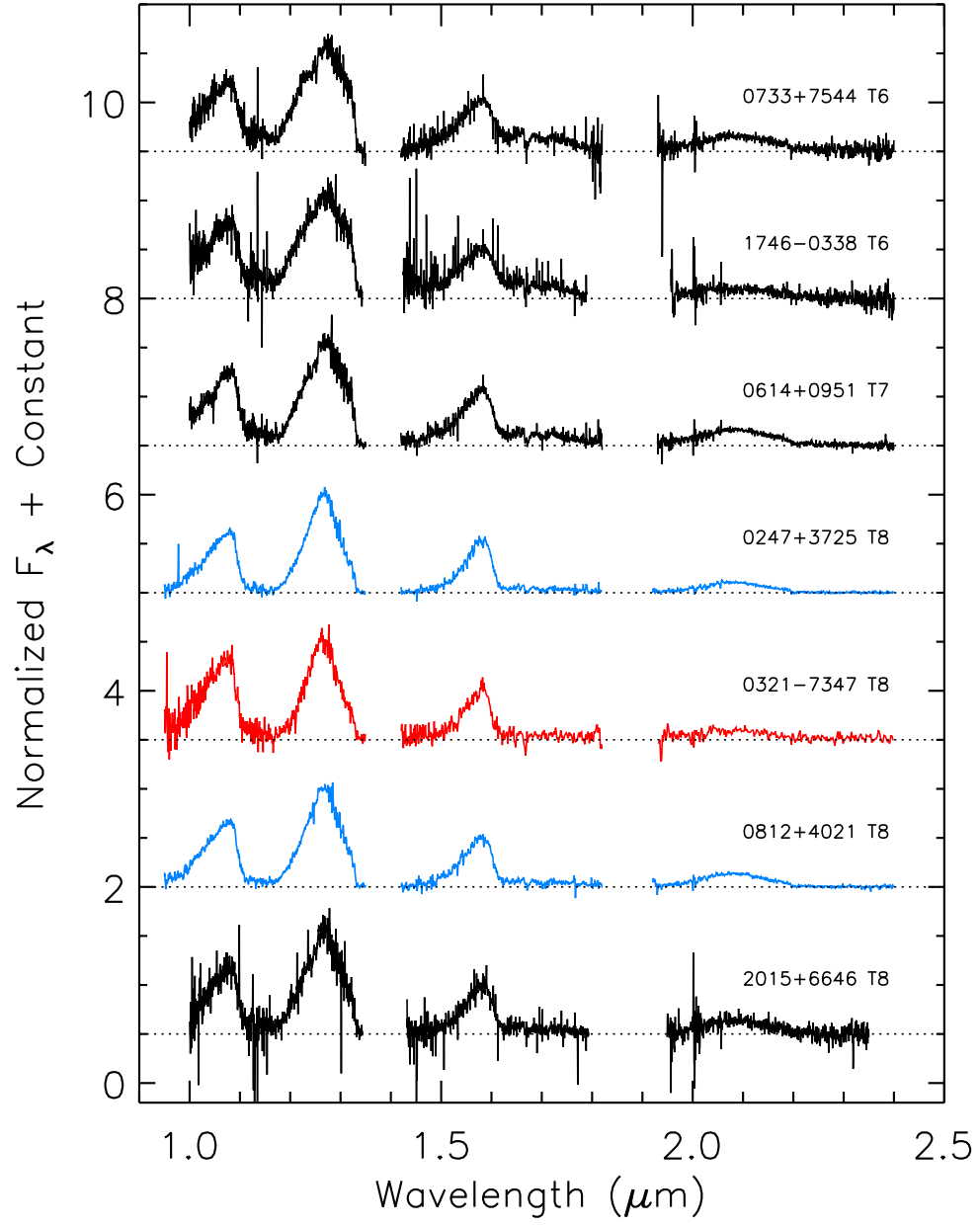
Fig. 10b.— Continued.
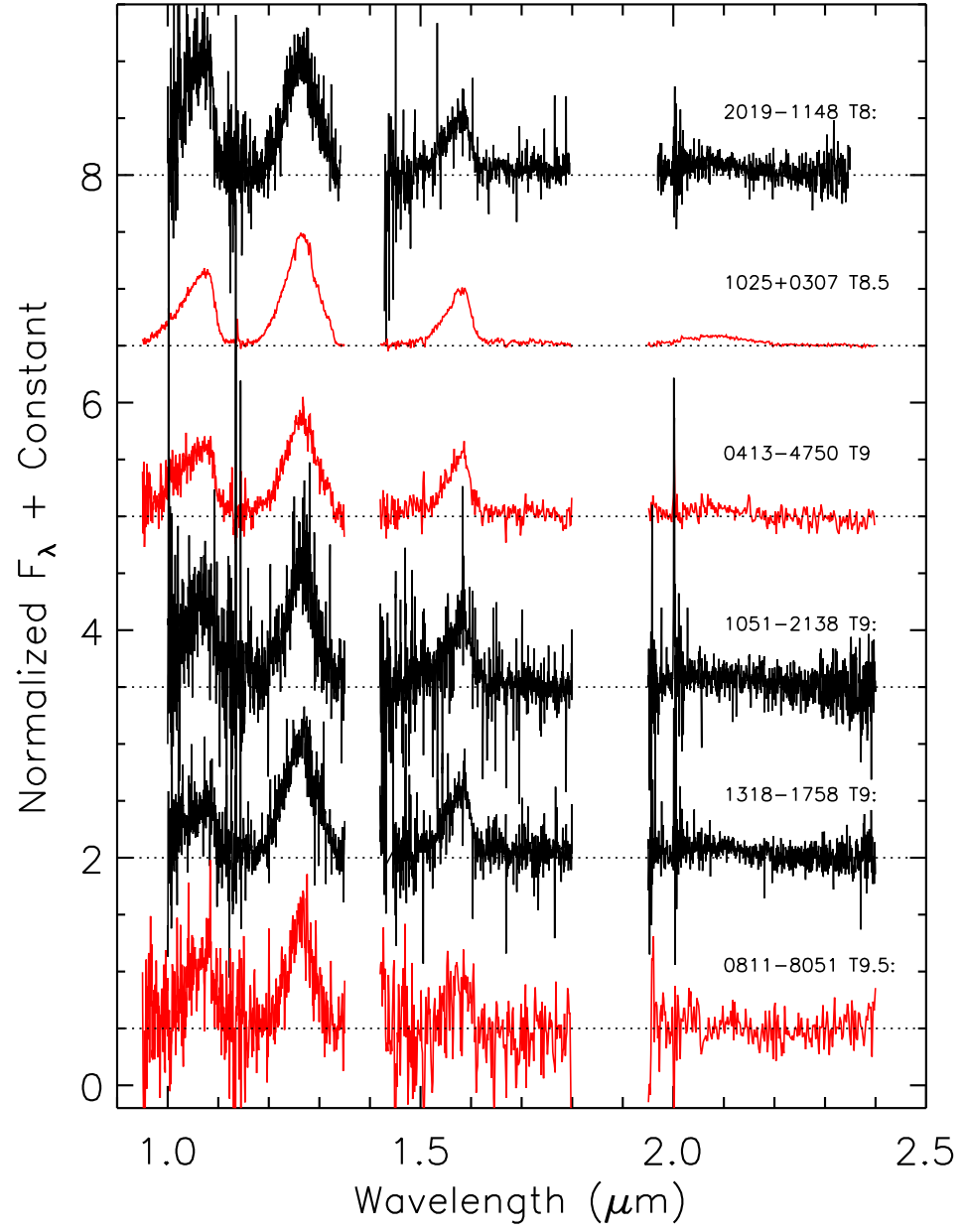
Fig. 10c.— Continued.
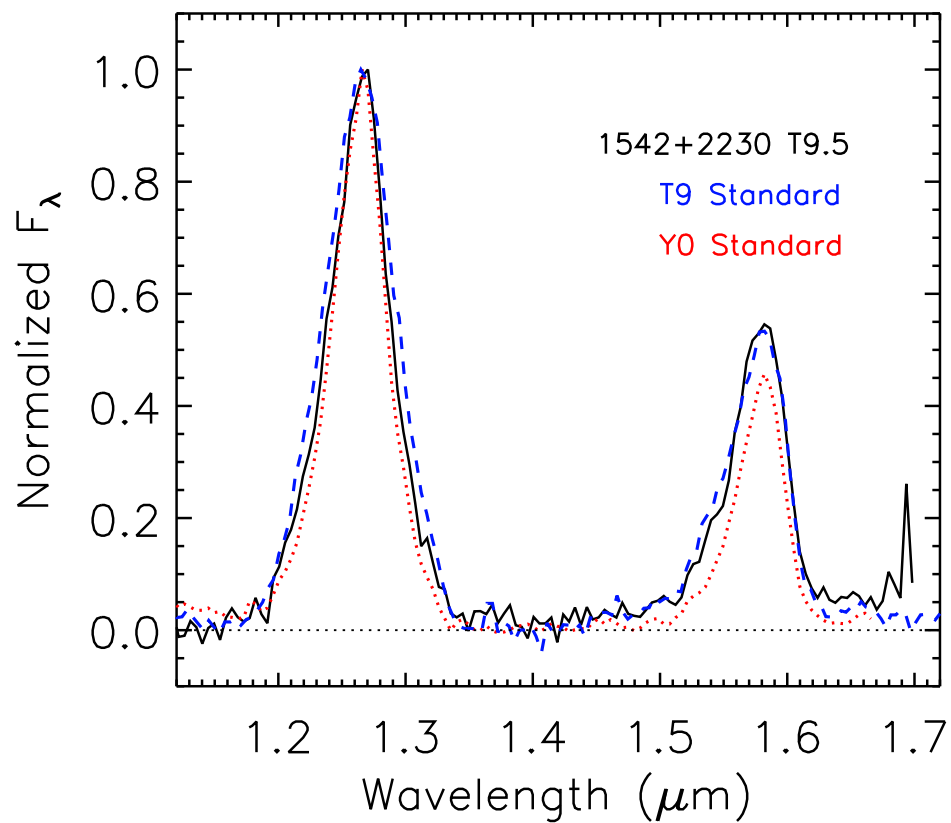
Fig. 11.— The HST/WFC3 spectrum of WISE J154214.00+223005.2 (T9.5). The T9 (UGPS J072227.51−054031.2) and Y0 (WISEP J173835.52+273258.9) spectral standards (Cushing et al. 2011) are included for comparison. Spectra have been normalized at 1.27μm.
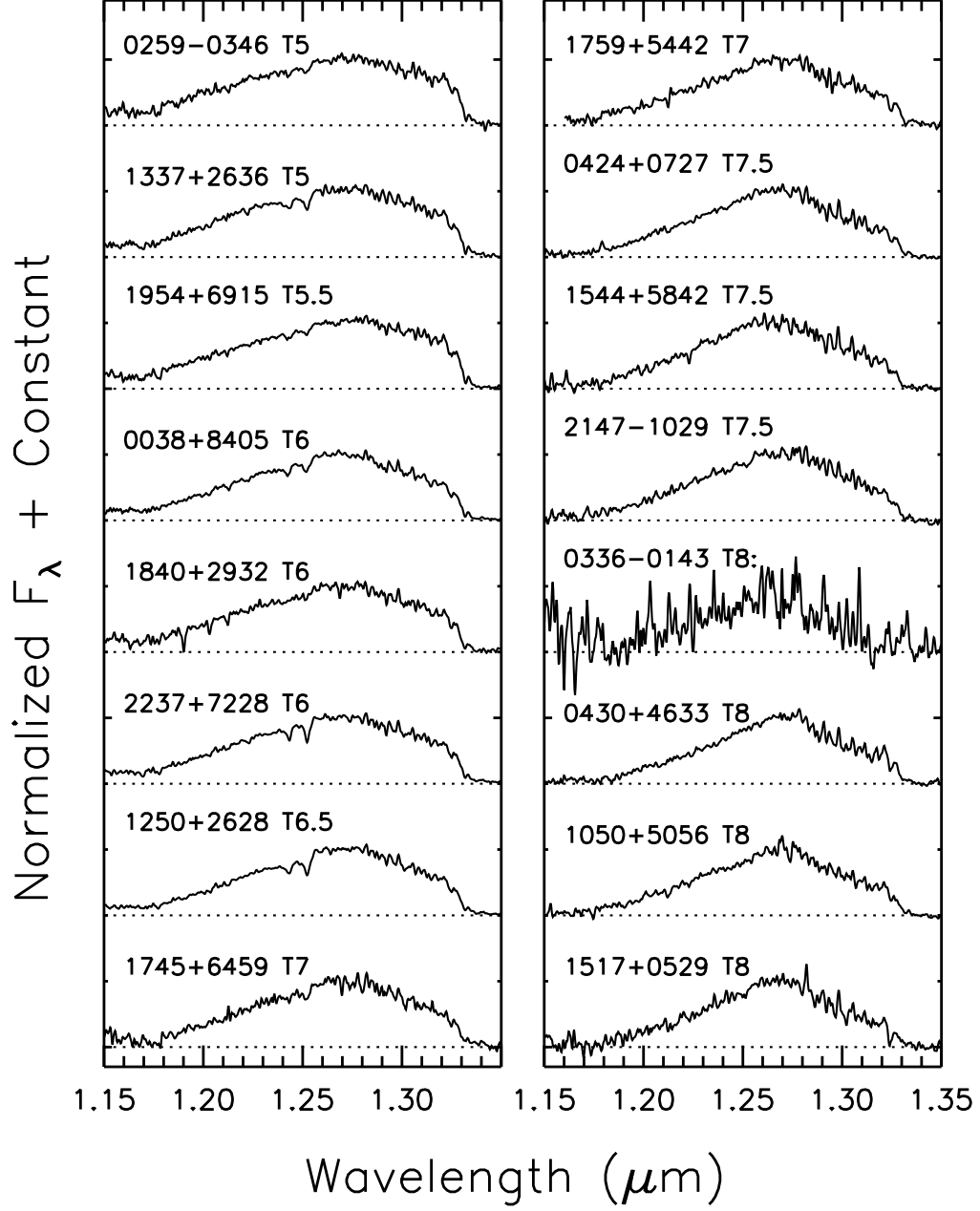
Fig. 12.— Keck/NIRSPEC J-band spectra of confirmed WISE brown dwarfs with spectral types from T5 to T9. Spectra have been normalized at 1.27μm and offset vertically.
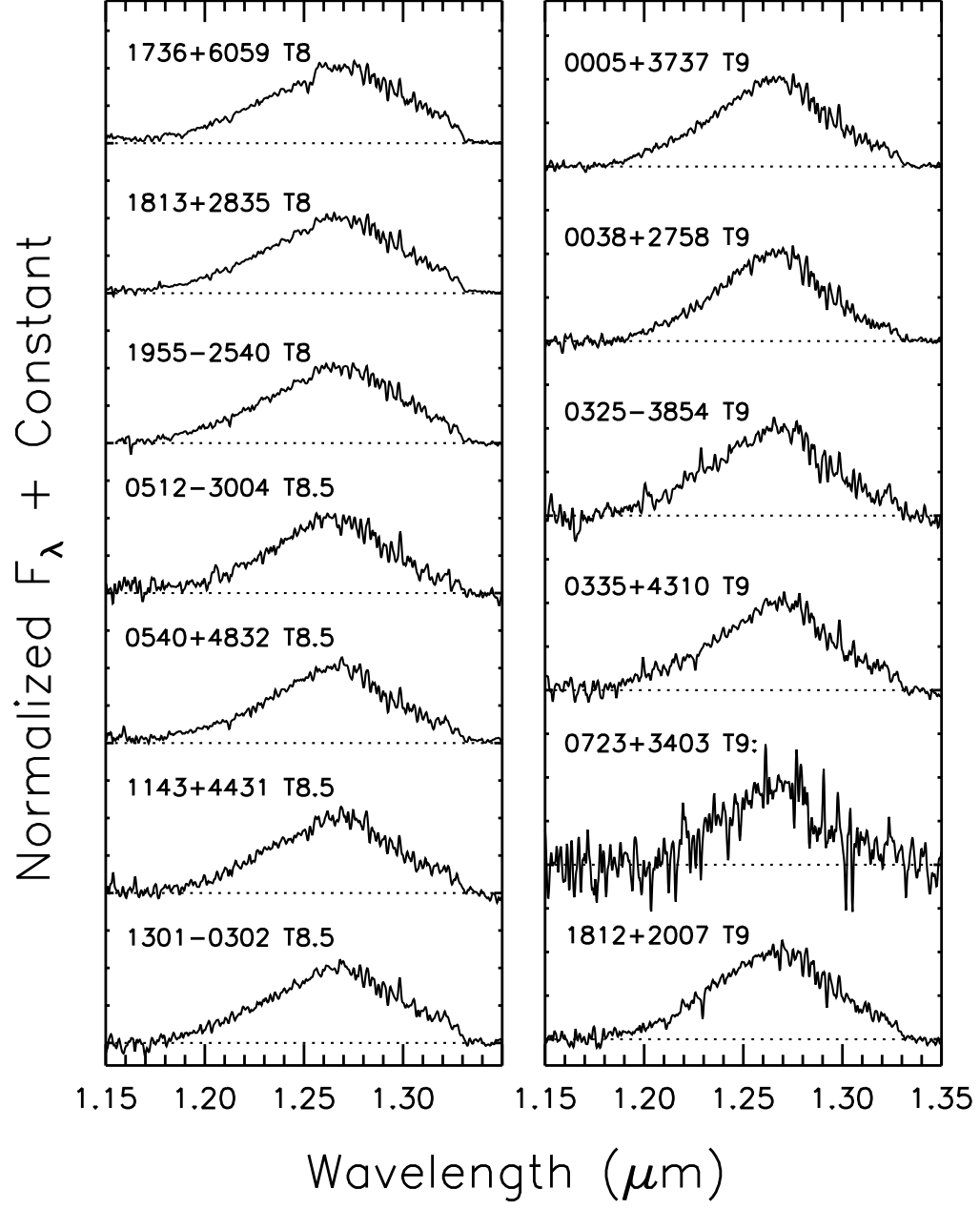
Fig. 12b.— Continued.
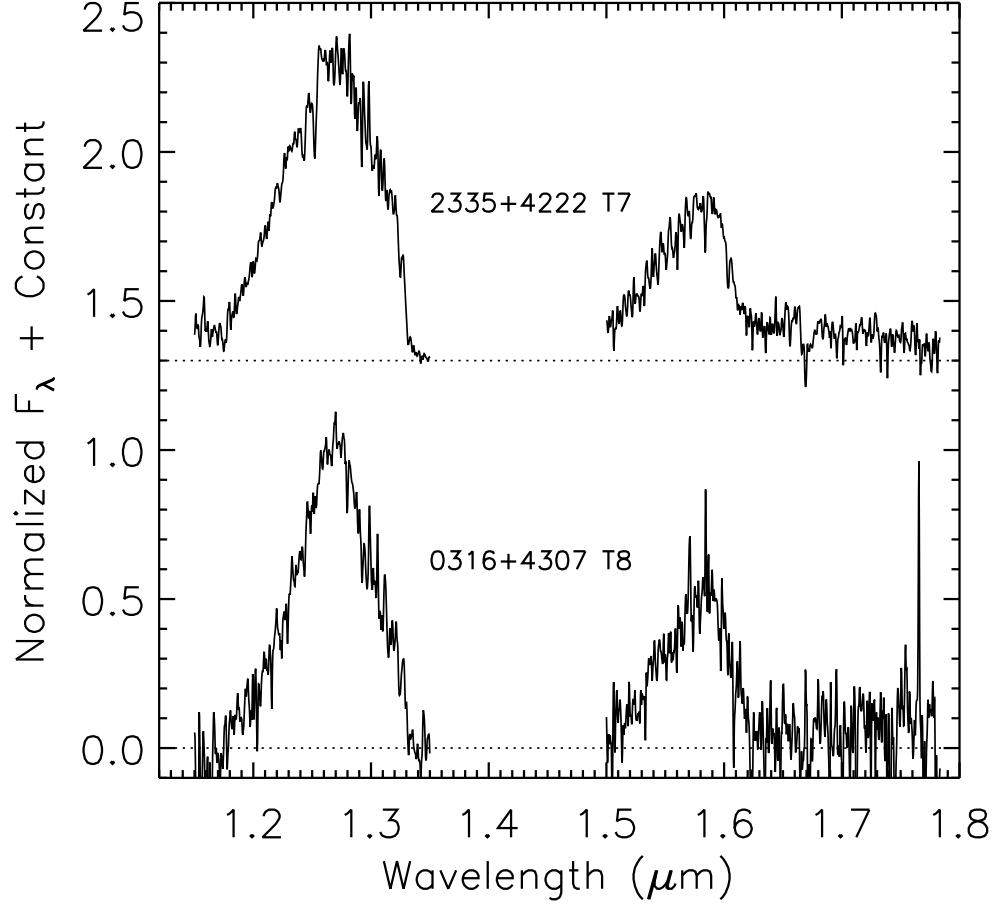
Fig. 13.— Keck/NIRSPEC J- and H-band spectra of confirmed WISE brown dwarfs WISE J233543.79+422255.2 (T7) and WISE J031624.35+430709.1 (T8). Spectra have been normalized at 1.27μm and offset vertically. The H-band spectra were scaled relative to the J-band data using the ratio of peak fluxes produced by REDSPEC (McLean et al. 2003).
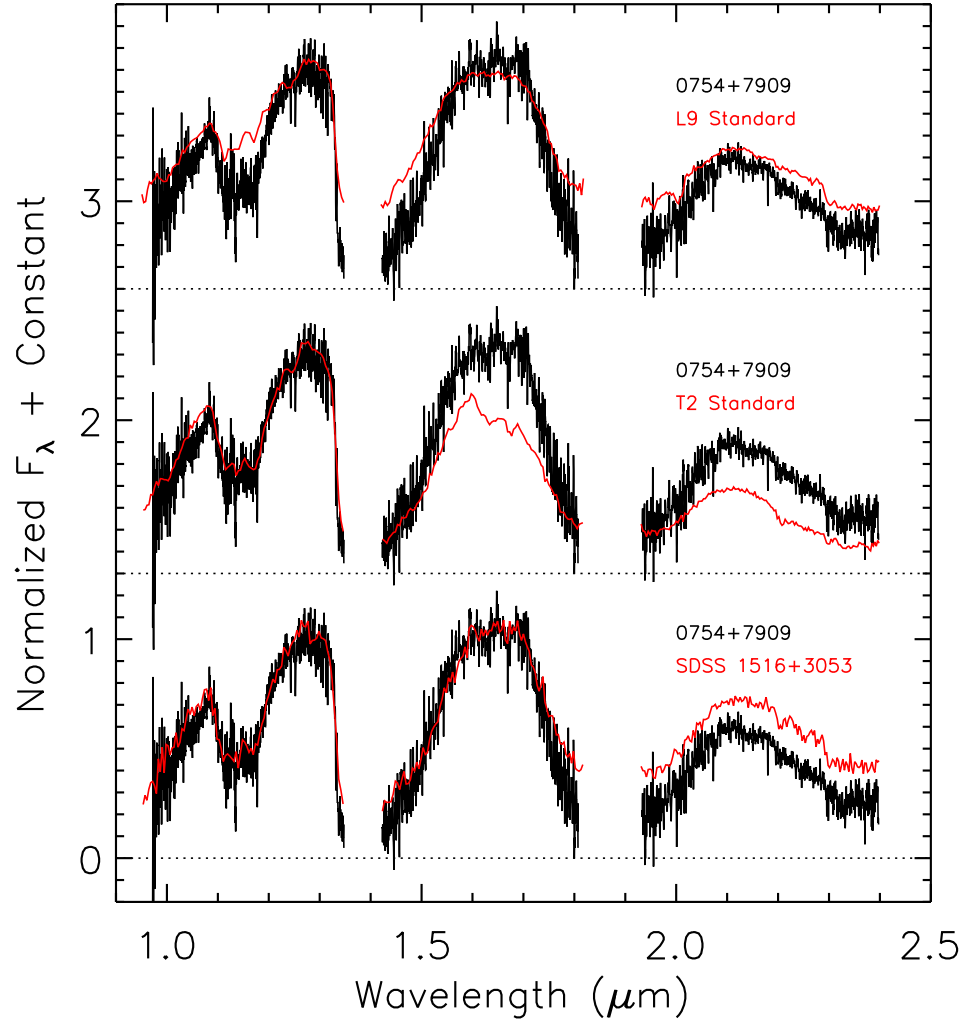
Fig. 14.— This Palomar/TSpec spectrum of WISE 0754+7909 is not easily classified as a L or T dwarf. SDSS J1516+3053 has been classified as a T0.5±1 (Chiu et al. 2006) and T1.5±2 (Burgasser et al. 2010) and is a better match in the J and H bands than the spectral standards. Spectra have been normalized at 1.27μm and offset vertically.
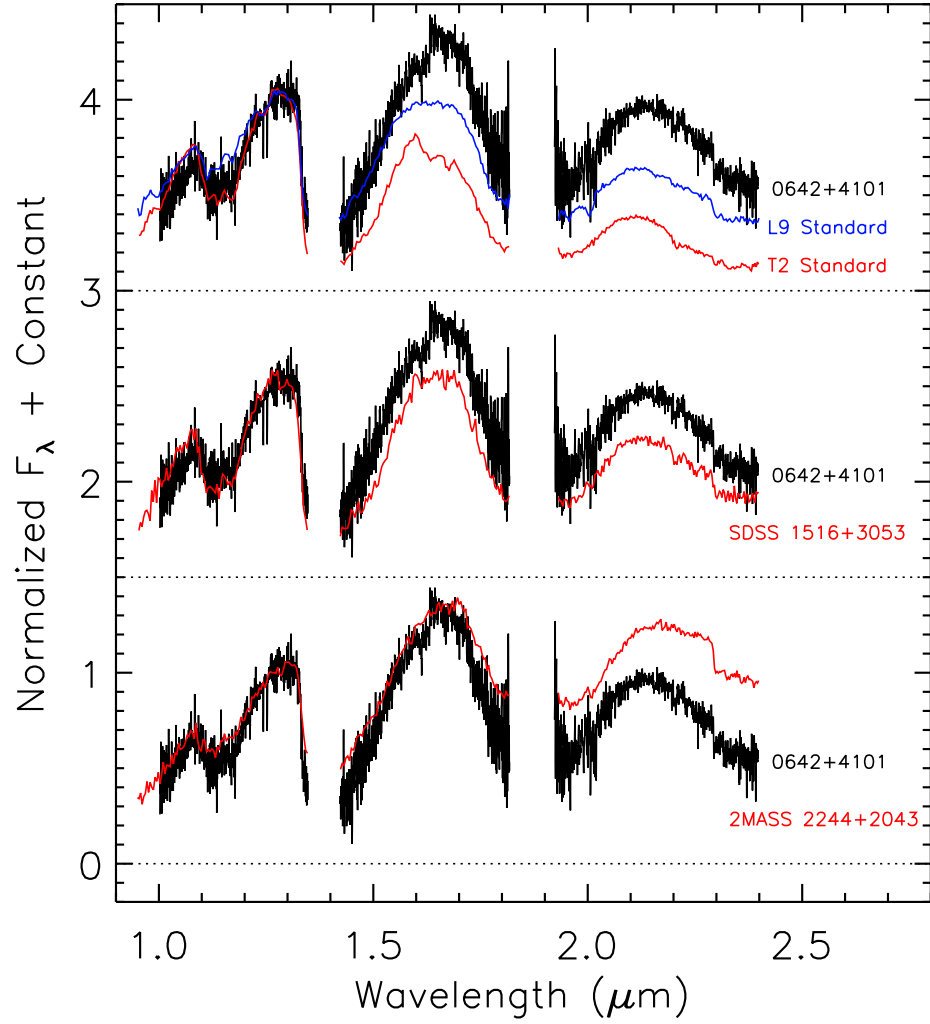
Fig. 15.— This Palomar/TSpec spectrum of WISE 0642+4101 is not easily classified as a L or T dwarf. It is redder than SDSS J1516+3053 (T1.5±2; Burgasser et al. 2010) and bluer than 2MASSW J2244+2043 (L7.5±2; Looper et al. 2008). Spectra have been normalized at 1.27μm and offset vertically.
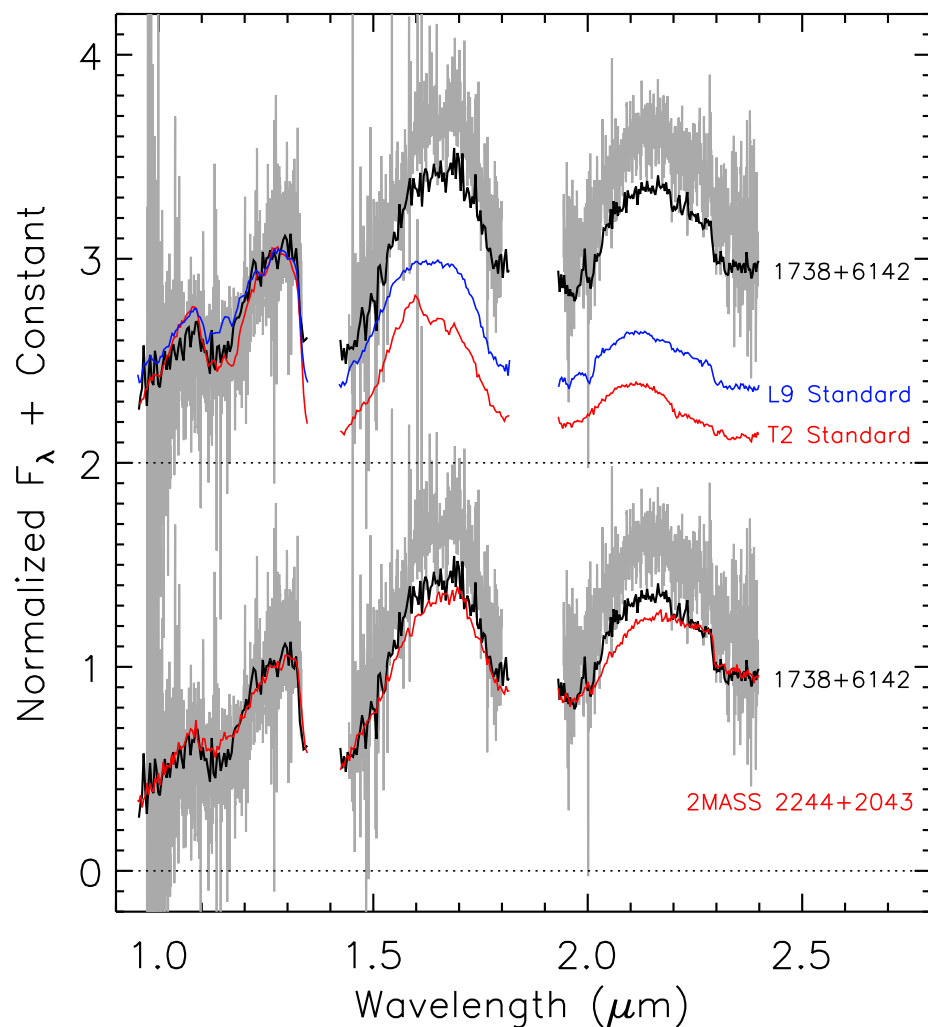
Fig. 16.— WISE 1738+6142 was observed with both Palomar/TSpec (gray) and IRTF/SpeX (black). If it is actually an L dwarf, it is the reddest one known and shows substantial variability. 2MASSW J2244+2043 (L7.5±2; Looper et al. 2008) is similar to this object, but not as red. Excess blue flux in the H and K bands may hint at a T dwarf companion or the presence of CH_4 in this extremely red object. Spectra have been normalized at 1.27μm and offset vertically.
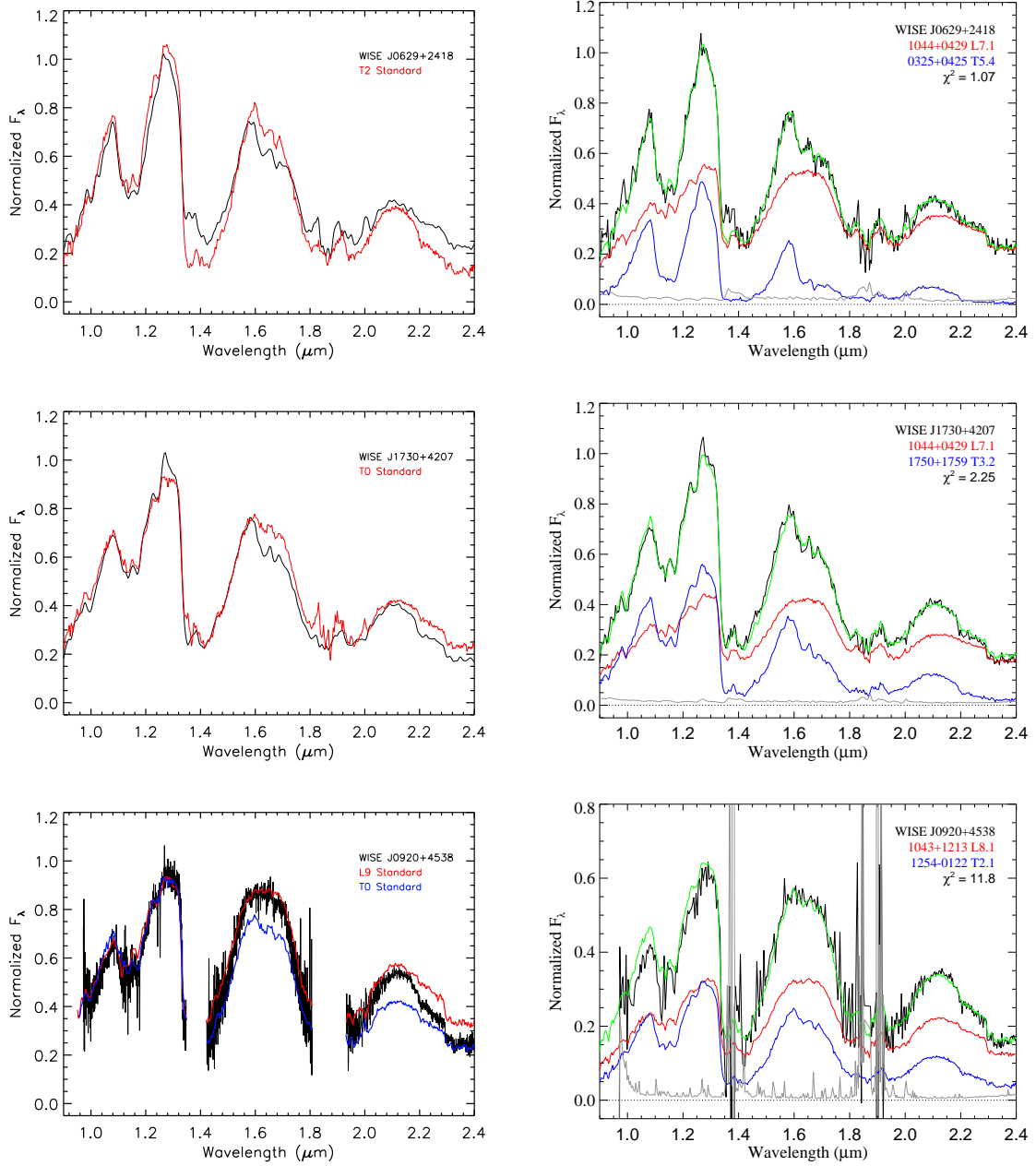
Fig. 17.— Binary candidates identified using the method of Burgasser et al. (2010). The left side shows the best matching spectral standard and the right side shows the best composite spectrum (green), along with the constituent templates. Spectra have been normalized at 1.27μm and offset vertically.
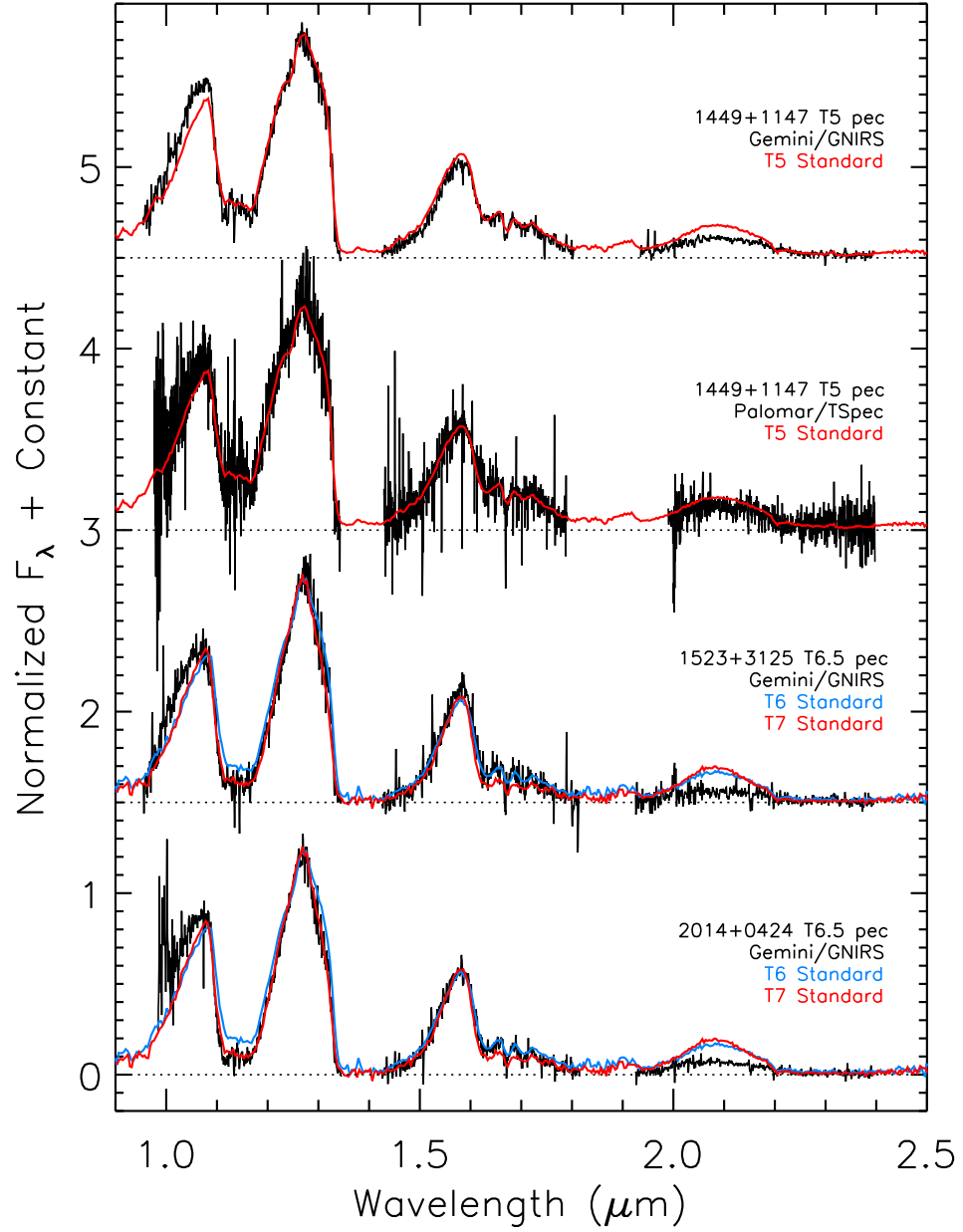
Fig. 18.— Spectra of peculiar early-type T dwarfs, shown in black, along with spectral standards. Two different observations of the peculiar T5, WISE J1449+1147, from Gemini/GNIRS and Palomar/TSpec are shown. Spectra have been normalized at 1.27μm and offset vertically.
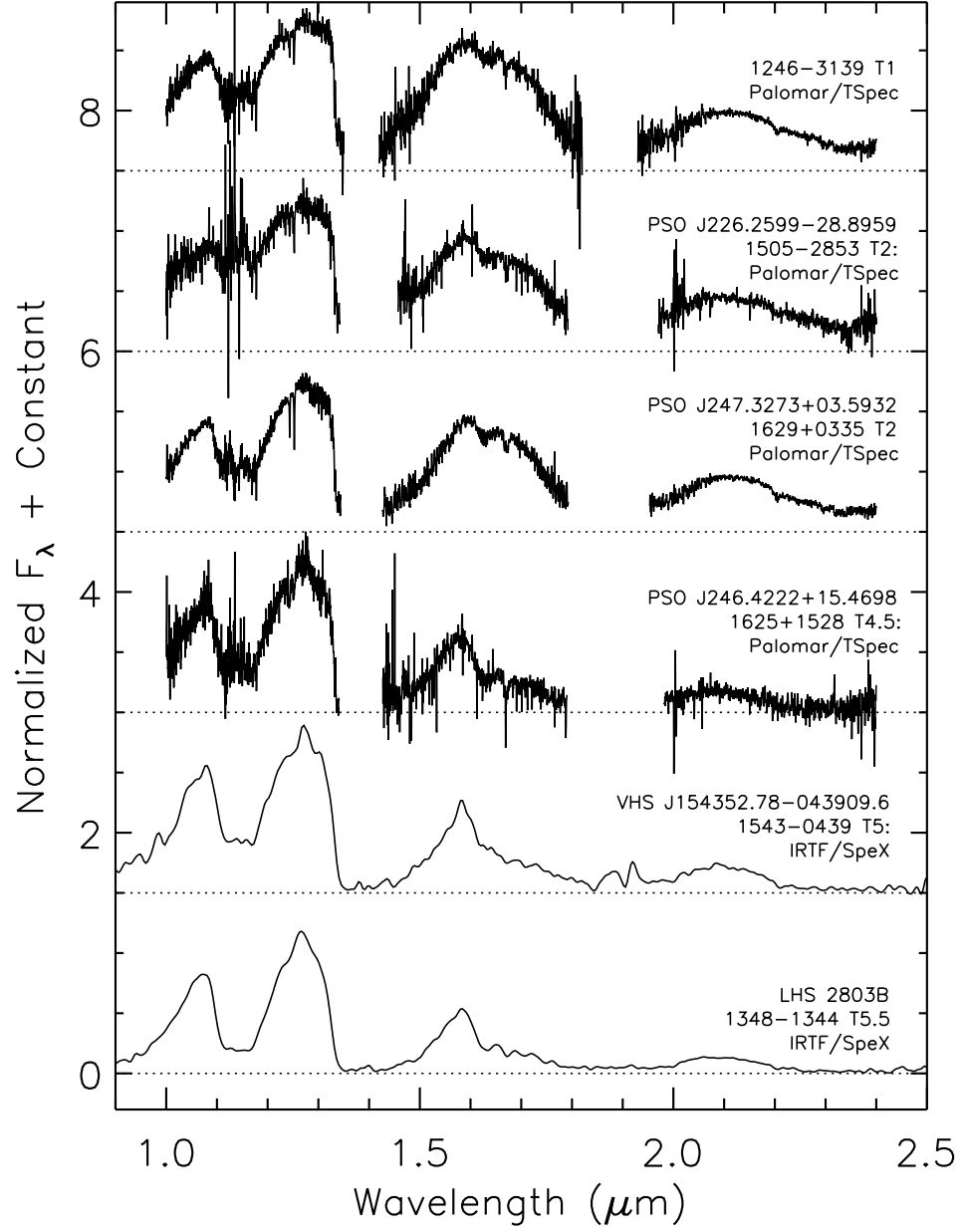
Fig. 19.— Spectra of previously identified T dwarfs from the literature. Spectra have been normalized at 1.27μm and offset vertically.
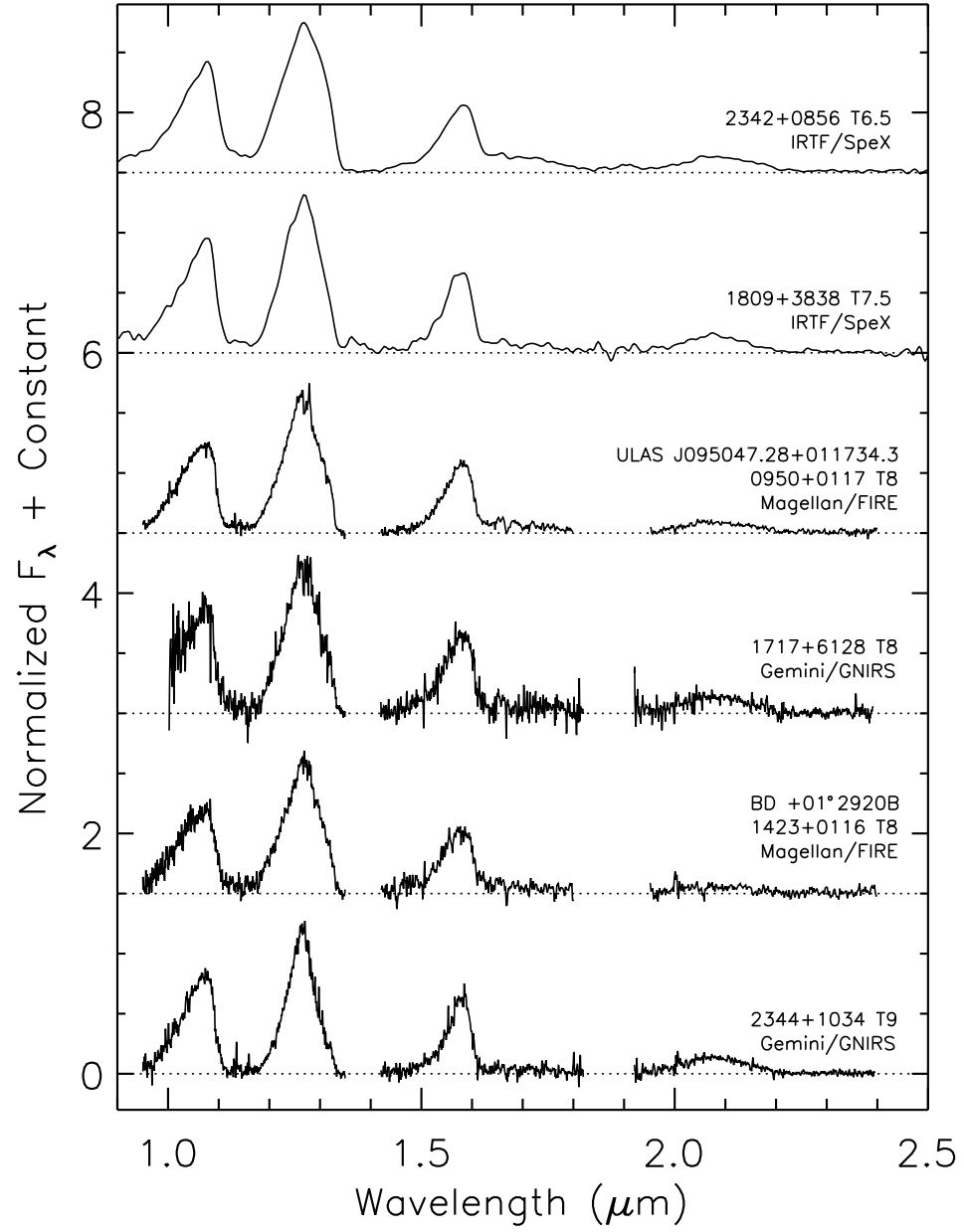
Fig. 19b.— Continued.
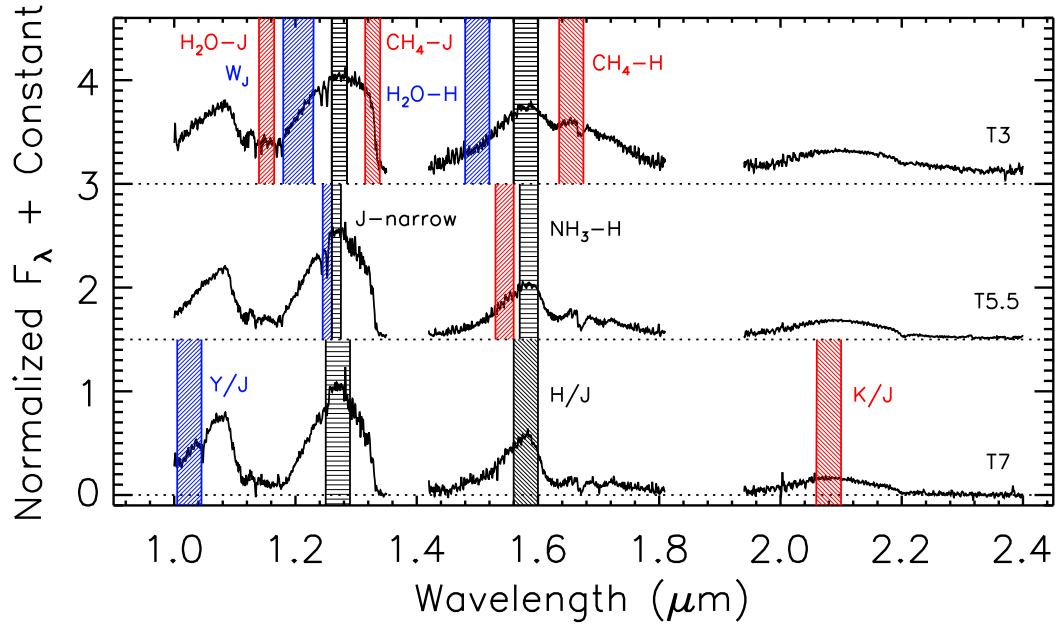
Fig. 20.— The wavelengths that define the spectral indices derived in Equations 1-10 are depicted for a series of Palomar/TSpec T dwarf spectra.
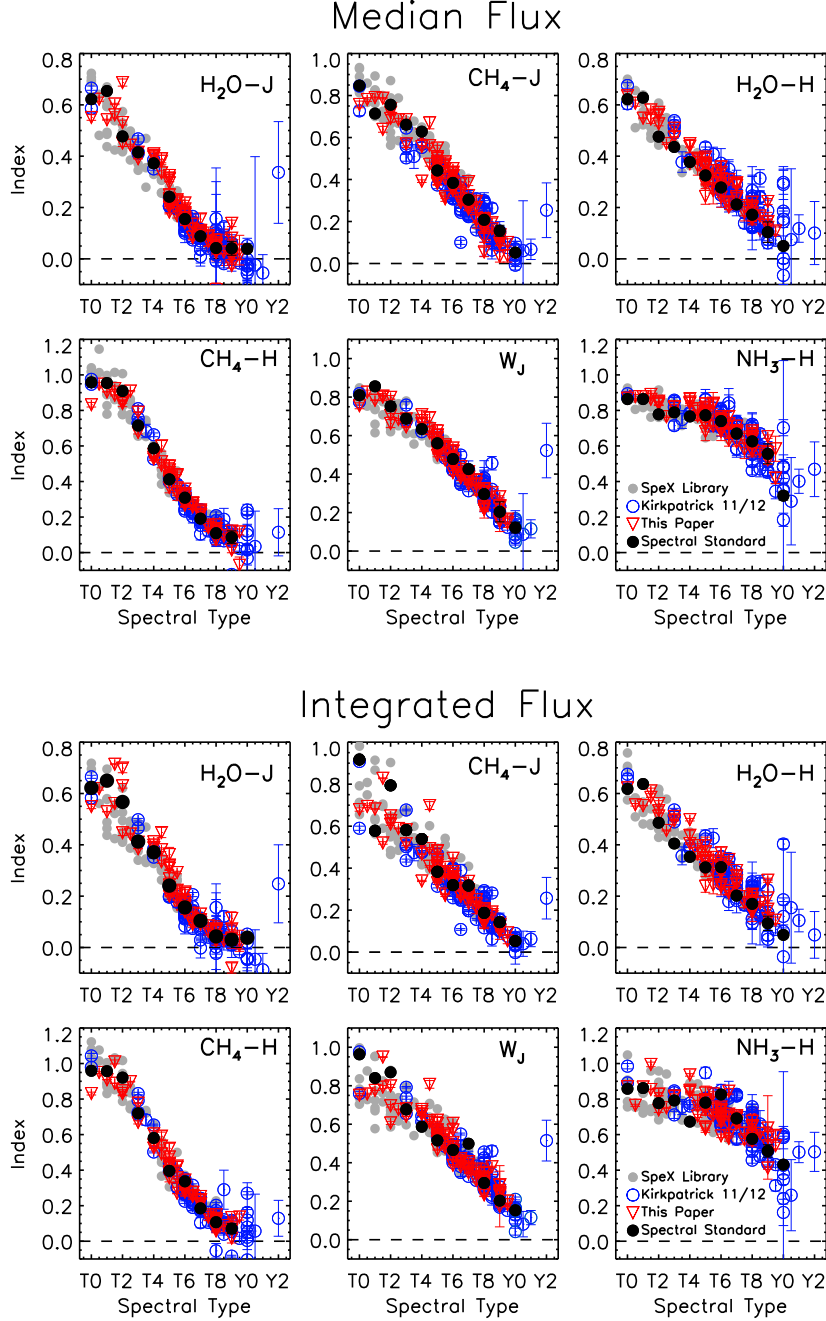
Fig. 21.— Six spectral indices from Burgasser et al. (2006), Warren et al. (2007) and Delorme et al. (2008), computed using the median flux and the integrated flux. The T dwarfs in this paper are marked by red triangles, and the T and Y dwarfs of Kirkpatrick et al. (2011, 2012) and Cushing et al. (2011) are marked as blue hollow circles. Also included are the T dwarfs from the SpeX Prism Library as gray filled circles, and spectral standards as black filled circles.
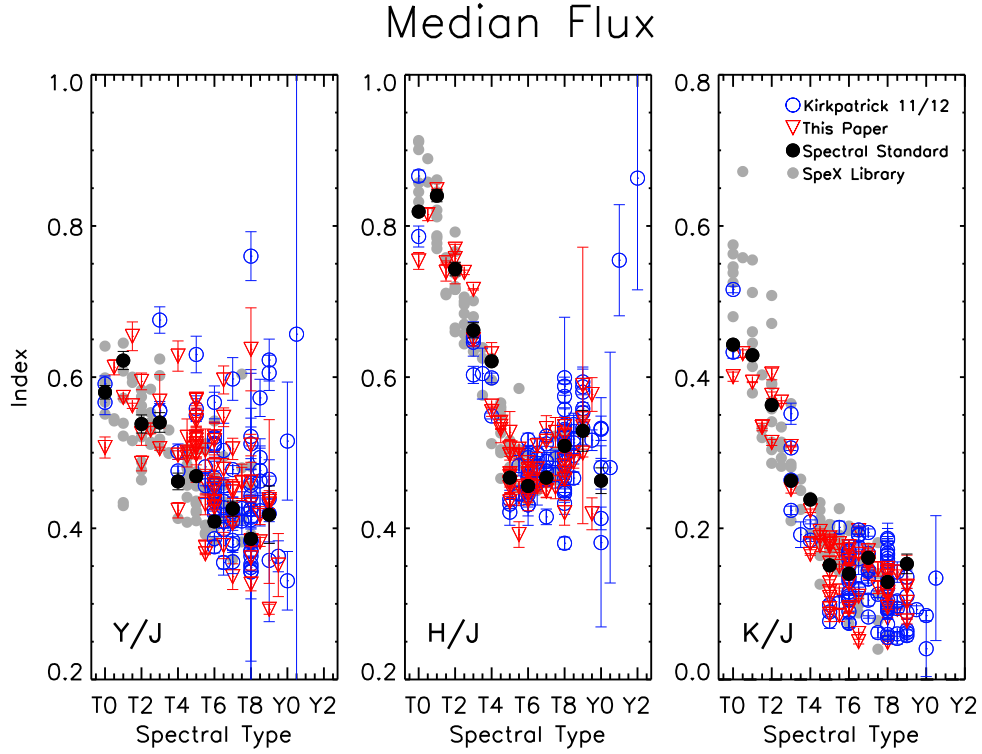
Fig. 22.— The peak flux ratios defined by Burgasser et al. (2004, 2006), computed using the median flux instead of the integrated flux. Same symbols as in Figure 21.
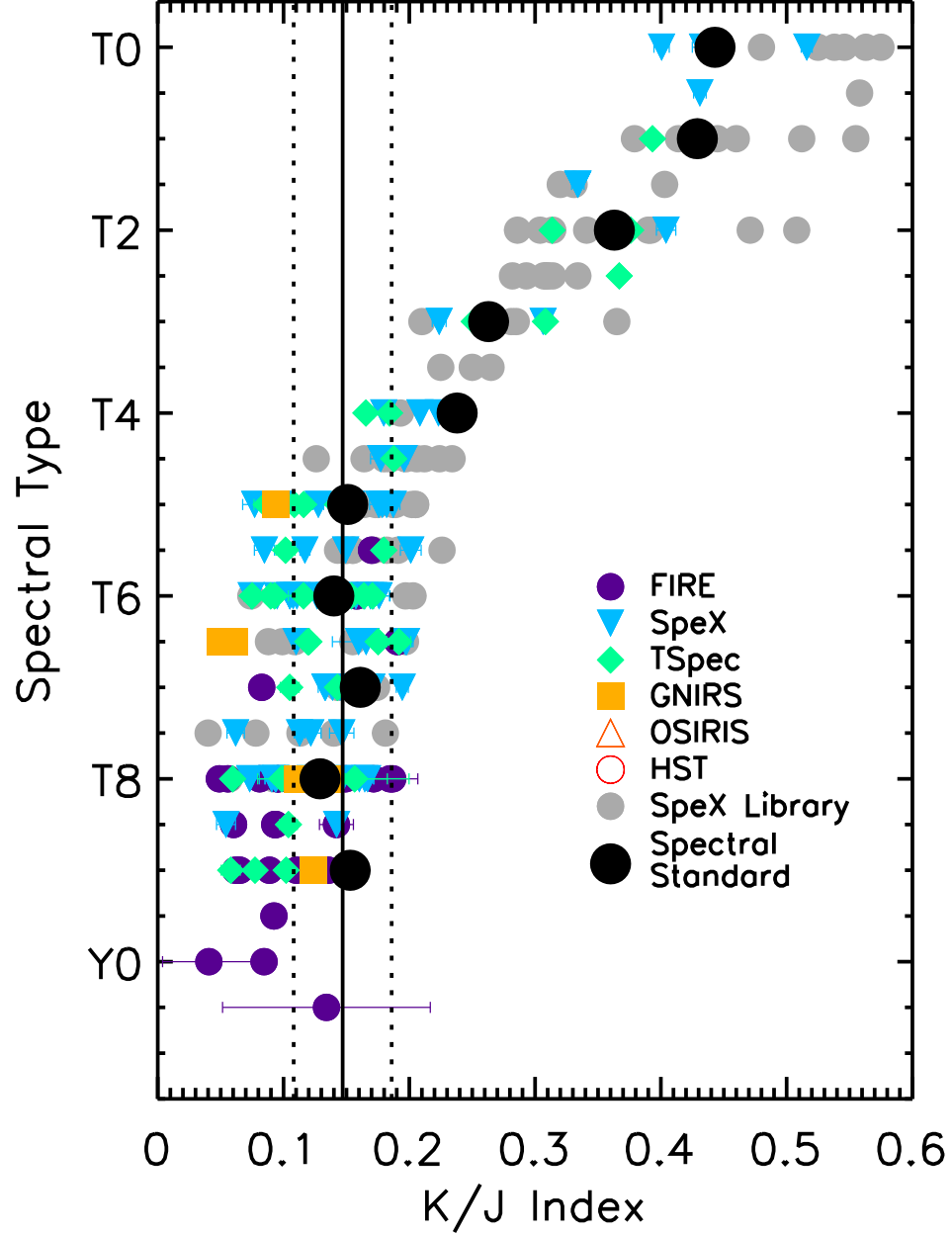
Fig. 23.— Spectral type versus K/J ratio for the same objects in Figure 22, sorted by spectrograph. The average K/J index for the T5-T9 spectral standards is 0.147±0.013, and the 3σ limits are shown here. We find that 54 out of 170 (about one third) of T5 or later dwarfs are below this limit, while only 18 out of 170 are above this limit.
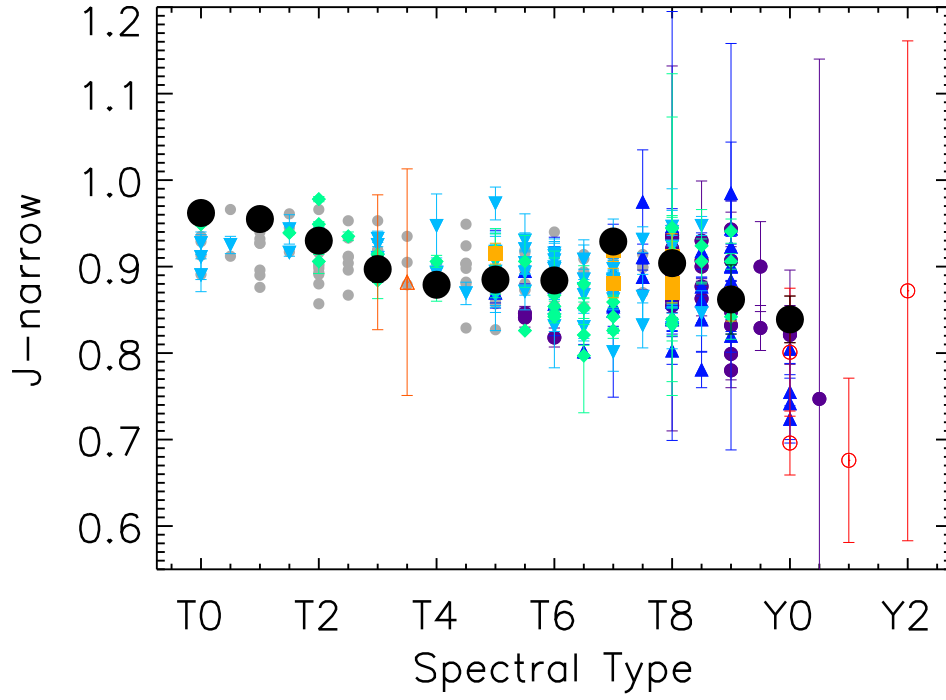
Fig. 24.— The J-narrow index for T and Y dwarfs in Figure 22. Undulation in the T dwarfs is due to changes in the 1.254μm KI line. Y dwarfs have smaller indices because of a narrowing of the J-band flux peak.
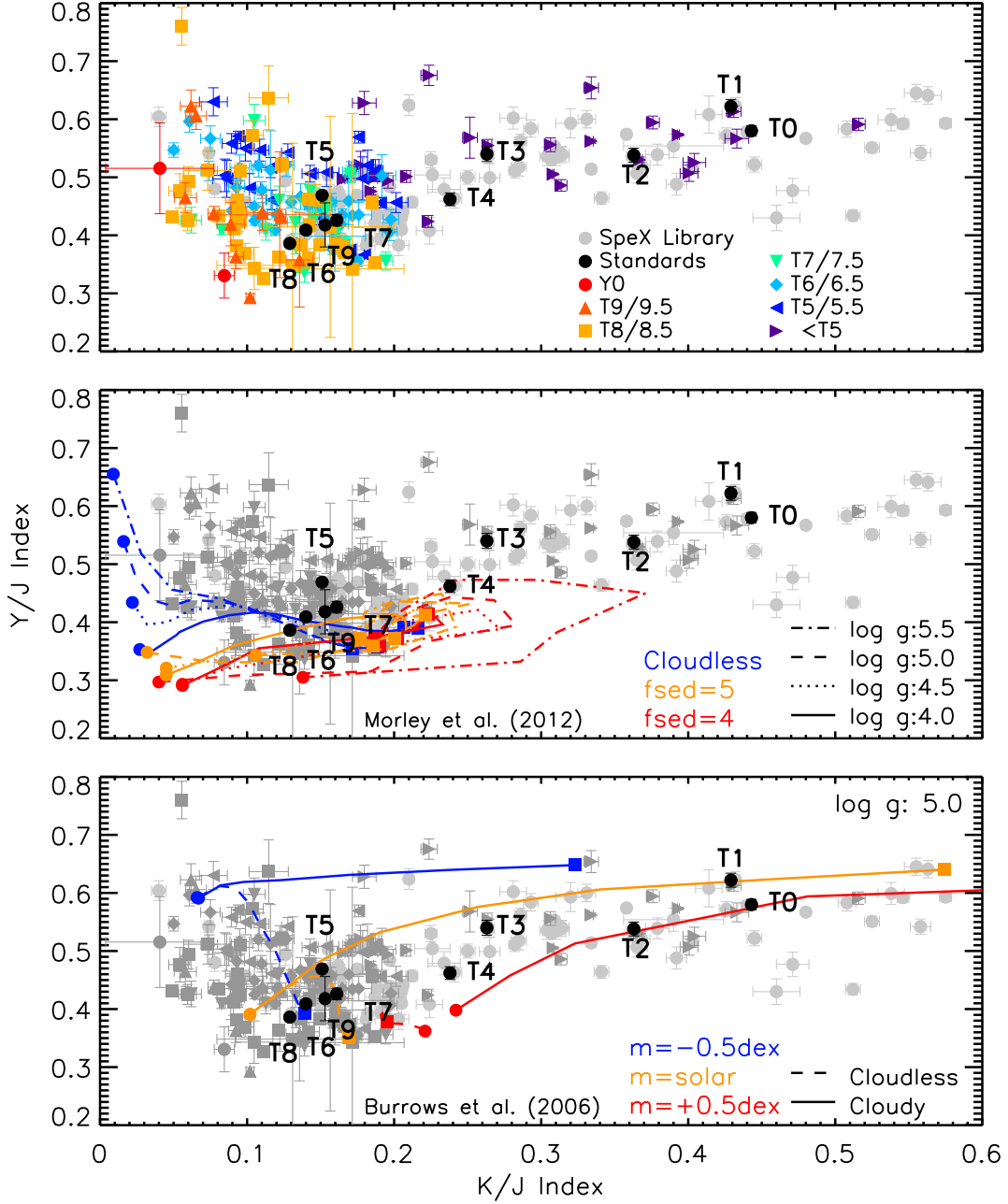
Fig. 25.— The Y/J versus K/J indices of late-type T dwarfs compared to models. Top: Index values sorted by spectral type. Middle: The Morley et al. (2012) sulfide cloud models (which do not include silicate clouds expected in early-type T dwarfs) are shown for log g =4, 4.5, 5, 5.5 (solid,dotted,dashed,dot-dash) and T_{eff}=400K to 1300K. Cloudless models are shown in blue, f_{sed}=5 in orange, and f_{sed}=4 in red. Bottom: The cloudy (solid lines) and clear (dashed lines) models from Burrows et al. (2006) with log g =5 and metallicities of solar and ±0.5dex with T_{eff}= 800K to 1700K. The highest temperature is marked with a square and the lowest temperature is marked with a circle.
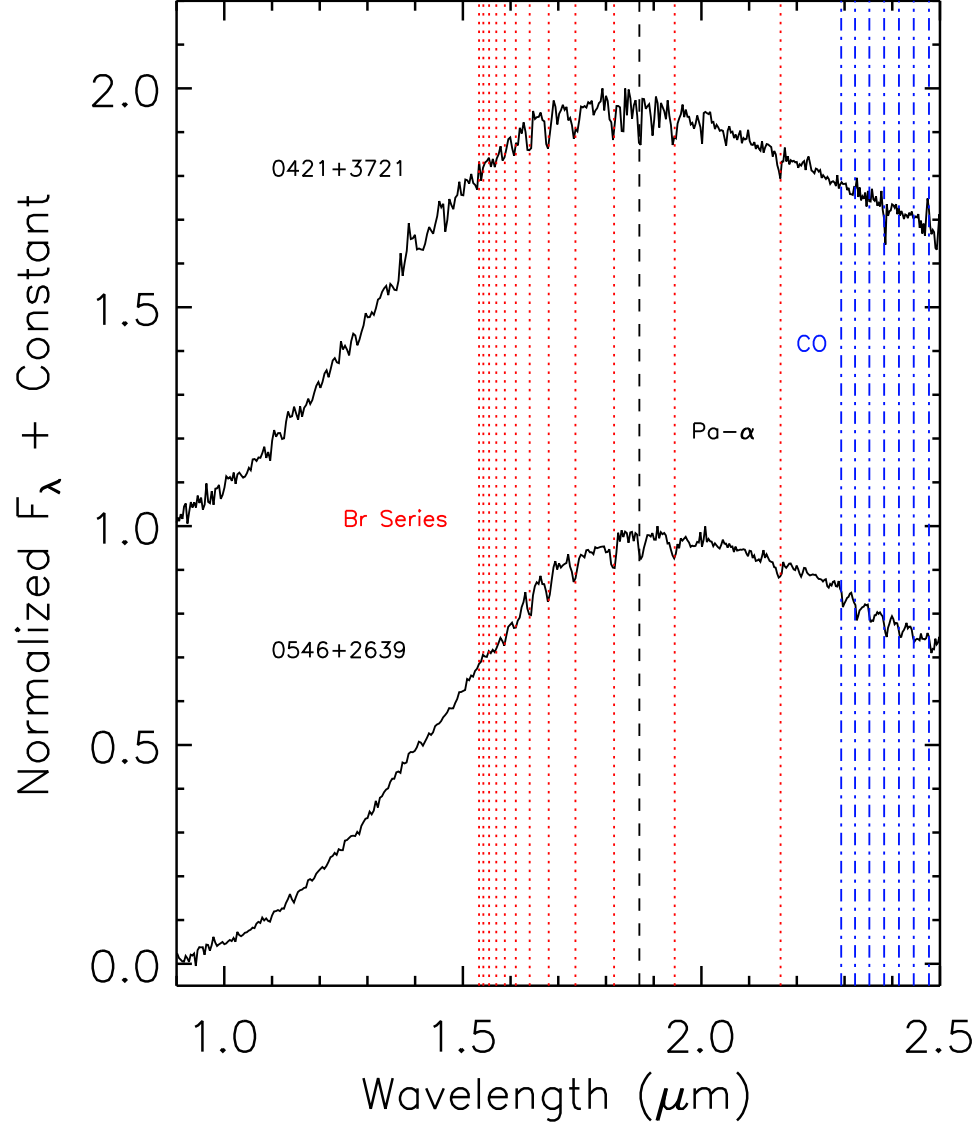
Fig. 26.— IRTF/SpeX spectra of two YSOs found in the same WISE color space as T dwarfs. Both sources lack clear emission features and display photospheric H(dotted and dashed lines) and CO(dash-dotted lines) absorption.
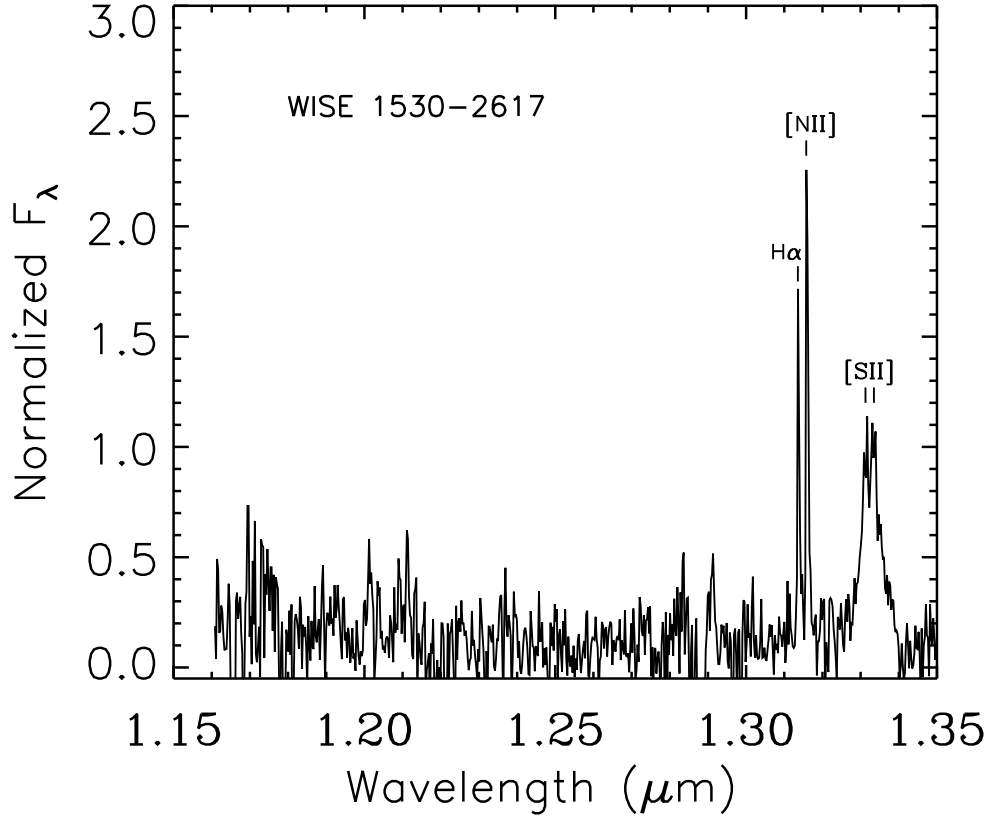
Fig. 27.— Keck/NIRSPEC spectrum of WISE J153015.18−261753.6, an AGN that is on the reddest edges of WISE brown dwarf color space. The Hα, [NII]λ6583, and broad double-peaked [SII]λλ6716, 6731 lines in the J band place this object at z=1.00.
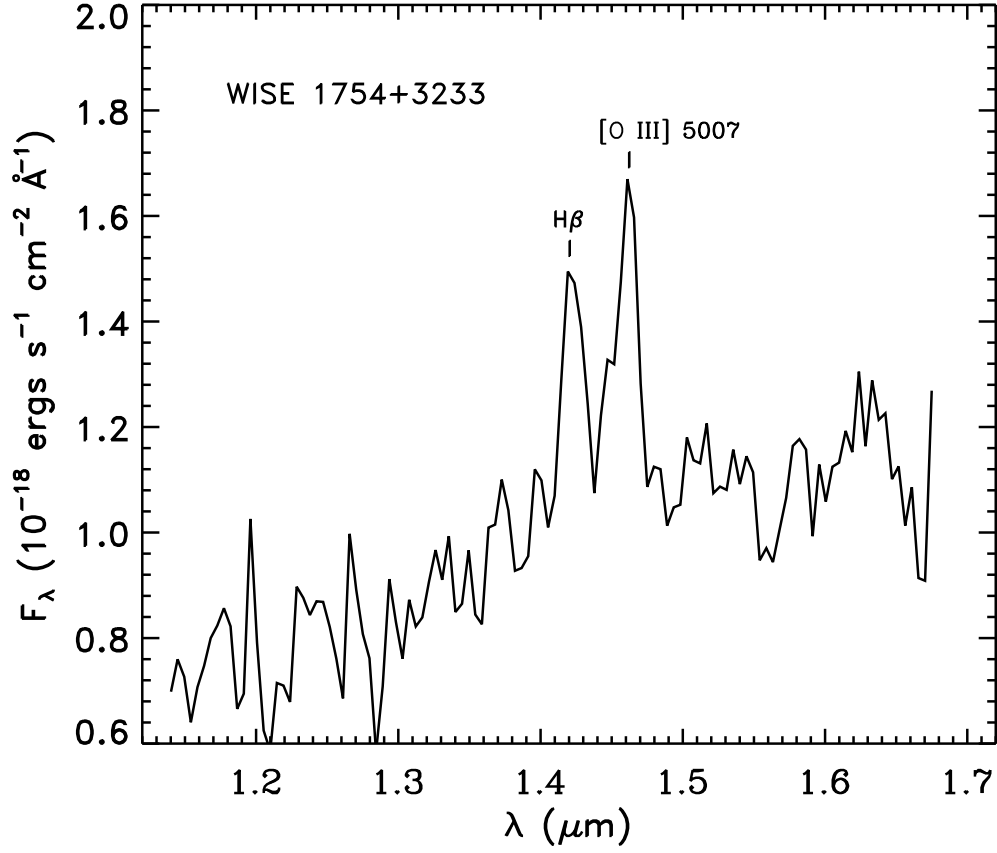
Fig. 28.— HST/WFC3 spectrum of WISE J175443.93+323332.5, an AGN interloper. The Hβ and [O III]λλ4959, 5007 lines in the H band place this object at z=1.92.
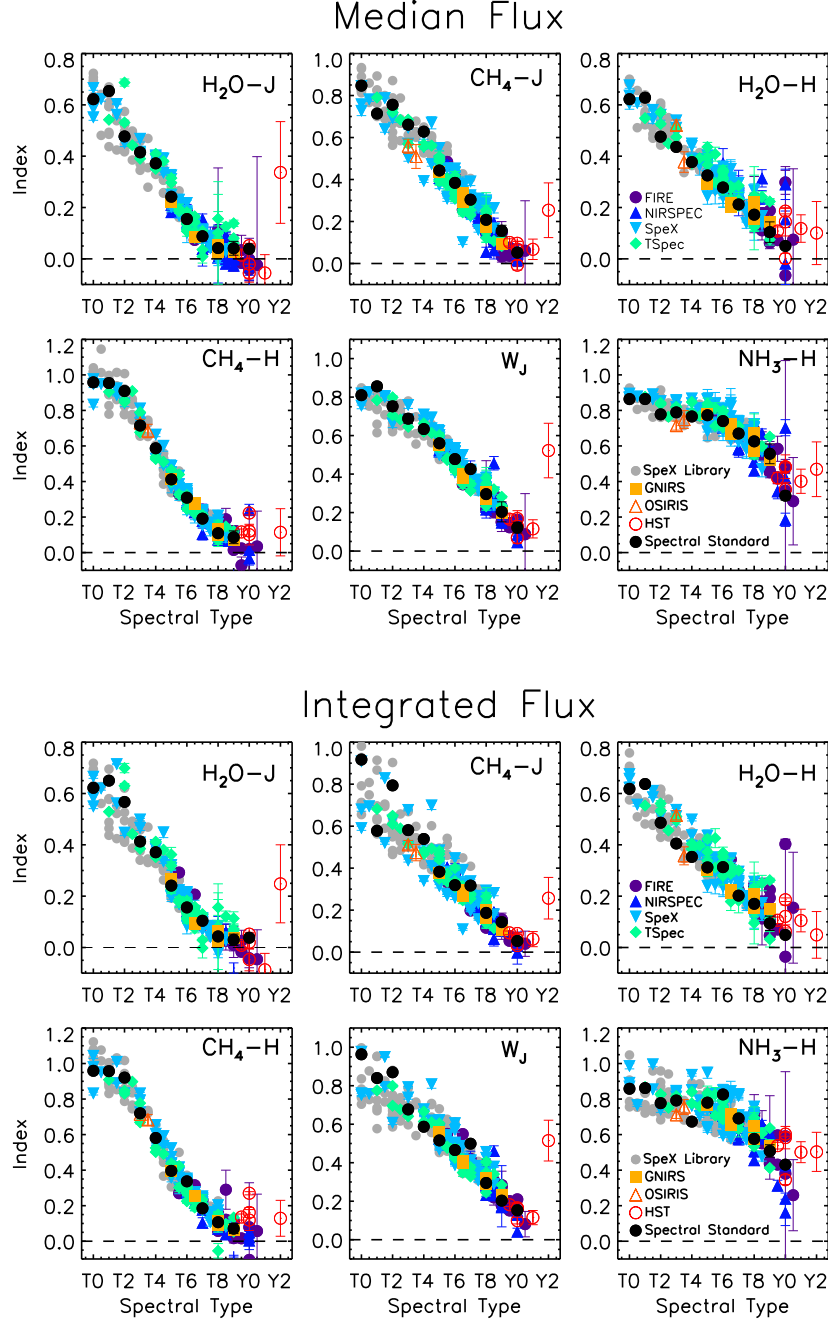
Fig. A1.— The six spectral indices from Burgasser et al. (2006), Warren et al. (2007) and Delorme et al. (2008), computed using the median flux and integrated flux for the T dwarfs in this paper and the T and Y dwarfs of Kirkpatrick et al. (2011, 2012) and Cushing et al. (2011). Objects are marked by instrument with the symbols and colors in the legend. Also included are the spectral standards as black filled circles and T dwarfs from the SpeX Prism Library as gray circles.
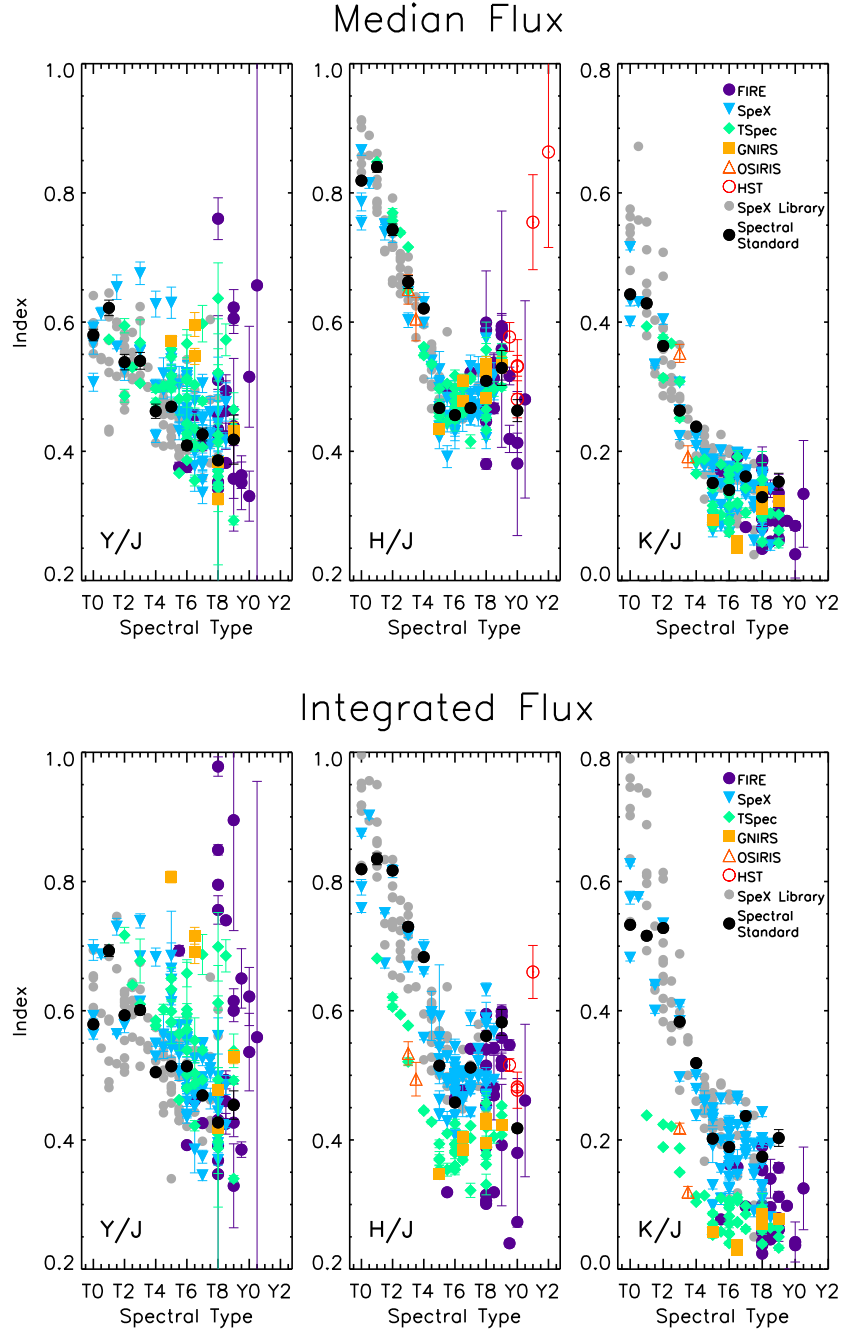
Fig. A2.— The peak flux ratios defined by Burgasser et al. (2004, 2006), computed using the median flux and the integrated flux. Same symbols as in Figure A1.